Article:
Aad, G. orcid.org/0000-0002-6665-4934, Aakvaag, E. orcid.org/0000-0001-7616-1554, Abbott, B. orcid.org/0000-0002-5888-2734 et al. (2885 more authors) (2024) Search for the nonresonant production of Higgs boson pairs via gluon fusion and vector-boson fusion in the b¯ bτ+τ− final state in proton-proton collisions at s =13 TeV with the ATLAS detector. Physical Review D, 110. 032012. ISSN 2470-0010

https://doi.org/10.1103/physrevd.110.032012

Search for the nonresonant production of Higgs boson pairs via gluon fusion and vector-boson fusion in the $b\bar{b}\tau^+\tau^-$ final state in proton-proton collisions at $\sqrt{s} = 13$ TeV with the ATLAS detector

G. Aad *et al.*[*]
(ATLAS Collaboration)

(Received 22 April 2024; accepted 9 July 2024; published 9 August 2024)

A search for the nonresonant production of Higgs boson pairs in the $HH \to b\bar{b}\tau^+\tau^-$ channel is performed using 140 fb^{-1} of proton-proton collisions at a center-of-mass energy of 13 TeV recorded by the ATLAS detector at the CERN Large Hadron Collider. The analysis strategy is optimized to probe anomalous values of the Higgs boson self-coupling modifier κ_λ and of the quartic $HHVV$ ($V = W, Z$) coupling modifier κ_{2V}. No significant excess above the expected background from Standard Model processes is observed. An observed (expected) upper limit $\mu_{HH} < 5.9(3.3)$ is set at 95% confidence-level on the Higgs boson pair production cross section normalized to its Standard Model prediction. The coupling modifiers are constrained to an observed (expected) 95% confidence interval of $-3.1 < \kappa_\lambda < 9.0$ ($-2.5 < \kappa_\lambda < 9.3$) and $-0.5 < \kappa_{2V} < 2.7$ ($-0.2 < \kappa_{2V} < 2.4$), assuming all other Higgs boson couplings are fixed to the Standard Model prediction. The results are also interpreted in the context of effective field theories via constraints on anomalous Higgs boson couplings and Higgs boson pair production cross sections assuming different kinematic benchmark scenarios.

DOI: 10.1103/PhysRevD.110.032012

I. INTRODUCTION

After the discovery of the Higgs boson (H) in 2012 [1,2], the ATLAS [3] and CMS [4] Collaborations at the Large Hadron Collider [5] (LHC) have been focusing on the measurement of its properties [6–12]. All features probed so far for this new particle are consistent with the Standard Model (SM) predictions [13–18] for a Higgs boson with an observed mass m_H near 125 GeV [19,20].

In this extensive measurement program, the properties of interactions involving multiple Higgs bosons remain to be verified. In the SM, these can be characterized by the trilinear and quartic self-couplings λ_{HHH} and λ_{HHHH}, which are both equal to the coefficient λ of the quartic term of the Higgs field potential $V(\phi) = \mu^2|\phi|^2 + \lambda|\phi|^4$. The quartic couplings g_{HHVV} ($V = W, Z$) characterize the interactions between two Higgs bosons and two W or Z bosons, and are related in the SM to the HWW and HZZ couplings g_{HVV} through the relation $g_{HHVV} = g_{HVV}/2\nu$, where ν is the vacuum expectation value of the Higgs field. Significant deviations from the SM predictions for these couplings would provide a strong sign of beyond the Standard Model (BSM) physics [21].

The most sensitive test of Higgs boson self-interactions comes from processes of Higgs boson pair production (HH) such as gluon fusion (ggF) and vector-boson fusion (VBF) HH production. Measuring the cross section of these processes offers a direct probe of the values of these couplings, through their scale factors with respect to the SM predictions: $\kappa_\lambda = \lambda_{HHH}/\lambda^{\mathrm{SM}}_{HHH}$, affecting both ggF and VBF production, and $\kappa_V = g_{HVV}/g^{\mathrm{SM}}_{HVV}$ and $\kappa_{2V} = g_{HHVV}/g^{\mathrm{SM}}_{HHVV}$, which only impact VBF production.

The dominant mode for HH production is ggF, with a cross section of $\sigma^{\mathrm{SM}}_{\mathrm{ggF}} = 31.1^{+2.1}_{-7.2}$ fb [22–29], calculated at next-to-next-to-leading order (NNLO) including finite top-quark-mass effects for $m_H = 125$ GeV at $\sqrt{s} = 13$ TeV, resulting from the destructive interference between the leading-order (LO) Feynman diagrams shown in Fig. 1. The second most common HH production mechanism at the LHC is VBF, with a total cross section of $\sigma^{\mathrm{SM}}_{\mathrm{VBF}} = 1.73 \pm 0.04$ fb [30–34] calculated at next-to-next-to-next-to-leading order (N^{3}LO) for $m_H = 125$ GeV at $\sqrt{s} = 13$ TeV. The LO diagrams for this process are shown in Fig. 2.

The most stringent constraints on SM HH production by the ATLAS Collaboration were obtained through a statistical combination [35] of the results in the $b\bar{b}\gamma\gamma$ [36], $b\bar{b}\tau^+\tau^-$ [37] and $b\bar{b}b\bar{b}$ [38] final states, exploiting the entire sample of proton-proton (pp) collisions provided by

[*]Full author list given at the end of the article.

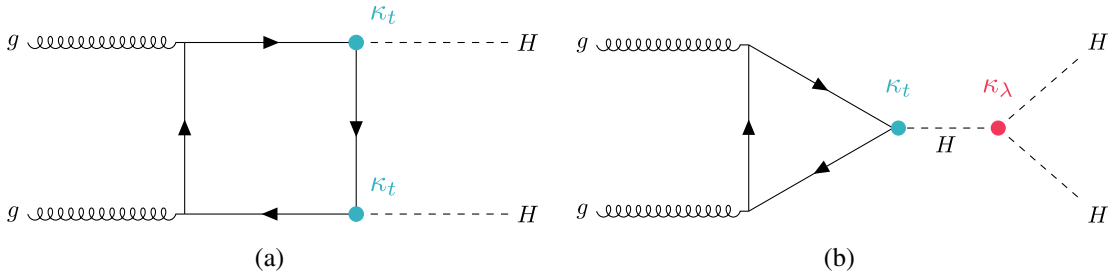

FIG. 1. Leading-order Feynman diagrams of the ggF HH production process: (a) box and (b) triangle diagrams. The Higgs self-coupling modifier is shown as κ_λ, while the modifier for the coupling of the Higgs boson to the top quark is shown as κ_t.

the LHC during its second phase (Run 2, 2015–2018). The 95% confidence level (CL) observed (expected) upper limit on the HH production signal strength $\mu_{HH} = (\sigma_{\text{ggF}} + \sigma_{\text{VBF}})/(\sigma^{\text{SM}}_{\text{ggF}} + \sigma^{\text{SM}}_{\text{VBF}})$ from the combination is 2.4 (2.9) with respect to the case $\mu_{HH} = 0$, which is later referred to as the *background-only hypothesis*. Using the values of the combination test statistic as a function of either κ_λ or κ_{2V}, when all other coupling modifiers are set to unity, the observed (expected with respect to the SM prediction) 95% confidence intervals (CIs) are $\kappa_\lambda \in [-0.6, 6.6]$ ($[-2.1, 7.8]$) and $\kappa_{2V} \in [0.1, 2.0]$ ($[0.0, 2.1]$). The CMS Collaboration also performed a combination of HH analyses in multiple final states, based on their full Run 2 dataset [12]. The observed (expected) 95% CL upper limit on μ_{HH} is 2.5 (3.4). The observed allowed ranges of κ_λ and κ_{2V} are restricted to $\kappa_\lambda \in [-1.24, 6.49]$ and $\kappa_{2V} \in [0.67, 1.38]$. No significant excess over the background-only hypothesis is observed by any of these analyses.

The $b\bar{b}\tau^+\tau^-$ final state captures 7.3% of all HH final states and provides a compromise between expected signal event yield and background contamination. This leads to a sensitivity similar to that of the $b\bar{b}b\bar{b}$ and $b\bar{b}\gamma\gamma$ decay modes. The latest ATLAS results for $HH \to b\bar{b}\tau^+\tau^-$ with the full LHC Run 2 dataset are documented in Ref. [37]. They result in an observed (expected) 95% CL upper limit on the total HH production cross section of 4.7 (3.9) times the SM prediction with respect to the background-only hypothesis. Moreover, observed (expected) 95% CIs on κ_λ and κ_{2V} are $\kappa_\lambda \in [-2.7, 9.5]$ ($[-3.1, 10.2]$) and $\kappa_{2V} \in [-0.6, 2.7]$ ($[-0.5, 2.7]$), respectively [35]. Recent results from the CMS Collaboration [39] set an observed (expected) upper limit of 3.3 (5.2) times the SM production cross section at 95% CL over the background-only hypothesis. Additionally, constraints are set on κ_λ and κ_{2V} with respect to the background-only hypothesis, leading to the observed (expected) 95% CL constraints $\kappa_\lambda \in [-1.7, 8.7]$ ($[-2.9, 9.8]$) and $\kappa_{2V} \in [-0.4, 2.6]$ ($[-0.6, 2.8]$).

In this paper, an updated search for nonresonant Higgs boson pair production in the $b\bar{b}\tau^+\tau^-$ final state with the full Run 2 ATLAS dataset is presented, superseding and expanding upon the nonresonant results of Ref. [37]. Compared with the previous publication, the overall object identification, trigger strategy and event selection in the signal-enriched regions is unchanged, but an optimized classification of the selected events is implemented to enhance the sensitivity to κ_λ and to the VBF production mode. Improved multivariate classifiers are used to exploit the kinematic features of SM VBF HH production to define a dedicated VBF category, which improves the sensitivity to anomalous values of the coupling modifiers κ_λ and κ_{2V}. Updated Monte Carlo (MC) predictions are used for describing the main backgrounds of top-quark pair production ($t\bar{t}$) and Z boson production in association with heavy-flavor quarks, leading to a more accurate modelling of these processes and enhancing the statistical power of the simulation. The event selection for the auxiliary measurement of the background from Z boson production in

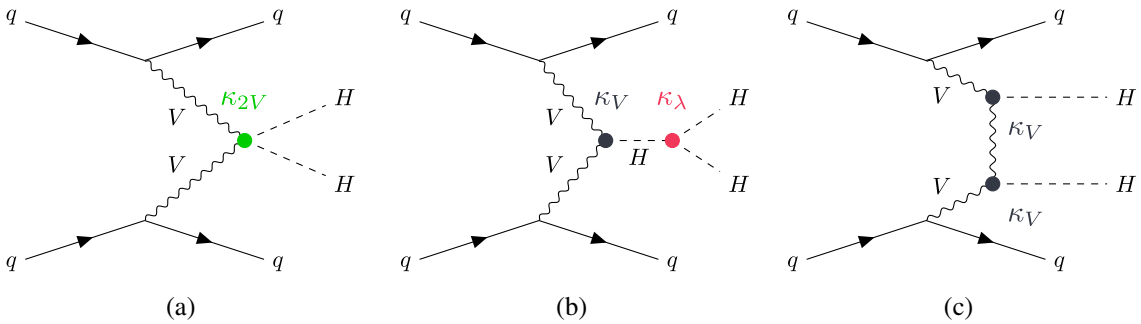

FIG. 2. Leading-order Feynman diagrams of the VBF HH production process. The g_{HHVV} coupling modifier is shown as κ_{2V}, the Higgs self-coupling modifier as κ_λ, and the modifier for the coupling of the Higgs boson to the SM vector bosons V as κ_V.

association with heavy-flavor quarks is adapted to improve the consistency of the kinematic properties of this process with the signal-enriched regions. Finally, the obtained results are reinterpreted in the context of effective field theories (EFTs). These changes in analysis set-up and strategy lead to an improvement of the expected 95% CL limit on μ_{HH} of 15%. The widths of the 95% CIs on κ_λ and κ_{2V} with respect to the SM expectation are reduced by 11% and 19%, respectively, compared with the analysis described in Ref. [37].

This paper is organized as follows. Section II describes the ATLAS detector. The collected dataset and the simulated event samples are covered in Section III. The event selection and categorization, along with the description of the multivariate classifiers, are described in Section IV. Section V lists the systematic uncertainties. Finally, Section VI summarizes the results, Section VII covers the conducted EFT interpretations, and the study is concluded in Section VIII.

II. ATLAS DETECTOR

The ATLAS experiment at the LHC is a multipurpose particle detector with a forward–backward symmetric cylindrical geometry and a near 4π coverage in solid angle.[1] It consists of an inner tracking detector surrounded by a thin superconducting solenoid providing a 2 T axial magnetic field, electromagnetic and hadron calorimeters, and a muon spectrometer. The inner tracking detector covers the pseudorapidity range $|\eta| < 2.5$. It consists of silicon pixel, silicon microstrip, and transition radiation tracking detectors. Lead/liquid-argon (LAr) sampling calorimeters provide electromagnetic (EM) energy measurements with high granularity. A steel/scintillator-tile hadron calorimeter covers the central pseudorapidity range ($|\eta| < 1.7$). The end cap and forward regions are instrumented with LAr calorimeters for both the EM and hadronic energy measurements up to $|\eta| = 4.9$. The muon spectrometer surrounds the calorimeters and is based on three large superconducting air-core toroidal magnets with eight coils each. The field integral of the toroids ranges between 2.0 and 6.0 T m across most of the detector. The muon spectrometer includes a system of precision tracking chambers and fast detectors for triggering. A two-level trigger system is used to select events. The first-level trigger is implemented in hardware and uses a subset of the detector information to accept events at a rate below 100 kHz. This is followed by a software-based trigger that reduces the accepted event rate to 1 kHz on average depending on the data-taking conditions. An extensive software suite [40] is used in simulation, in the reconstruction and analysis of real and simulated events, in detector operations, and in the trigger and data acquisition systems of the experiment.

[1]ATLAS uses a right-handed coordinate system with its origin at the nominal interaction point (IP) in the center of the detector and the z-axis along the beam pipe. The x-axis points from the IP to the center of the LHC ring, and the y-axis points upward. Polar coordinates (r, ϕ) are used in the transverse plane, ϕ being the azimuthal angle around the z-axis. The pseudorapidity is defined in terms of the polar angle θ as $\eta = -\ln\tan(\theta/2)$. Angular distance is measured in units of $\Delta R \equiv \sqrt{(\Delta\eta)^2 + (\Delta\phi)^2}$.

III. DATA AND SIMULATED EVENT SAMPLES

The search presented in this paper uses the pp collision dataset collected by the ATLAS experiment during the LHC Run 2 at a center-of-mass energy of $\sqrt{s} = 13$ TeV. After data quality requirements [41], the integrated luminosity of the dataset is 140.1 ± 1.2 fb^{-1} [42,43].

The samples of simulated events used for this study are summarized in Table I, and they correspond to those already employed in the previous publication [37], with a few important updates aimed at improving the statistical power of the simulated samples for the main background processes providing a more accurate simulation of the HH signal. All generated samples are passed through a detailed simulation of the ATLAS detector response [44] based on GEANT4 [45].

The production of $t\bar{t}$ events, and of single-top-quark events in the $Wt-$, $s-$ and $t-$channels is simulated using the POWHEG BOX V2 [46] generator together with the NNPDF3.0NLO parton distribution functions (PDF) set [47]. The simulated events are interfaced to PYTHIA8.230 [48] for parton showering and hadronization using the A14 tune [49] together with the NNPDF2.3LO [50] PDF set. The setup of the MC event generator for these production processes is unchanged with respect to Ref. [37]. For $t\bar{t}$ processes the size of the sample is increased by including two statistically independent sets of events. The first sample is simulated with the requirement of at least one top quark decaying into a leptonic final state, while in the second sample both top quarks are forced to decay leptonically. The combination of these samples results in a decrease in the statistical uncertainty related to the $t\bar{t}$ simulation by a factor of approximately two in the selected phase space compared to using only the first sample, as was done in Ref. [37].

For events containing a W or a Z boson produced in association with jets, new samples are produced with the SHERPA2.2.11 generator [51]. Events are simulated using NLO matrix elements for up to two partons, and LO matrix elements for up to five partons calculated using the OPENLOOPS [52–55] and Comix [56] matrix-element generators. For these samples, the NNPDF3.0NNLO PDF set is used with dedicated parton shower, matched to the matrix element via the MEPS@NLO prescription [57]. The electroweak input scheme is updated compared to the previous version, along with corrected heavy-flavor hadron production fractions. The SHERPA2.2.11 generator allows faster per-event generation time, with significant reduction

TABLE I. Generators used to simulate the signal and background processes. If not otherwise specified, the order of the cross-section calculation refers to the expansion in the strong coupling constant (α_S). The acronyms ME, PS and UE are used for matrix element, parton shower and underlying event, respectively. More details on the simulation of the signal and background samples are described in the text and in Ref. [37]. (†) The NNLO(QCD) + NLO(EW) cross-section calculation for the $pp \to ZH$ process already includes the $gg \to ZH$ contribution. The $qq \to ZH$ process is normalized to the NNLO(QCD) + NLO(EW) cross section for the $pp \to ZH$ process, after subtracting the $gg \to ZH$ contribution.

Process	ME generator	ME QCD order	PDF set	PS and hadronization	UE model tune	Cross-section order
Signal						
$gg \to HH$ (ggF)	POWHEG BOX V2 [46]	NLO	PDF4LHC15NLO [58]	PYTHIA8.244 [48]	A14 [49]	NNLO FTApprox
$qq \to qqHH$ (VBF)	MADGRAPH5_AMC@NLO 2.7.3 [60]	LO	NNPDF3.0NLO [47]	PYTHIA8.244	A14	$N^3LO(QCD)$
Top-quark						
$t\bar{t}$	POWHEG BOX V2	NLO	NNPDF3.0NLO	PYTHIA8.230	A14	NNLO + NNLL
t-channel	POWHEG BOX V2	NLO	NNPDF3.0NLO	PYTHIA8.230	A14	NLO
s-channel	POWHEG BOX V2	NLO	NNPDF3.0NLO	PYTHIA8.230	A14	NLO
Wt	POWHEG BOX V2	NLO	NNPDF3.0NLO	PYTHIA8.230	A14	NLO
$t\bar{t}Z$	SHERPA2.2.1 [51]	NLO	NNPDF3.0NNLO	SHERPA 2.2.1	···	NLO
$t\bar{t}W$	SHERPA2.2.8	NLO	NNPDF3.0NNLO	SHERPA2.2.8	···	NLO
Vector boson+jets						
W/Z + jets	SHERPA2.2.11	NLO($\leq$ 2 jets) LO(3,4 jets)	NNPDF3.0NNLO	SHERPA2.2.11	···	NNLO
Diboson						
WW, WZ, ZZ	SHERPA2.2.1	NLO($\leq$ 1 jets) LO(2,3 jets)	NNPDF3.0NNLO	SHERPA2.2.1	···	NLO
Single Higgs boson						
ggF	POWHEG BOX V2	NNLO	PDF4LHC15NNLO	PYTHIA8.212	AZNLO [59]	$N^3LO(QCD) + NLO(EW)$
VBF	POWHEG BOX V2	NLO	PDF4LHC15NLO	PYTHIA8.212	AZNLO	$NNLO(QCD) + NLO(EW)$
$qq \to WH$	POWHEG BOX V2	NLO	PDF4LHC15NLO	PYTHIA8.212	AZNLO	$NNLO(QCD) + NLO(EW)$
$qq \to ZH$	POWHEG BOX V2	NLO	PDF4LHC15NLO	PYTHIA8.212	AZNLO	$NNLO(QCD) + NLO(EW)^\dagger$
$gg \to ZH$	POWHEG BOX V2	NLO	PDF4LHC15NLO	PYTHIA8.212	AZNLO	NLO + NLL
$t\bar{t}H$	POWHEG BOX V2	NLO	NNPDF3.0NLO	PYTHIA8.230	A14	$NLO(QCD) + NLO(EW)$

of the negative weight fraction. Using a sample generated with SHERPA2.2.11 instead of the sample generated with SHERPA2.2.1 that was used in Ref. [37] results in a reduction of the MC statistical uncertainty ranging from 30% to 60%, depending on the flavor composition of the events and the analysis region.

Diboson (WW, WZ and ZZ) and $t\bar{t}Z$ production processes are simulated with the 2.2.1 generator, whereas the $t\bar{t}W$ production process is simulated with the SHERPA2.2.8 generator. These samples use the NNPDF3.0NNLO PDF set with dedicated parton shower tuning developed by the SHERPA authors. Single Higgs boson production is considered as part of the background in this search, and its production modes are simulated using the POWHEG BOX V2 generator and either the PDF4LHC15NLO [58] with the AZNLO [59] tune or the NNPDF3.0NLO PDF sets with the A14 tune. The setup of the MC event generator for these production processes is unchanged with respect to Ref. [37].

Signal samples consist of simulated events from nonresonant ggF and VBF production of Higgs boson pairs, with one Higgs boson decaying into $b\bar{b}$ and the other one to $\tau^+\tau^-$. The simulated ggF events are generated with the POWHEG BOX V2 generator at NLO with finite top-quark mass, and using the PDF4LHC15NLO PDF set. The VBF events are generated at LO using the MADGRAPH5_AMC@NLO2.7.3 [60] generator with the NNPDF3.0NLO PDF set. Parton shower and hadronization are simulated using PYTHIA8.244 with the A14 tune and the NNPDF2.3LO PDF set. A reweighting technique based on the particle-level invariant mass m_{HH} of the Higgs boson pair is applied to the $\kappa_\lambda = 1$ sample to determine the ggF HH signal yield and kinematic distributions for any value of κ_λ [61]. The particle-level m_{HH} spectrum for any generic value of κ_λ is calculated from the m_{HH} distributions of three ggF HH samples generated for $\kappa_\lambda = 0$, 1 or 20. To determine the potential nonclosure in the reweighting process from residual kinematic effects, an additional ggF HH sample is generated with the same settings as the nominal sample but with the non-SM value of the self-coupling modifier $\kappa_\lambda = 10$, and then passed through detector simulation and reconstruction algorithms. The reweighting procedure is validated by comparing the predicted event yields and kinematic distributions of the simulated sample generated with $\kappa_\lambda = 1$ and reweighted to $\kappa_\lambda = 10$ with those of the simulated sample generated under the hypothesis $\kappa_\lambda = 10$. Furthermore, 12 additional VBF HH samples are generated and simulated with the same setup as the nominal VBF sample, but using non-SM combinations of the coupling modifiers κ_λ, κ_{2V} and κ_V. A basis for a linear combination is formed by the SM sample and five of the other 12 samples, corresponding to the combinations of the κ_λ, κ_{2V} and κ_V couplings (1, 1.5, 1), (0, 1, 1), (10, 1, 1), (1, 3, 1), (−5, 1, 0.5). This approach is used to determine the expected VBF HH yields and distributions for any value of κ_λ, κ_{2V} and κ_V. The remaining seven samples are compared to the corresponding predictions from the interpolation procedure for validation purposes. The same procedure was used in the measurements presented in Ref. [35]. For both the ggF and the VBF production mode, good closure between the simulated and reweighted samples for alternative κ_λ, κ_V and κ_{2V} values is observed within statistical uncertainties.

The Higgs boson mass is assumed to be 125 GeV in both the simulation and the analysis of the data. All samples are normalized to the same cross-section calculations detailed in Ref. [37]. The impacts of the differences with respect to the best-fit values of the m_H measurements reported in Refs. [19,20] and the effects of the corresponding experimental uncertainties on m_H, are negligible.

IV. EVENT SELECTION AND CATEGORIZATION

Events are selected in three separate signal regions (SRs), which remain unchanged with respect to Ref. [37]. The $\tau_{\text{had}}\tau_{\text{had}}$ signal region (SR) targets fully hadronic decay modes of the τ-lepton pair, where the presence of two oppositely charged hadronically decaying τ leptons (τ_{had}) is determined by detector signatures compatible with the expected visible decay products ($\tau_{\text{had-vis}}$). Two $\tau_{\text{lep}}\tau_{\text{had}}$ SRs target events with a leptonic decay of a τ lepton (τ_{lep}) into an electron or a muon, and an oppositely charged $\tau_{\text{had-vis}}$. The electron and muon channels are considered together. The decay channel with both τ leptons decaying leptonically is not studied in this paper but is instead covered in Ref. [62]. A control region (CR) is defined to constrain the background from Z bosons produced in association with two jets initiated by b or c quarks (referred to as Z + HF in the following), and top-quark pair production processes. In all regions the presence of two b-jets is also required. These four regions are briefly summarized in Sec. IV A. Selected events are split into different categories to enhance the sensitivity to the coupling modifiers κ_λ and κ_{2V}, as described in Sec. IV B. In each category a multivariate approach based on boosted decision trees (BDTs) is adopted to build the final discriminants, as detailed in Sec. IV C. The identification and reconstruction of electrons, muons, $\tau_{\text{had-vis}}$, jets from the hadronization of quarks and gluons, b-tagged jets, and missing transverse momentum ($\vec{p}_{\text{T}}^{\text{miss}}$) is identical to what was documented in Ref. [37].

A. Preselection

Events in the $\tau_{\text{had}}\tau_{\text{had}}$ SR are selected using a combination of single-$\tau_{\text{had-vis}}$ triggers (STTs) and di-$\tau_{\text{had-vis}}$ triggers (DTTs), and are required to have two $\tau_{\text{had-vis}}$ with opposite charge. An electron and muon veto is applied to ensure orthogonality with the $\tau_{\text{lep}}\tau_{\text{had}}$ SRs. In the $\tau_{\text{had}}\tau_{\text{had}}$ SR event selection, the offline[2] transverse momentum (p_{T}) thresholds for the $\tau_{\text{had-vis}}$ range between 100 GeV and 180 GeV

[2]In this paper, offline objects are those reconstructed after the data were collected, as opposed to trigger-level objects.

for STT events depending on the data-taking period, while they are set at 40 GeV (30 GeV) for the (sub-)leading $\tau_{\text{had-vis}}$ for DTT events. For events selected by the STTs a second $\tau_{\text{had-vis}}$-candidate is required, with an offline p_{T} threshold of 25 GeV. Additional offline requirements for the DTTs are that either one extra jet with an offline p_{T} threshold set to 80 GeV is in the event, and the $\tau_{\text{had-vis}}$ are reconstructed within $\Delta R = 2.5$ of each other, or that two extra jets with offline p_{T} thresholds set to 45 GeV are present in the event. For events that satisfy both the STTs and DTTs, the offline requirements used for the STTs are applied.

Events containing exactly an electron or muon and one $\tau_{\text{had-vis}}$ with opposite charge are split into two mutually exclusive SRs, depending on whether they satisfy a single-lepton trigger (SLT) or a lepton-plus-$\tau_{\text{had-vis}}$ trigger (LTT), named the $\tau_{\text{lep}}\tau_{\text{had}}$ SLT SR and the $\tau_{\text{lep}}\tau_{\text{had}}$ LTT SR, respectively. Only events failing the $\tau_{\text{lep}}\tau_{\text{had}}$ SLT SR selection are considered for the $\tau_{\text{lep}}\tau_{\text{had}}$ LTT SR. Depending on the data-taking period, the offline electron (muon) selected by the SLT is required to have $p_{\text{T}}^{e} > 25$ GeV or $p_{\text{T}}^{e} > 27$ GeV ($p_{\text{T}}^{\mu} > 21$ GeV or $p_{\text{T}}^{\mu} > 27$ GeV). Events selected in the $\tau_{\text{lep}}\tau_{\text{had}}$ LTT SR are required to contain either an electron or a muon with offline p_{T} thresholds set to $p_{\text{T}}^{e} > 18$ GeV and $p_{\text{T}}^{\mu} > 15$ GeV respectively, along with a $\tau_{\text{had-vis}}$ with an offline p_{T} threshold set to 30 GeV.

Events in all SRs are required to have $m_{\tau\tau}^{\text{MMC}} > 60$ GeV.[3] To target $H \to b\bar{b}$ decays, events are required to contain exactly two b-tagged jets in the pseudorapidity region of $|\eta| < 2.5$, satisfying the criteria of the "DL1r" b-tagging algorithm with a nominal efficiency of 77% for b jets [64]. The two selected b-tagged jets have to satisfy minimum p_{T} thresholds of 45 and 20 GeV respectively, in addition to any trigger-dependent requirements. In the $\tau_{\text{lep}}\tau_{\text{had}}$ SRs the invariant mass of the b-tagged jet pair (m_{bb}) is required to be lower than 150 GeV to reject background $t\bar{t}$ events, and a $\tau_{\text{had-vis}}$ with p_{T} of at least 20 GeV is required in the $\tau_{\text{lep}}\tau_{\text{had}}$ SLT SR, while $p_{\text{T}} > 30$ GeV is required in the $\tau_{\text{lep}}\tau_{\text{had}}$ LTT SR, in addition to any trigger-dependent requirements.

Events in the CR are required to contain exactly two electrons or two muons of opposite charge with a dilepton invariant mass ($m_{\ell\ell}$) within the range of 75 GeV $< m_{\ell\ell} <$ 110 GeV, and exactly two b-tagged jets. The m_{bb} is required to be less than 40 GeV or greater than 210 GeV to avoid overlap with other analyses targeting $H \to b\bar{b}$ decays. Compared with Ref. [37], the requirement on the transverse momentum of the selected leptons is raised to $p_{\text{T}} > 40$ GeV (from $p_{\text{T}} > 9$ GeV), while the leading b-tagged jet is required to have $p_{\text{T}} > 45$ GeV.

[3]The invariant mass of the τ-lepton pair ($m_{\tau\tau}^{\text{MMC}}$) is estimated by using the missing mass calculator (MMC) [63].

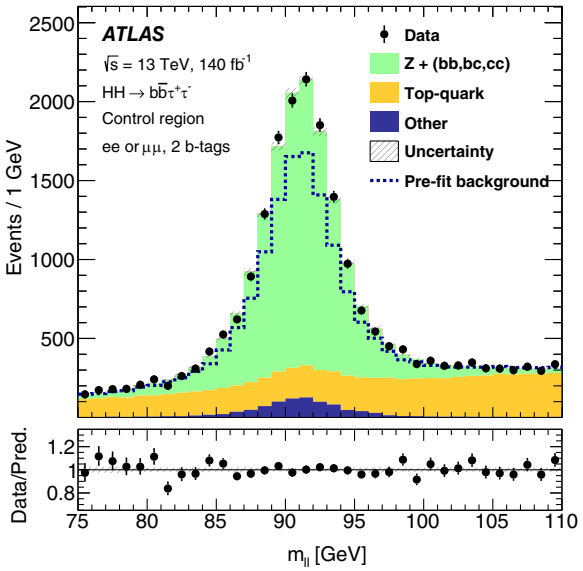

FIG. 3. Predicted and observed $m_{\ell\ell}$ distributions in the CR, with the normalization, shape and total uncertainty of the backgrounds as determined from the likelihood fit to data described in Sec. VI. The background processes named "Other" contain contributions from Z-boson production in association with less than two jets initiated by b or c quarks, W-boson production, vector boson pair production, $t\bar{t}W$ and $t\bar{t}Z$ production, and single Higgs boson production processes. The dashed histogram shows the total prefit background. The lower panel shows the ratio of data to the total postfit background. The hatched bands in the upper and lower panels show the combined statistical and systematic uncertainties in the total background.

This selection provides a closer alignment between the kinematic properties of events selected in the CR and the SRs. Figure 3 shows the predicted and observed $m_{\ell\ell}$ distributions in the CR, after the likelihood fit described in Sec. VI.

The main sources of background in the SRs after this preselection are from top-quark, $Z+$jets, $W+$jets, diboson, single Higgs boson and multijet production. Depending on the source, the background contamination is estimated by using data-driven or simulation-based techniques, or a combination of both. The normalizations of simulated $t\bar{t}$ and $Z+$HF backgrounds are determined from data in the likelihood fits of signal and control regions described in Sec. VI. A reconstructed $\tau_{\text{had-vis}}$ candidate in these background events can originate either from a τ_{had} decay (true-$\tau_{\text{had-vis}}$), or from a misidentified quark- or gluon-initiated jet (fake-$\tau_{\text{had-vis}}$). Events in which an electron or a muon is misidentified as a $\tau_{\text{had-vis}}$ represent a small additional background. The processes that contribute most to background events with fake-$\tau_{\text{had-vis}}$ candidate are $t\bar{t}$ and multijet production. In $t\bar{t}$ events, fake-$\tau_{\text{had-vis}}$ candidates typically originate from quark-initiated jets from the top-quark decay. In multijet events, both quark- and gluon-initiated jets are a source for fake-$\tau_{\text{had-vis}}$ candidates. Events

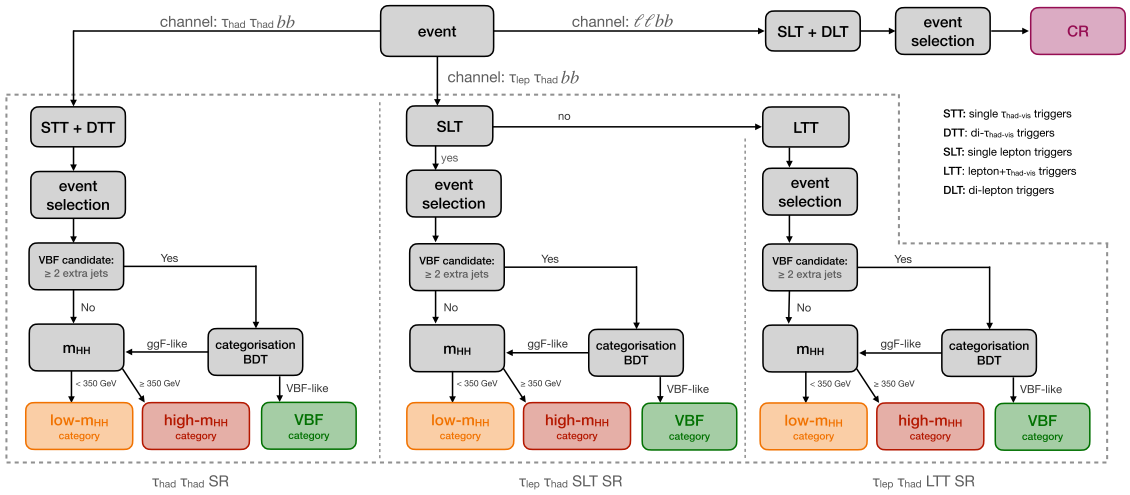

FIG. 4. Flowchart summarizing the definition of the $\tau_{\text{had}}\tau_{\text{had}}$ SR, the $\tau_{\text{lep}}\tau_{\text{had}}$ SLT SR, the $\tau_{\text{lep}}\tau_{\text{had}}$ LTT SR and the dedicated CR defined in Sec. IV. The flowchart shows the selection criteria applied to define the corresponding ggF low-m_{HH}, ggF high-m_{HH} and VBF categories for each analysis SR, leading to a total number of nine analysis categories and an additional CR.

with fake-$\tau_{\text{had-vis}}$ candidate in $t\bar{t}$ and multijet production are estimated from techniques relying on both simulated events and data, described in Ref. [37], which prove to provide an accurate modelling of the variables used for the event categorization and multivariate techniques described in this Section. The estimate of this background relies on a good description of the fundamental properties of τ leptons in the three analysis SRs, which are unchanged compared to Ref. [37]. In the $\tau_{\text{lep}}\tau_{\text{had}}$ regions a combined fake-factor method is used to estimate $t\bar{t}$ and multijet events with fake-$\tau_{\text{had-vis}}$, by employing two groups of regions: the identification (ID) regions containing one identified $\tau_{\text{had-vis}}$, and the anti-identification (anti-ID) regions containing one reconstructed $\tau_{\text{had-vis}}$ with modified requirements (anti-$\tau_{\text{had-vis}}$), leading to an enriched fake-$\tau_{\text{had-vis}}$ contribution. Fake factors are derived separately for $t\bar{t}$ and multijet events in dedicated ID and anti-ID control regions, and are combined to scale events from the anti-ID SRs to obtain the fake-$\tau_{\text{had-vis}}$ background prediction in the $\tau_{\text{lep}}\tau_{\text{had}}$ SRs. In the $\tau_{\text{had}}\tau_{\text{had}}$ regions two separate methods are used to estimate the backgrounds with fake-$\tau_{\text{had-vis}}$ from $t\bar{t}$ and multijet production. Multi-jet events can only enter the SRs when both $\tau_{\text{had-vis}}$ are fake, and their contribution is estimated by using a fake-factor method. Fake-factors are derived for the multijet background in a dedicated set of ID control regions, defined for events with two identified $\tau_{\text{had-vis}}$, and anti-ID control regions for events with one identified $\tau_{\text{had-vis}}$ and one anti-$\tau_{\text{had-vis}}$ candidate. The fake-factors are applied to scale events from the anti-ID SRs to obtain the multijet fake-$\tau_{\text{had-vis}}$ background prediction in the $\tau_{\text{had}}\tau_{\text{had}}$ SRs. Background events with fake-$\tau_{\text{had-vis}}$ from $t\bar{t}$ production in the $\tau_{\text{had}}\tau_{\text{had}}$ SRs are estimated using simulation, while correcting the fake-$\tau_{\text{had-vis}}$ misidentification efficiencies with scale factors derived from data in the $t\bar{t}$ control region defined for the fake-factor estimate in the $\tau_{\text{lep}}\tau_{\text{had}}$ channel. The modelling of events with a fake-$\tau_{\text{had-vis}}$ candidate from background processes other than $t\bar{t}$ and multijet production is performed using MC simulation, as they represent a minor contribution to the total background. Simulated event samples are used to model background events containing true-$\tau_{\text{had-vis}}$ and events with an electron or a muon misidentified as a $\tau_{\text{had-vis}}$ candidate. The changes introduced to the MC simulation detailed in Sec. III are found to have a negligible impact on the data-driven estimate of the background.

B. Event categorization

Events selected in each SR described in Sec. IV A are split into three separate categories. To enhance the sensitivity to the coupling modifier κ_{2V}, a dedicated VBF category is defined with a multivariate approach, defining a dedicated BDT to select events with characteristic features of VBF HH production, separately for each analysis SR. These are referred to as *categorization BDTs* in the following. The distribution of the invariant mass of the HH system (m_{HH}) in ggF HH events is significantly affected by the value of κ_λ. Hence, events not falling in the VBF category are split into two m_{HH} categories, targeting ggF HH production with κ_λ values close to the SM expectation (ggF high-m_{HH}) or significantly different from it (ggF low-m_{HH}). The three categories are mutually exclusive, and they are defined separately for each SR following the procedure outlined in Figure 4, leading to a total of nine event categories. First, VBF candidate events are identified by requiring the presence of at least two jets in addition to the ones associated with the $H \to b\bar{b}$ decay. These events are used to train the categorization BDTs to separate ggF and VBF HH production modes in event topologies with additional jets. Events

satisfying a SR-dependent selection on the output of these BDTs are assigned to the VBF category. Events failing the VBF selection are assigned to the ggF categories, together with events not selected as VBF candidates.

The categorization BDTs are built using the toolkit for multivariate data analysis (TMVA [65]) using ggF HH events as signal and VBF HH events as background, scaled such that the total event yield is the same for both processes. A dedicated version of the BDT is trained in each SR respectively. To make use of the complete set of simulated events for the BDT training, optimization and evaluation, the events are split into three samples of equal size, A, B and C. The performance of the BDTs trained on sample A (respectively B, C), is optimized using sample B (C, A) and evaluated with sample C (A, B), ensuring an unbiased estimate of the performance of the BDTs. The selected data events are split into three samples, each analysed with one of the three separately trained BDTs. The output distributions of the BDTs evaluated on samples A, B and C are merged for both simulated and data events to produce the final discriminant. The number of trees and their depth are chosen to maximise the BDT separation power, quantified by the value of the number-counting significance z [66] computed from the binned distribution of the BDT discriminant.

The minimal set of training variables that optimizes the BDT separation power is determined starting from a small set and iteratively adding variables one at a time from a predefined list of candidate variables. The variable leading to the largest increase (or minimal decrease[4]) in significance z is included, until no changes are observed. The starting set of variables comprizes the invariant mass of the VBF jets (m_{jj}^{VBF}), defined as the two jets with the highest p_{T} not associated with the $H \to b\bar{b}$ decay, and their pseudorapidity gap ($\Delta\eta_{jj}^{\mathrm{VBF}}$). The final set of variables for the categorization BDTs in each SR is summarized in Table II. It includes the product of VBF jet pseudorapidities (VBF $\eta_0 \times \eta_1$), their angular separations ($\Delta\phi_{jj}^{\mathrm{VBF}}$ and $\Delta R_{jj}^{\mathrm{VBF}}$) and m_{HH}. In addition, the Fox-Wolfram moments f_i of ith order [67] and their modified definitions for usage in hadron collider experiments h_i [68] can further increase the separation power, together with the centrality[5] (C) and the invariant mass (m_{Eff}) of the system composed by the selected τ leptons, the missing transverse momentum vector $\vec{p}_{\mathrm{T}}^{\,\mathrm{miss}}$ and the selected jets. The predicted and observed distributions of the resulting BDT scores are shown in Fig. 5 for all three SRs. VBF candidate events are assigned to the VBF category if their BDT score is evaluated below a certain threshold. The value of this threshold is optimized to achieve the best upper limits on HH production for ggF and VBF production modes separately and combined, along with the best exclusion limits for the coupling modifiers κ_λ and κ_{2V} from the likelihood fit described in Section VI. The categorization BDT cut values are set to 0.1, −0.13 and −0.1 for the $\tau_{\mathrm{had}}\tau_{\mathrm{had}}$, $\tau_{\mathrm{lep}}\tau_{\mathrm{had}}$ SLT and $\tau_{\mathrm{lep}}\tau_{\mathrm{had}}$ LTT SRs, respectively.

TABLE II. Input variables for the categorization BDTs in each of the three SRs. The superscripts a and c specify the selection of jets that are taken into account for the calculation in addition to the two τ-lepton candidates and the $\vec{p}_{\mathrm{T}}^{\,\mathrm{miss}}$ vector. For variables with a c, only the four-momenta of central jets, i.e., jets with $|\eta| < 2.5$, are included, while an a indicates that all available jets are included.

Variable	$\tau_{\mathrm{had}}\tau_{\mathrm{had}}$	$\tau_{\mathrm{lep}}\tau_{\mathrm{had}}$ SLT	$\tau_{\mathrm{lep}}\tau_{\mathrm{had}}$ LTT
m_{jj}^{VBF}	✓	✓	✓
$\Delta\eta_{jj}^{\mathrm{VBF}}$	✓	✓	✓
VBF $\eta_0 \times \eta_1$	✓	✓	
$\Delta\phi_{jj}^{\mathrm{VBF}}$	✓		
$\Delta R_{jj}^{\mathrm{VBF}}$		✓	✓
$\Delta R_{\tau\tau}$	✓		
m_{HH}	✓		
f_2^a	✓		
C^a		✓	✓
m_{Eff}^a		✓	✓
f_0^c		✓	
f_0^a			✓
h_3^a			✓

Events not retained in the VBF category are split into low-m_{HH} and high-m_{HH} categories targeting ggF HH production. While the ggF HH cross section increases for κ_λ values larger than the SM expectation and close to the current experimental sensitivity ($\kappa_\lambda \sim 6$ [35]), the softer m_{HH} spectrum leads to smaller detector acceptance and selection efficiency. The event split into different regions of m_{HH} allows to partially disentangle these effects, improving the sensitivity to higher κ_λ values. The splitting value is chosen to be 350 GeV since the effect of the interference between the box and triangle diagrams on the differential ggF HH production cross section is maximal there.

C. Multivariate discriminants

Based on the event categorization described in Sec. IV B, an additional set of multivariate discriminants making use of BDTs is trained and evaluated in each of the analysis SRs separately to achieve optimal separation between the HH signal and the background. One dedicated BDT is

[4]Variables showing minimal decrease of the z significance are retained to mitigate the impact of statistical fluctuations on the optimization, potentially leading to prematurely terminating the iterative procedure. In the final selection only variables improving the BDT sensitivity are retained.

[5]The centrality of a set of four-momenta of index i is defined as $C = \frac{\sum_i p_{\mathrm{T}}(i)}{\sum_i E(i)}$.

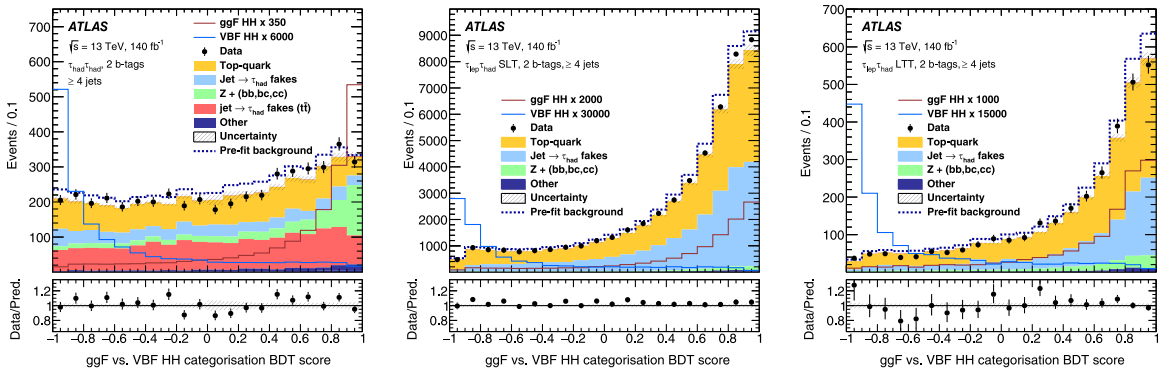

(a) (b) (c)

FIG. 5. Predicted and observed distributions of the categorization BDT scores in (a) the $\tau_{\text{had}}\tau_{\text{had}}$, (b) the $\tau_{\text{lep}}\tau_{\text{had}}$ SLT and (c) the $\tau_{\text{lep}}\tau_{\text{had}}$ LTT SRs, for all candidate VBF events. The background distributions are shown as obtained from the combined likelihood fit to data described in Sec. VI. The background processes named "Other" contain contributions from Z-boson production in association with less than two jets initiated by b or c quarks, W-boson production, vector boson pair production, $t\bar{t}W$ and $t\bar{t}Z$ production, and single Higgs boson production processes. The ggF and VBF HH signal distributions are overlaid and scaled to the factor indicated in the legend times the SM expectation. The dashed histogram shows the total prefit background. The lower panels show the ratio of data to the total postfit sum of signal and background. The hatched bands in the upper and lower panels show the combined statistical and systematic uncertainties in the total prediction.

trained for each analysis SR ($\tau_{\text{had}}\tau_{\text{had}}$, $\tau_{\text{lep}}\tau_{\text{had}}$ SLT, $\tau_{\text{lep}}\tau_{\text{had}}$ LTT) and each category (ggF low-m_{HH}, ggF high-m_{HH} and VBF), leading to nine separate BDTs. In the ggF high-m_{HH} and VBF categories, the signal corresponds to the ggF and VBF SM production of HH pairs, respectively. In the ggF low-m_{HH} category the signal is defined as ggF HH production with $\kappa_\lambda = 10$. During training, the sum of all backgrounds normalized to their respective cross sections is used, which is scaled such that the total background yield matches that of the corresponding signal sample. The backgrounds containing $\tau_{\text{had-vis}}$ from misidentified quark- or gluon-initiated jets are modeled using simulation, except for the multijet background in the $\tau_{\text{had}}\tau_{\text{had}}$ category, where the data-driven estimate introduced in Sec. IV A is used. The BDTs evaluated in the low-m_{HH} and high-m_{HH} categories are trained on the event samples selected in the respective categories. The BDTs evaluated in the VBF categories are trained on events from both the VBF and ggF categories to maximize the available sample size.

To make use of the complete set of simulated events for the BDT training, optimization and evaluation, the events are split into three samples, following the same procedure described in Sec. IV B. The number of trees and their depth are chosen to maximize the BDT separation power, quantified by the value of the signal significance z computed from the binned distribution of the BDT output.

The input variables used for the BDTs are chosen to maximize the BDT separation power, separately for each trained BDT. A list of variables is built for each BDT, ordered according to their impact on the signal significance z, following the same procedure as described in Sec. IV B. In each analysis SR and category the starting set comprises the following variables: the invariant mass of the two selected b-jets (m_{bb}), the invariant mass of the τ-lepton pair ($m_{\tau\tau}^{\text{MMC}}$), the m_{HH} reconstructed from the selected b-jet and τ-lepton pairs, the angular separation between b-jets (ΔR_{bb}) and between τ-leptons ($\Delta R_{\tau\tau}$). In the $\tau_{\text{lep}}\tau_{\text{had}}$ LTT high-m_{HH} category ΔR_{bb} is not included, and in the $\tau_{\text{lep}}\tau_{\text{had}}$ LTT VBF category both ΔR_{bb} and $\Delta R_{\tau\tau}$ are removed. The additional variables included in the BDT training through a z-based optimization as described in Sec. IV B can be grouped in several categories. Variables that require the presence of a charged lepton are not included for the $\tau_{\text{had}}\tau_{\text{had}}$ SR. Higgs boson candidates H are reconstructed from either b-jet or τ-lepton pairs. For the low-m_{HH} and high-m_{HH} categories, variables describing the kinematic properties of the selected b-jets and τ leptons are included: the transverse momentum of the leading and subleading b-jets and τ leptons, along with the pseudorapidity of the τ leptons and the transverse mass of each of the τ leptons and $\vec{p}_{\text{T}}^{\text{miss}}$. The angular separation between the (sub)leading b-jet and the (sub)leading τ lepton is included, along with the angular separation between the leading b-jet and the subleading τ lepton, the pseudorapidity separation and the transverse momentum difference between the selected τ-lepton candidate and the charged lepton. Variables related to the reconstructed H candidate topologies include: the azimuthal angular separation between the b-jet pair and the τ-lepton pair, and between either the b-jet or the τ-lepton pair and the magnitude $E_{\text{T}}^{\text{miss}}$ of $\vec{p}_{\text{T}}^{\text{miss}}$, the azimuthal angle of the selected b-jet (or τ-lepton) pair relative to the H candidate rest frame, along with the transverse momentum of the b-jet and τ-lepton pairs. The separation power is further increased by including variables

describing the hadronic activity in candidate events, such as the number of selected hadronic jets, the scalar sum of jet transverse momenta (H_{T}), the effective mass of the τ-lepton pair and all jets with $|\eta| < 2.5$, the $E_{\mathrm{T}}^{\mathrm{miss}}$, the stransverse mass [69] (M_{T2}), the azimuthal angular separation between the selected charged lepton and the $\vec{p}_{\mathrm{T}}^{\mathrm{miss}}$. Additional variables are included to characterize event properties, such as the transverse mass of the W boson candidate in the $\tau_{\mathrm{lep}}\tau_{\mathrm{had}}$ SRs (defined as the transverse mass of the selected lepton and the $\vec{p}_{\mathrm{T}}^{\mathrm{miss}}$), the topness variable [70] as defined in Ref. [71] assuming either $\sigma_t = 5$ GeV, $\sigma_W = 5$ GeV (T_1) or $\sigma_t = 15$ GeV, $\sigma_W = 5$ GeV (T_2), the reduced invariant mass of the HH system (defined as $m_{HH}{}^{*} = m_{HH} - m_{bb} - m_{\tau\tau}^{\mathrm{MMC}} + 250$ GeV), the scaled invariant mass of the HH system (defined by scaling the four-momenta of both H candidates by the ratio $125\ \mathrm{GeV}/m_H$, where m_H is the H candidate invariant mass), the transverse momentum of the reconstructed HH system and the effective mass of the HH decay products. To construct the $E_{\mathrm{T}}^{\mathrm{miss}}$ centrality, the transverse plane is transformed such that the directions of the $\tau_{\text{had-vis}}$ candidates or leptons are orthogonal, and that the smaller ϕ angle between them defines the positive quadrant of the transformed plane. Then the $E_{\mathrm{T}}^{\mathrm{miss}}$ centrality is defined as the sum of the x and y components of the $\vec{p}_{\mathrm{T}}^{\mathrm{miss}}$ unit vector in this transformed plane. Dedicated variables describing characteristic event configurations are included via a selection of Fox-Wolfram moments (as defined in Sec. IV B), circularity, sphericity, thrust and planar flow variables reconstructed from the HH decay products. Finally, the b-tagging information is provided by the quantile distribution of the DL1r tagger output for the selected b-jets, which is included as a training variable. For the VBF categories the first five variables listed in Table II are also included, along with circularity, sphericity and planar flow variables reconstructed from the τ-lepton pair and all selected jets, to target the specific features of VBF HH events.

V. SYSTEMATIC UNCERTAINTIES

While the largest source of uncertainty in this analysis comes from the limited number of data events, systematic uncertainties can affect the signal and background estimates. Uncertainties originating from the detector response in the selection and reconstruction of the used objects are included as documented in Ref. [37]. Statistical uncertainties in the predicted background processes are modeled using a simplified version of the Beeston-Barlow technique [72], in which only the uncertainty in the total background contribution in each bin is considered. An uncertainty in the full Run 2 integrated luminosity of 0.83% [42], from measurements using the LUCID-2 [43] detector and a complementary measurement using the inner detector and calorimeters, is assigned to physics processes whose normalizations are taken from simulation.

For all processes whose estimation relies on MC simulation, the impact of various sources of theoretical uncertainties in their cross section, on the fractional contribution to each analysis category within each SR, as well as on the shape of the BDTs introduced in Sec. IV C is considered. The total normalization of $t\bar{t}$ and $Z + \mathrm{HF}$ backgrounds is determined via the likelihood fit described in Sec. VI; therefore, no uncertainty is included for their cross-section calculation. For $t\bar{t}$ and $Z + \mathrm{HF}$ backgrounds, the uncertainty in the fractional contribution in each analysis category is computed as the relative variation in acceptance with respect to the dedicated CR introduced in Sec. IV, while for other processes this is evaluated as the absolute acceptance variation in each analysis category. To assess an uncertainty in the shape of the BDT output, a dedicated rebinning algorithm is applied to ensure that only statistically significant shape variations are considered. In the signal-enriched region of the BDT distribution, the statistical uncertainty of each bin is required to be below a process- and variation-dependent threshold (ranging from 5% to 15%), while in the background-enriched region of the distribution the fraction of total events per bin is required to be larger than 5%. For each process, the impact of each source of uncertainty in the fractional contribution in each analysis category is correlated with the uncertainty in the shape of the BDT score in the corresponding category, in the likelihood fit described in Section VI. All sources of uncertainty are evaluated separately and correlated across the three analysis SRs. The uncertainties in the SM cross-section calculations for all processes are unchanged with respect to Ref. [37], along with the full uncertainty estimate for smaller background processes including Z+light-flavor jets, $W +$ jets, diboson and single-top-quark production in the $s-$ and $t-$channels.

The $t\bar{t}$ hard-scatter and parton-shower uncertainties are evaluated by comparing the nominal sample with samples generated using MADGRAPH5_AMC@NLO+PYTHIA8 and POWHEG BOX V2+HERWIG7.04 [73,74], respectively. The hard-scatter uncertainty also accounts for uncertainties in the matching and merging of the matrix-element calculation with the parton-shower algorithm. The uncertainty in missing higher-order QCD corrections and the modeling of initial-state QCD radiation is assessed via independent variations of the renormalization and factorization scales in the hard-scatter calculation, of the showering tune VAR3C parameter [49] and of the h_{damp}[6] parameter, while for the modeling of final state QCD radiation alternative choices of factorization and renormalization scales in the showering

[6]The h_{damp} parameter regulates the p_{T} of the first additional emission beyond the Born configuration in the POWHEG BOX generator, controlling the matching of the matrix element to the parton shower.

algorithm are considered. Finally, uncertainties in the PDF and the value of the strong coupling constant α_S are also evaluated. All sources of uncertainty have an impact on the shape of the BDT score and the $t\bar{t}$ fractional contribution in each analysis category. The largest effect on the latter is due to parton-shower variations and ranges between 1% and 10% of the nominal values, depending on the analysis category and SR.

For Z + HF processes the uncertainty in the modelling of the hard scatter and the parton shower are evaluated by comparing the nominal sample with a MADGRAPH5_AMC@NLO+PYTHIA8 sample with up to three additional partons in the final state at NLO accuracy in the QCD coupling, in which additional jet multiplicities are merged together with the FxFx NLO matrix-element and parton-shower merging prescription [75]. The A14 parton-shower tune and the NNPDF2.3LO PDF set are used for this alternative sample. Uncertainties from missing higher-order QCD corrections are evaluated with renormalization and factorization scale variations from the nominal samples, along with PDF and α_S variations. The effect of higher-order electroweak corrections for Z + HF processes is found to be negligible, and thus not included. Uncertainties in the matching between matrix element calculation and parton shower are considered via variations of the SHERPA matching parameter (CKKW) and the resummation scale (QSF). All sources of uncertainty have an impact on the Z + HF fractional contribution in each analysis category, with the largest effect due to renormalization and factorization scale variations ranging up to 13% of the nominal values depending on the analysis category and SR. The uncertainty in the modelling of the hard scatter and the parton shower, from the comparison with the alternative MADGRAPH5_AMC@NLO+PYTHIA8, is the only source of uncertainty with a significant impact on the shape of the BDT score in the analysis SRs. The same source of uncertainty is found to have a non-negligible impact on the shape of the $m_{\ell\ell}$ variable in the CR, which is included as a dedicated uncertainty uncorrelated from the BDT score shape uncertainty in the likelihood fit. Finally, an additional systematic uncertainty is included to cover the residual difference between data and MC simulation in the dedicated CR, as a function of the transverse momentum of the selected lepton pair. This uncertainty is applied in all analysis SRs as a function of the transverse momentum of the τ-lepton pair selected from the MC truth record.

For single-top-quark processes only uncertainties related to the Wt−channel are considered, as it is found to be dominant compared with s− and t− channel contributions. The hard-scatter and the parton-shower uncertainties are evaluated by comparing the nominal sample with alternative MADGRAPH5_AMC@NLO+PYTHIA8 and POWHEG BOX V2+HERWIG7 samples. The uncertainty in the modelling of QCD radiation is evaluated by varying the showering tune VAR3C, along with independent variations of the renormalization and factorization scales in the hard-scatter and parton-shower calculations. The uncertainty related to the interference between the $t\bar{t}$ and the Wt−channel single-top-quark processes is evaluated by comparing the nominal Wt-channel sample produced with the diagram removal scheme to an alternative sample produced with the diagram subtraction scheme [76]. Finally, uncertainties in the PDF are also evaluated. All sources of uncertainty have an impact on the Wt−channel single-top-quark fractional contribution in each analysis category. Variations due to the uncertainty in the Wt−channel interference scheme range from 1% to 7% in the low-m_{HH} categories, from 23% to 29% in the high-m_{HH} categories and from 14% to 34% in VBF categories. Uncertainties in the Wt−channel interference scheme are also evaluated on the shape of the BDT score, rather than on the p_{T} of the b-tagged jet pair as in Ref. [37]. The hard-scatter and parton-shower uncertainties range from 15% to 36% on the Wt−channel fractional contribution, depending on the analysis category and SR. Uncertainties in the modeling of QCD radiation are found to have a significant impact on the shape of the BDT score.

An uncertainty of 100% is applied on the normalization of single Higgs boson in the ggF, VBF and associated production WH mechanisms where the Higgs boson decays into a τ-lepton pair, to account for difficulties in the modelling of these processes in association with heavy-flavor jets [77,78]. Uncertainties from missing higher-order QCD corrections are evaluated with independent variations of the renormalization and factorization scales from the nominal samples, along with PDF and α_S variations. Parton-shower uncertainties are evaluated by comparing the nominal sample to alternative POWHEG BOX V2+HERWIG7 samples for associated production ZH and $t\bar{t}H$ processes. For $t\bar{t}H$ processes the hard-scatter uncertainties are derived by comparing the nominal samples to MADGRAPH5_AMC@NLO+PYTHIA8 predictions, and uncertainties in the modelling of QCD radiation are assessed via variations of the showering tune VAR3C, along with independent variations of the renormalization and factorization scales in the parton-shower algorithm. All sources of uncertainty have an impact on the single-Higgs-boson fractional contribution in each analysis category, while only parton-shower uncertainties are included as variations of the BDT score for the ZH and $t\bar{t}H$ processes.

For the SM ggF and VBF HH signal processes, uncertainties from missing higher-order QCD corrections are assessed via independent variations of the renormalization and factorization scales in the hard-scatter calculation, along with PDF and α_S variations. Parton-shower uncertainties are evaluated by comparing the nominal samples with alternative POWHEG BOX V2+HERWIG7 samples. All sources of uncertainty have an impact on the signal fractional contribution in each analysis category, while only parton-shower uncertainties are included as variations of the BDT score. Cross-section uncertainties for

single-Higgs-boson and HH processes [29] follow the same approach detailed in Ref. [37], along with uncertainties in the $H \to b\bar{b}$ and $H \to \tau^+\tau^-$ branching ratios [79].

A dedicated uncertainty in the reweighting method applied to the ggF HH samples to model alternative κ_λ hypotheses, described in Sec. III, is defined via a comparison of the SM ggF HH samples with an alternative sample generated assuming $\kappa_\lambda = 10$. The SM sample and the $\kappa_\lambda = 10$ sample are reweighted to a wide range of κ_λ values and the acceptance values of both predictions are compared independently in each category. The maximum of the obtained deviations is taken as an uncertainty and applied to the $\kappa_\lambda = 0$ and $\kappa_\lambda = 20$ templates used for the linear combination of signal samples in the fit. These deviations range from 2% to 4% in the ggF categories and from 20% to 40% in the VBF categories. The uncertainty in the VBF categories arises from the m_{HH}-based reweighting method not accounting for additional radiation produced with the HH pair, to which the categorization BDTs are highly sensitive. The linear combination of VBF HH samples described in Sec. III is found to accurately model alternative κ_λ and κ_{2V} hypothesis; therefore, no dedicated uncertainty is considered.

The estimate of systematic uncertainties affecting the data-driven background follows the approach described in Ref. [37]. Uncertainties in the fractional contribution of the data-driven background and on the shape of the BDT score are derived in all the analysis SRs and categories.

VI. RESULTS

The statistical procedures applied for extracting results are the same as in Refs. [35,37]. The global likelihood function $L(\alpha, \theta)$ is constructed from the binned distribution of the BDT output score for signal, background and data distributions in the nine orthogonal analysis categories described in Sec. IV, together with the $m_{\ell\ell}$ distribution in the dedicated CR. The set α contains the parameters of interest (POI) of the measurement, while θ is the ensemble of nuisance parameters, corresponding to systematic uncertainties constrained by auxiliary measurements in control regions or by theoretical predictions, or to parameters such as the $t\bar{t}$ and Z + HF background yields, which are *a priori* unconstrained.

A dedicated procedure is applied to transform the BDT discriminant to obtain a smoother distribution for the background processes and a finer binning in the regions with the largest signal contribution, while preserving a sufficiently large number of background events in each bin, similarly to Ref. [37]. Starting from finely binned histograms, bins are iteratively merged starting from the most signal-enriched bins until they satisfy the condition of $10f_s + 5f_b > 1$, where f_s and f_b are the fractions of signal and background contained in the bin, respectively. The relative statistical uncertainty in the predicted background contribution has to be below 20%, and at least three expected background events are required per bin. The $m_{\ell\ell}$ distribution in the CR is binned uniformly with a width of 1 GeV.

The constraints on the coupling modifiers are determined using a profile likelihood ratio $\Lambda(\alpha, \theta)$ as the test statistic, computed from the likelihood function in the asymptotic approximation [66], where the POI α are the coupling modifiers κ. The procedure adopted in Ref. [35] is used to set constraints on κ_λ and κ_{2V}, expressed as 68% and 95% CIs. Signal strength upper limits are derived using the CL_s method [80] with the procedure described in Ref. [37]. Upper limits are set on the overall μ_{HH} and on the separate signal strength parameters $\mu_{\text{ggF}} = \sigma_{\text{ggF}}/\sigma^{\text{SM}}_{\text{ggF}}$ and $\mu_{\text{VBF}} = \sigma_{\text{VBF}}/\sigma^{\text{SM}}_{\text{VBF}}$. The expected results are obtained with Asimov datasets [66] generated from the likelihood function after setting all nuisance parameters to their maximum-likelihood estimate in the fit to the data and fixing the POIs to the values corresponding to the hypothesis under test. The asymptotic results are found to agree within 7% with the upper limits obtained using pseudoexperiments. Figure 6 shows the BDT score distribution in the nine orthogonal categories, after performing the maximum-likelihood fit to data for the $L(\mu_{HH}, \theta)$ function. Good agreement between the data and the prediction is found within the assessed uncertainties.

The maximum-likelihood estimator for the total HH production signal strength is found to be $\hat{\mu}_{HH} = 2.2 \pm 1.7$ by the combined fit to data. The uncertainty in the fitted signal strength is obtained from the variation of log-likelihood-based test statistic Λ by one unit, and includes both statistical and systematic uncertainties. The maximum-likelihood estimator for the unconstrained normalization factor of the $t\bar{t}$ and Z + HF backgrounds are measured at 0.96 ± 0.03 and 1.34 ± 0.08, respectively, by the combined fit to data. An observed 95% CL upper limit of 5.9 is set on μ_{HH}, to be compared with an expected limit of 3.3 in the background-only hypothesis ($\mu_{HH} = 0$), corresponding to an observed (expected) significance with respect to the background-only hypothesis of $1.4(0.75)\sigma$. From the simultaneous fit of μ_{ggF} and μ_{VBF}, observed (expected) 95% CL upper limits are $\mu_{\text{ggF}} < 5.8(3.4)$ and $\mu_{\text{VBF}} < 91(73)$, respectively, for each production mode, assuming that the signal strength parameters can vary independently for each production mode. If μ_{VBF} is fixed to the SM prediction, the observed (expected) 95% CL upper limit is $\mu_{\text{ggF}} < 5.9(3.4)$. Similarly, if μ_{ggF} is fixed to the SM prediction, the observed (expected) 95% upper limit is $\mu_{\text{VBF}} < 93(72)$.

Expected upper limits for the separate production mode signal strengths are derived with respect to the background-only hypothesis. The signal strength upper limits are summarized in Table III and Fig. 7, in each SR individually along with the combined fit. The results for the individual SRs are obtained from the combined likelihood fit of the BDT score distributions in the categories of a single SR

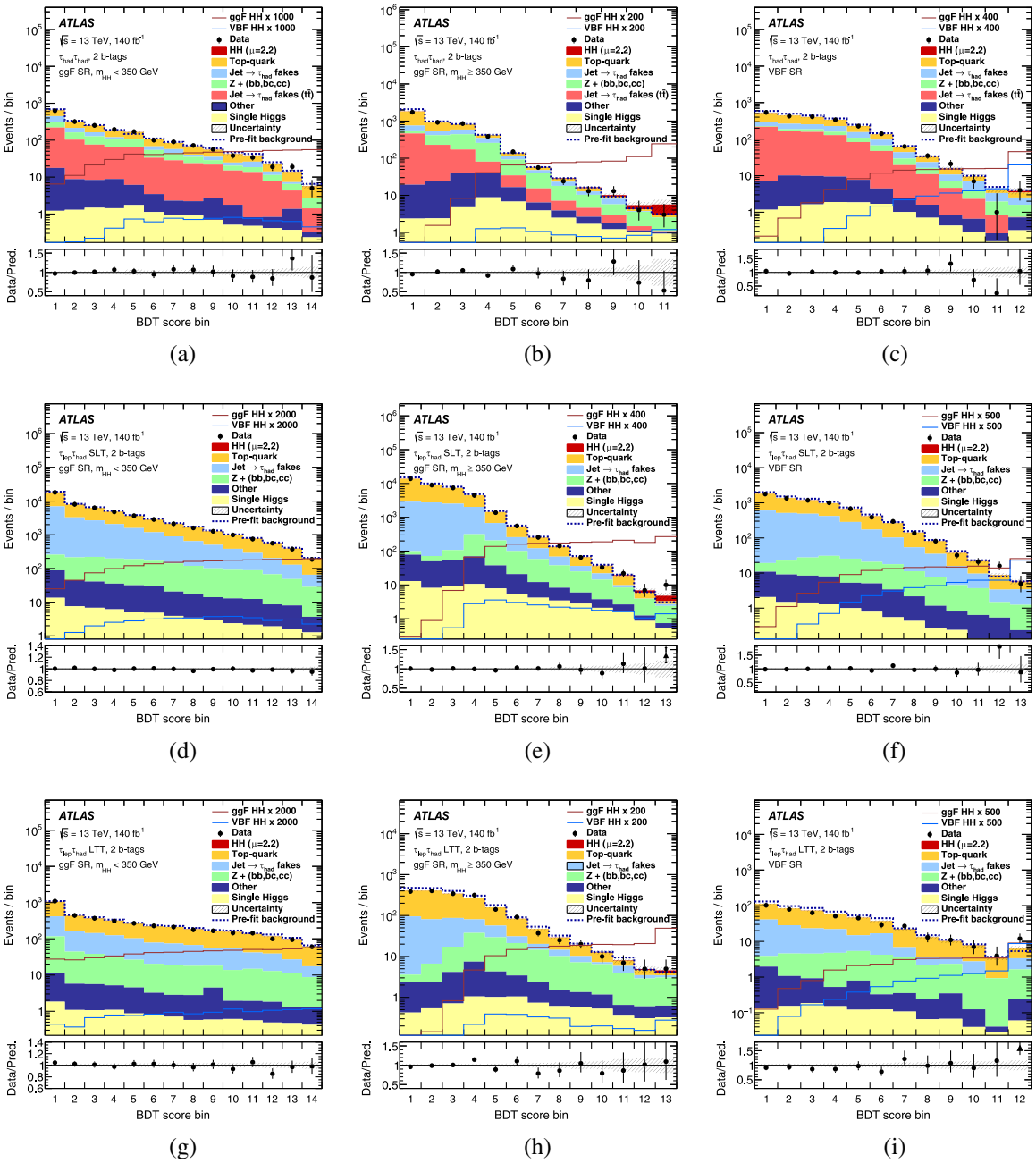

FIG. 6. Predicted and observed distribution of the BDT score in (left) the low-m_{HH}, (middle column) the high-m_{HH} and (right) the VBF categories of (top) the $\tau_{\text{had}}\tau_{\text{had}}$, (middle row) the $\tau_{\text{lep}}\tau_{\text{had}}$ SLT and (bottom) the $\tau_{\text{lep}}\tau_{\text{had}}$ LTT SRs. The signal and background distributions are shown at postfit level as obtained from the combined likelihood fit to data described in Section VI. The background processes named "Other" contain contributions from Z-boson production in association with less than two jets initiated by b or c quarks, W-boson production, vector boson pair production, $t\bar{t}W$ and $t\bar{t}Z$ production processes. The "HH" signal contribution is scaled to the fitted signal strength μ_{HH} from the combined likelihood fit times the SM expectation. The ggF and VBF HH signal distributions are overlaid and scaled to the factor indicated in the legend times the SM expectation. The dashed histograms show the total prefit background. The lower panels show the ratio of data to the total postfit sum of signal and background, where the hatched bands show the statistical and systematic uncertainties of this prediction. The BDT score distributions are shown with the binning used in the likelihood fit. For visualization purposes each bin is displayed with uniform width and an index labeling it.

with the $m_{\ell\ell}$ distribution from the dedicated CR. The observed limit on μ_{HH} from the combined fit is looser than the expected one as a result of an excess in the $\tau_{\text{lep}}\tau_{\text{had}}$ SLT SR, in the high-m_{HH} category. This excess corresponds to a local significance of 2.3σ with respect to the SM hypothesis ($\mu_{HH} = 1$), and a local significance of 2.7σ with respect to

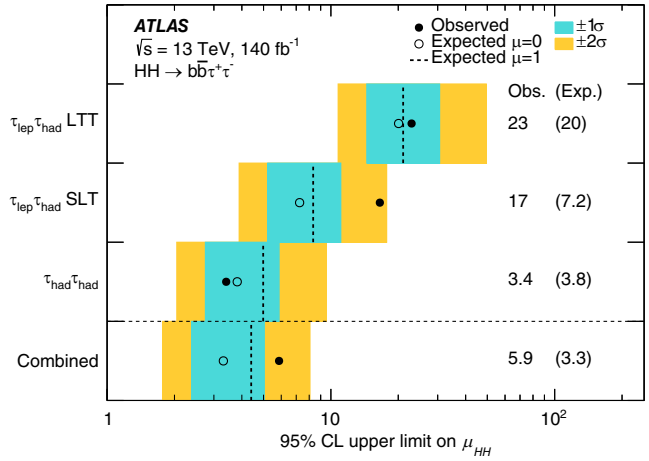

FIG. 7. Summary of observed (filled circles) and expected (open circles) 95% CL upper limits on μ_{HH} from the fit of each individual channel and the combined fit in the background-only ($\mu_{HH} = 0$) hypothesis. The dashed lines indicate the expected 95% CL upper limits on μ_{HH} in the SM hypothesis ($\mu_{HH} = 1$). The inner and outer bands indicate the $\pm 1\sigma$ and $\pm 2\sigma$ variations, respectively, on the expected limit with respect to the background-only hypothesis due to statistical and systematic uncertainties.

the background-only hypothesis, as obtained from the individual fit of the $\tau_{\text{lep}}\tau_{\text{had}}$ SLT SR.

The observed and expected values of $-2\ln\Lambda$ as a function of the coupling modifiers κ_λ and κ_{2V} are shown in Fig. 8, under the hypothesis that all other coupling modifiers are equal to their SM predictions. The combined fit allows to set observed (expected) 95% CIs of $\kappa_\lambda \in [-3.1, 9.0]([-2.5, 9.3])$ (assuming $\kappa_{2V} = 1$) and $\kappa_{2V} \in [-0.5, 2.7]([-0.2, 2.4])$ (assuming $\kappa_\lambda = 1$). Additional constraints are set on κ_λ and κ_{2V} assuming that both coupling modifiers can vary simultaneously. The resulting observed and expected two-dimensional 68% and 95% contours are shown in Fig. 9. The observed and expected constraints on κ_λ reported in this paper are affected by the issue concerning the ggF HH prediction for BSM scenarios in POWHEG reported in the erratum of Ref. [81] and do not include the changes to resolve this issue described in Ref. [82]. If the ggF HH signal yields in the analysis categories are scaled based on the ratio of the predicted differential ggF HH cross sections with and without the changes described in Ref. [82], the width of the 95% CI on κ_λ changes by less than 5%.

As in Ref. [37], the analysis sensitivity is primarily limited by the statistical uncertainty of the data. The leading systematic uncertainty in the measurement of μ_{HH} is the uncertainty in the ggF HH production cross section arising from variations of the QCD scales and the top-quark mass scheme. The next leading sources of uncertainty are the statistical precision of the background MC samples and the uncertainty related to the interference between the Wt and $t\bar{t}$ processes. The combined impact of all sources of systematic uncertainties leads to an increase in the expected upper limits on the signal strength μ_{HH} by 23% and to a widening of the expected 95% CI for κ_λ and κ_{2V} by 9% and 2%, respectively, with respect to the case in which systematic uncertainties are neglected (excluding the $t\bar{t}$ and $Z + \text{HF}$ floating normalization and MC statistical uncertainties).

Based on a consistent statistical procedure for evaluating the 95% CIs and upper limits as described at the beginning of this section, these results can be compared with the previous analysis of Ref. [37]. The approach presented in this paper leads to an increase (reduction) of the observed (expected) upper limit on the signal strength μ_{HH} by 25% (15%), along with new results for the upper limits on the separate ggF and VBF HH production mode signal strengths. The width of the observed (expected) CI for κ_λ is reduced by $< 1\%$ (11%) and the width of the observed (expected) CI for κ_{2V} is reduced by 2% (19%) compared with the previous analysis.

The compatibility, considering statistical and systematic uncertainties, between the upper limit at 95% CL on the signal strength μ_{HH} from this study and that of Ref. [37] is evaluated using a bootstrap technique [83] separately for the independent SR fits and for the combined fit.

TABLE III. Observed and expected 95% CL upper limits on μ_{HH}, μ_{ggF} and μ_{VBF} from the individual SR likelihood fits as well as the combined results. The μ_{ggF} and μ_{VBF} limits are quoted both from the results of the simultaneous fit of both signal strengths (central column), and from independent fits for the individual production modes, assuming the other to be as predicted by the SM. The uncertainties quoted on the combined expected upper limits correspond to the 1σ uncertainty band.

		μ_{HH}	μ_{ggF}	μ_{VBF}	μ_{ggF} ($\mu_{\text{VBF}} = 1$)	μ_{VBF} ($\mu_{\text{ggF}} = 1$)
$\tau_{\text{had}}\tau_{\text{had}}$	Observed	3.4	3.6	87	3.5	80
	Expected	3.8	3.9	102	3.9	99
$\tau_{\text{lep}}\tau_{\text{had}}$ SLT	Observed	17	17	136	17	158
	Expected	7.2	7.4	129	7.4	127
$\tau_{\text{lep}}\tau_{\text{had}}$ LTT	Observed	23	18	765	22	733
	Expected	20	21	359	20	350
Combined	Observed	5.9	5.8	91	5.9	93
	Expected	$3.3^{+1.7}_{-0.9}$	$3.4^{+1.8}_{-1.0}$	73^{+32}_{-21}	$3.4^{+1.8}_{-0.9}$	72^{+32}_{-20}

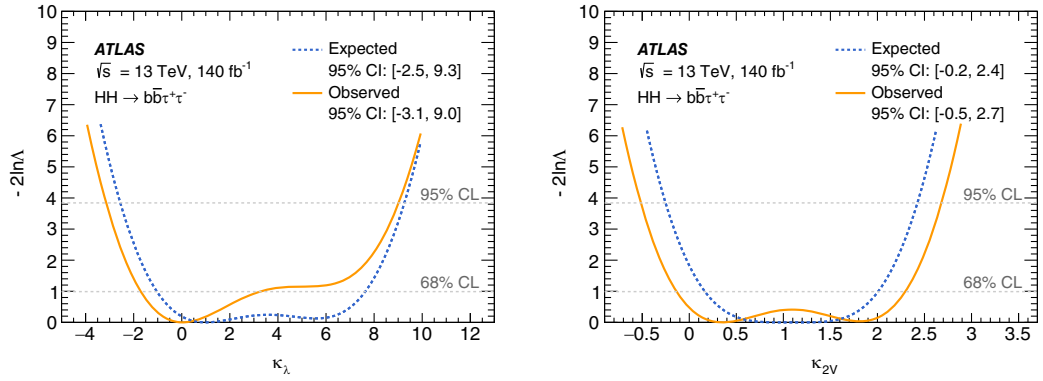

FIG. 8. Values of $-2\ln\Lambda$ for different (a) κ_λ and (b) κ_{2V} hypotheses obtained from fits to the data (solid orange) and an Asimov dataset (dashed blue) constructed under the SM hypothesis. In each case, all coupling modifiers but the scanned parameter are fixed to their SM values.

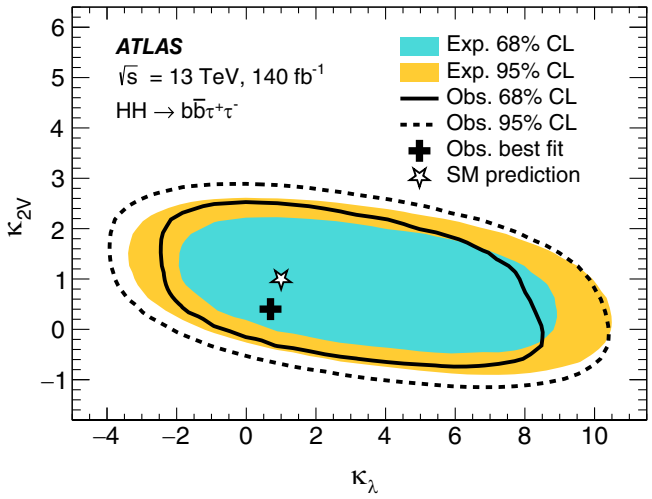

FIG. 9. Likelihood contours at 68% (solid line) and 95% (dashed line) CL in the (κ_λ, κ_{2V}) parameter space, when all other coupling modifiers are fixed to one. The corresponding expected contours are shown by the inner and outer shaded regions. The SM prediction is indicated by the star, while the best-fit value is denoted by the black cross.

The compatibility between the two results is at the level of 1σ for the individual fit of the $\tau_{\text{had}}\tau_{\text{had}}$ SR, of 2.5σ for the individual fit of the $\tau_{\text{lep}}\tau_{\text{had}}$ SLT SR, and of 0.1σ for the individual fit of the $\tau_{\text{lep}}\tau_{\text{had}}$ LTT SR. The compatibility is at the level of 0.8σ for the combined fit.

VII. EFFECTIVE FIELD THEORY INTERPRETATION

Effective field theory approaches can be employed to parametrize effects of new particles and anomalous couplings on the HH production rates and Higgs boson decay rates, assuming that the energy scale of the underlying BSM processes is far too high to be probed directly. Interpretations of the results in the context of the Higgs effective field theory (HEFT) and SM effective field theory (SMEFT) are presented in this section, following closely the procedure in Refs. [38,84].

The SMEFT interpretation is based on the effective Lagrangian

$$\mathcal{L}_{\text{SMEFT}} = \mathcal{L}_{\text{SM}} + \frac{1}{\Lambda_{\text{EFT}}^2}\sum_k c_k^{(6)} O_k^{(6)},$$

where $\mathcal{L}_{\text{SM}}$ is the SM Lagrangian and Λ_{EFT} is the energy scale of the new physics phenomena, which is set to 1 TeV. The $c_k^{(6)}$ are the Wilson coefficients corresponding to an operator $O_k^{(6)}$ of mass dimension 6. The Warsaw basis [85] is chosen for the dimension-6 operators, and constraints are placed on the Wilson coefficients c_H and $c_{H\Box}$. They correspond to the operators $(\phi^\dagger\phi)^3$ and $(\phi^\dagger\phi)\Box(\phi^\dagger\phi)$, respectively. While the VBF HH contribution is affected by variations of c_H and $c_{H\Box}$, the SMEFT preserves the Higgs doublet structure of the SM, which implies cancellations between the LO diagrams Figs. 2(a) and 2(c). Therefore, the change in the expected VBF HH contribution is small, and the process is ignored for the SMEFT interpretations, as it is dominated by the ggF HH contribution in all considered coupling scenarios.

For the HEFT interpretation, two studies are conducted. First, cross-section limits are placed on the seven m_{HH} shape benchmark scenarios defined in Ref. [86]. As described in Ref. [87], these benchmark scenarios have been determined using a clustering algorithm that identifies distinct shapes of the m_{HH} spectrum that can be obtained by varying five Wilson coefficients in the HEFT framework. In addition to the study of these benchmark scenarios, the Wilson coefficients c_{tthh} and c_{gghh} are considered, which quantify the strengths of the effective $t\bar{t}HH$ and $ggHH$ couplings, respectively. The Wilson coefficient of the only considered anomalous coupling that affects VBF HH

production at NLO precision is c_{hhh}, which is equivalent to κ_λ. Due to the much smaller overall expected yield compared with ggF HH production, and the decorrelation of the two production modes through the event categorization, the impact of VBF HH contribution on the m_{HH} shape benchmark limits is expected to be negligible, even when taking c_{hhh} variations into account. Hence, it is ignored in the following, i.e., μ_{VBF} is set to 0.

Signal predictions for ggF HH production assuming different effective coupling strengths are obtained from the SM sample. For this purpose, a reweighting method is used that assigns each event a weight corresponding to the ratio of the differential NLO cross section (in m_{HH}) predicted by the SM and the hypothesis of interest. These weights are taken from Ref. [86]. Possible effects of the anomalous couplings on the Higgs boson branching fractions are neglected. The SMEFT coefficients can also affect single Higgs boson processes. To take these effects on production cross sections and branching fractions into account, the procedure in Ref. [88] is adopted.

For a continuous parametrization of the effect of the Wilson coefficients on the predicted ggF HH distributions, the linear combination method described in Ref. [61] is applied to the ggF HH cross section dependence on the respective Wilson coefficients. The basis samples for the Wilson coefficients are chosen to be close to the 95% CL limits in order to reduce the effect of large cancellations between the basis samples on the obtained results. The values of the couplings $(c_{gghh}, c_{tthh}, c_{hhh})$ that define the ten samples making up the basis for measuring the HEFT Wilson coefficients are (0, 0, 1), $(-0.3, 0, 1)$, (0.4, 0,1), $(0, -0.2, 1)$, $(0, 0.7, 1)$, $(0, 0, -2.5)$, $(0, 0, 9)$, $(0.4, 0, -2.5)$, $(0, 1, -10)$, $(0.4, -0.2, 1)$. The six values of $(c_H, c_{H\Box})$ used for the SMEFT interpretation are (0, 0), $(-17, 0)$, (7, 0), $(0, -7)$, (0, 13), $(7, -7)$.

Uncertainties on the ggF HH event yield from the reweighting procedure are derived using comparisons to alternative MC samples generated with different assumed coupling values. They are produced for the seven HEFT m_{HH} shape benchmarks and for $c_{gghh/tthh} \in \{-0.5, 0.5, 1\}$ using POWHEG BOX V2 interfaced with PYTHIA8.244 for parton showering and hadronization. The uncertainty assessment for variations in c_H is based on the LO relation $\kappa_\lambda = 1 - 2\frac{v^4}{m_H^2 \Lambda_{\mathrm{EFT}}^2} c_H + 3\frac{v^2}{\Lambda_{\mathrm{EFT}}^2}(c_{H\Box} - \frac{1}{4} c_{HD})$ [86], which allows for a comparison to a $\kappa_\lambda = 10$ sample. Here, c_{HD} is the Wilson coefficient corresponding to the dimension-6 operator $(\phi^\dagger D_\mu \phi)^*(\phi^\dagger D^\mu \phi)$. For $c_{H\Box}$, alternative samples with $c_{H\Box} \in \{-9.5, 7\}$ are used. Additionally, the signal modeling uncertainties are evaluated for each signal configuration, as described in Sec. V. For scans of Wilson coefficients, the modeling uncertainties are computed for all signal configurations used in the linear combination approach. The maximal obtained deviation is taken as the final value for each source of uncertainty.

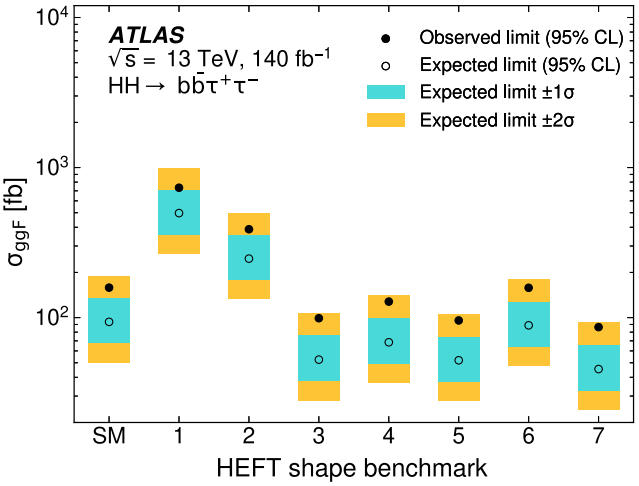

FIG. 10. Observed (filled circles) and expected (open circles) 95% CL upper limits on the ggF HH production cross section with respect to the background-only hypothesis in the SM and each of the seven HEFT shape benchmarks obtained from the combined fit. The inner and outer bands show the $\pm 1\sigma$ and $\pm 2\sigma$ variations on the expected upper limit. The contribution from VBF HH production is neglected for this result.

The 95% CL upper limits on the ggF HH cross section assuming the different benchmark m_{HH} shapes are summarized in Fig. 10. The following changes are made in the fit model with respect to the measurement of signal strength limits described in Section VI. The ggF HH prediction is replaced depending on the benchmark scenario, while the contribution from VBF HH production is neglected. Moreover, as this is a cross section measurement, no uncertainties in the ggF HH production cross section are taken into account. Overall, it is observed that lower average signal m_{HH} values, as represented by benchmarks 1 and 2, lead to weaker constraints.

The Wilson coefficients are probed with the same profile likelihood ratio scan as for κ_λ and κ_{2V} in Sec. VI. The one-dimensional constraints on the HEFT and SMEFT Wilson coefficients are summarized in Table IV.

TABLE IV. Observed and expected 95% CIs on HEFT and SMEFT Wilson coefficients, obtained from one-dimensional scans of $-2\ln\Lambda$ in fits to the observed data and an Asimov dataset constructed under the SM hypothesis. In each case, only the scanned Wilson coefficient is varied while all others are fixed to their respective SM predicted value. The contribution from VBF HH production is neglected for this result. The SM value for all considered Wilson coefficients is 0, hence no sign of BSM physics is found.

Wilson coefficient	Observed 95% CI	Expected 95% CI
c_{gghh}	$[-0.51, 0.58]$	$[-0.42, 0.44]$
c_{tthh}	$[-0.40, 0.84]$	$[-0.32, 0.72]$
c_H	$[-19.4, 10.0]$	$[-19.1, 8.6]$
$c_{H\Box}$	$[-12.6, 11.6]$	$[-8.5, 11.1]$

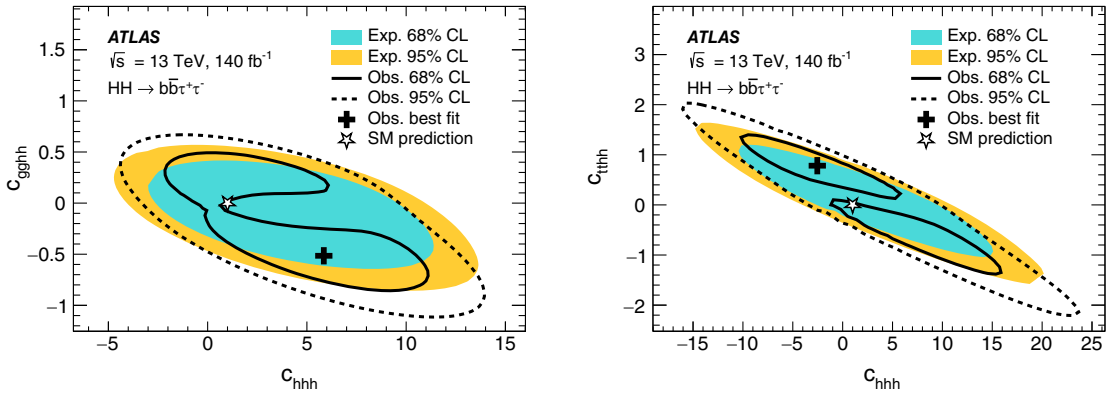

FIG. 11. Likelihood contours at 68% (solid line) and 95% (dashed line) CL in (a) the (c_{hhh}, c_{gghh}) and (b)the (c_{hhh}, c_{tthh}) parameter space, when all other Wilson coefficients are fixed to their SM values. The corresponding expected contours are shown by the inner and outer shaded regions. The SM prediction is indicated by the star, while the best-fit value is denoted by the black cross.

The observed and expected constraints on the ggF HH cross section limits assuming the HEFT shape benchmarks shown in Fig. 10 and the CIs on individual Wilson coefficients reported in Table IV are affected by the issue concerning the ggF HH prediction for BSM scenarios in POWHEG reported in the erratum of Ref. [81] and do not include the changes to resolve this issue described in Ref. [82]. If the ggF HH signal yields in the analysis categories are scaled based on the ratio of the predicted differential ggF HH cross sections with and without the changes described in Ref. [82], the expected limits and CIs changes by less than 10%.

Two-dimensional 68% and 95% CL likelihood contours are measured for the HEFT Wilson coefficients c_{gghh} and c_{tthh}, respectively, as a function of c_{hhh}. They are shown in Fig. 11. In addition, two-dimensional contours are measured for the SMEFT coefficients c_H and $c_{H\Box}$, as shown in Fig. 12. The observed nonparabolic features in the two-dimensional contours, such as the double-minimum structure in Fig. 11(b), stem from different best-fit Wilson coefficient values in the $\tau_{\text{lep}}\tau_{\text{had}}$ SLT and $\tau_{\text{had}}\tau_{\text{had}}$ high-m_{HH} categories, which drive the sensitivity of the combined fit. The excess in the SLT high-m_{HH} category leads to a 68% CL rejection of the region between the two 68% CL contours, as those Wilson coefficient combinations correspond to the lowest signal yields. The tighter 68% CL contour at $c_{gghh} \approx 0$ in Fig. 11(a) can also be attributed to this excess. As the signal yield is minimal around $c_{hhh} = 3$, for higher c_{hhh} the $-2\ln\Lambda$ value will decrease in the $\tau_{\text{lep}}\tau_{\text{had}}$ SLT high-m_{HH} category, while it increases in the $\tau_{\text{had}}\tau_{\text{had}}$ high-m_{HH} category that does not feature an excess. Hence, the slope of the combined $-2\ln\Lambda$ function is small in that region of the parameter space, leading to the observed behavior. The same effect can also be seen in Fig. 8(a).

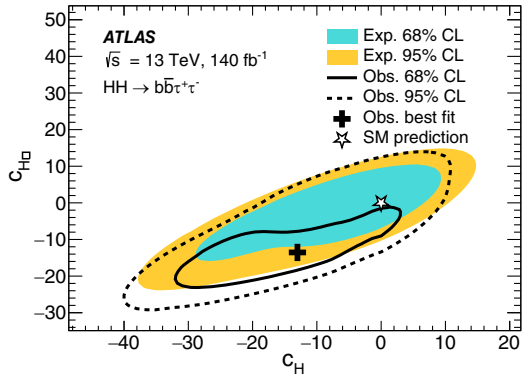

FIG. 12. Likelihood contours at 68% (solid line) and 95% (dashed line) CL in the (c_H, $c_{H\Box}$) parameter space, when all other Wilson coefficients are fixed to their SM values. The corresponding expected contours are shown by the inner and outer shaded regions. The SM prediction is indicated by the star, while the best-fit value is denoted by the black cross.

VIII. CONLUSION

An updated search for nonresonant Higgs boson pair production in the $b\bar{b}\tau^+\tau^-$ final state has been performed using the full Run 2 ATLAS dataset, corresponding to 140 fb^{-1} of proton-proton collisions at a center-of-mass energy of 13 TeV. The results supersede and expand on those of a previous search based on the same dataset described in Ref. [37]. Compared with the previous publication, the event classification has been reoptimized to enhance the sensitivity to κ_λ and to the VBF production mode. Improved multivariate classifiers are used to build the final discriminants, increasing the sensitivity to SM HH production and to anomalous values of the coupling modifiers κ_λ and κ_{2V}. The analysis sensitivity is improved by 11% to 19%, depending on the parameter of interest. Results interpreted in terms of ggF and VBF production

modes have been added, compared with the results of Ref. [37]. The statistical procedure for the interpretation of the observed yields in terms of the signal coupling modifiers has been updated from scans of cross section limits to profile likelihood ratio scans.

No evidence of HH signal is found. An observed 95% CL upper limit of 5.9 is set on the HH production signal strength μ_{HH}, to be compared with an expected limit of 3.3 in the background-only ($\mu_{HH} = 0$) hypothesis. The observed limit on μ_{HH} is looser than the expected one as a result of a mild excess in the $\tau_{\text{lep}}\tau_{\text{had}}$ SLT SR, in the high-m_{HH} category. The corresponding observed (expected) 95% confidence intervals for the self-coupling modifier κ_λ and the quartic coupling modifier κ_{2V} are $-3.1 < \kappa_\lambda < 9.0$ $(-2.5 < \kappa_\lambda < 9.3)$ and $-0.5 < \kappa_{2V} < 2.7$ $(-0.2 < \kappa_{2V} < 2.4)$, respectively. Based on these improvements, 95% CL upper limits are set on the HH production cross section in the seven shape benchmark scenarios proposed in Ref. [86]. Moreover, one-dimensional constraints are set on the Wilson coefficients c_H and $c_{H\Box}$ in the SMEFT framework as well as on c_{gghh} and c_{tthh} in the HEFT framework.

ACKNOWLEDGMENTS

We thank CERN for the very successful operation of the LHC and its injectors, as well as the support staff at CERN and at our institutions worldwide without whom ATLAS could not be operated efficiently. The crucial computing support from all WLCG partners is acknowledged gratefully, in particular from CERN, the ATLAS Tier-1 facilities at TRIUMF/SFU (Canada), NDGF (Denmark, Norway, Sweden), CC-IN2P3 (France), KIT/GridKA (Germany), INFN-CNAF (Italy), NL-T1 (Netherlands), PIC (Spain), RAL (UK) and BNL (USA), the Tier-2 facilities worldwide and large non-WLCG resource providers. Major contributors of computing resources are listed in Ref. [89]. We gratefully acknowledge the support of ANPCyT, Argentina; YerPhI, Armenia; ARC, Australia; BMWFW and FWF, Austria; ANAS, Azerbaijan; CNPq and FAPESP, Brazil; NSERC, NRC and CFI, Canada; CERN; ANID, Chile; CAS, MOST and NSFC, China; Minciencias, Colombia; MEYS CR, Czech Republic; DNRF and DNSRC, Denmark; IN2P3-CNRS and CEA-DRF/IRFU, France; SRNSFG, Georgia; BMBF, HGF and MPG, Germany; GSRI, Greece; RGC and Hong Kong SAR, China; ISF and Benoziyo Center, Israel; INFN, Italy; MEXT and JSPS, Japan; CNRST, Morocco; NWO, Netherlands; RCN, Norway; MEiN, Poland; FCT, Portugal; MNE/IFA, Romania; MESTD, Serbia; MSSR, Slovakia; ARRS and MIZŠ, Slovenia; DSI/NRF, South Africa; MICINN, Spain; SRC and Wallenberg Foundation, Sweden; SERI, SNSF and Cantons of Bern and Geneva, Switzerland; MOST, Taipei; TENMAK, Türkiye; STFC, United Kingdom; DOE and NSF, United States of America. Individual groups and members have received support from BCKDF, CANARIE, CRC and DRAC, Canada; CERN-CZ, PRIMUS 21/SCI/017 and UNCE SCI/013, Czech Republic; COST, ERC, ERDF, Horizon 2020, ICSC-NextGenerationEU and Marie Skłodowska-Curie Actions, European Union; Investissements d'Avenir Labex, Investissements d'Avenir Idex and ANR, France; DFG and AvH Foundation, Germany; Herakleitos, Thales and Aristeia programmes co-financed by EU-ESF and the Greek NSRF, Greece; BSF-NSF and MINERVA, Israel; Norwegian Financial Mechanism 2014-2021, Norway; NCN and NAWA, Poland; La Caixa Banking Foundation, CERCA Programme Generalitat de Catalunya and PROMETEO and GenT Programmes Generalitat Valenciana, Spain; Göran Gustafssons Stiftelse, Sweden; The Royal Society and Leverhulme Trust, United Kingdom. In addition, individual members wish to acknowledge support from CERN: European Organization for Nuclear Research (CERN PJAS); Chile: Agencia Nacional de Investigación y Desarrollo (FONDECYT 1190886, FONDECYT 1210400, FONDECYT 1230812, FONDECYT 1230987); China: National Natural Science Foundation of China (NSFC—12175119, NSFC 12275265, NSFC-12075060); Czech Republic: PRIMUS Research Programme (PRIMUS/21/SCI/017); European Union: European Research Council (ERC—948254, ERC 101089007), Horizon 2020 Framework Programme (MUCCA—CHIST-ERA-19-XAI-00), European Union, Future Artificial Intelligence Research (FAIR-NextGenerationEU PE00000013), Italian Center for High Performance Computing, Big Data and Quantum Computing (ICSC, NextGenerationEU); France: Agence Nationale de la Recherche (ANR-20-CE31-0013, ANR-21-CE31-0013, ANR-21-CE31-0022), Investissements d'Avenir Labex (ANR-11-LABX-0012); Germany: Baden-Württemberg Stiftung (BW Stiftung-Postdoc Eliteprogramme), Deutsche Forschungsgemeinschaft (DFG—469666862, DFG—CR 312/5-2); Italy: Istituto Nazionale di Fisica Nucleare (ICSC, NextGenerationEU); Japan: Japan Society for the Promotion of Science (JSPS KAKENHI JP21H05085, JSPS KAKENHI JP22H01227, JSPS KAKENHI JP22H04944, JSPS KAKENHI JP22KK0227); Netherlands: Netherlands Organisation for Scientific Research (NWO Veni 2020—VI.Veni.202.179); Norway: Research Council of Norway (RCN-314472); Poland: Polish National Agency for Academic Exchange (PPN/PPO/2020/1/00002/U/00001), Polish National Science Centre (NCN 2021/42/E/ST2/00350, NCN OPUS nr 2022/47/B/ST2/03059, NCN UMO-2019/34/E/ST2/00393, UMO-2020/37/B/ST2/01043, UMO-2021/40/C/ST2/00187, UMO-2022/47/O/ST2/00148); Slovenia: Slovenian Research Agency (ARIS grant J1-3010); Spain: BBVA Foundation (LEO22-1-603), Generalitat Valenciana (Artemisa, FEDER, IDIFEDER/2018/048), La Caixa Banking Foundation (LCF/BQ/PI20/

11760025), Ministry of Science and Innovation (MCIN & NextGenEU PCI2022-135018-2, MICIN & FEDER PID2021-125273NB, RYC2019-028510-I, RYC2020-030254-I, RYC2021-031273-I, RYC2022-038164-I), PROMETEO and GenT Programmes Generalitat Valenciana (CIDEGENT/2019/023, CIDEGENT/2019/027); Sweden: Swedish Research Council (VR 2018-00482, VR 2022-03845, VR 2022-04683, VR grant 2021-03651), Knut and Alice Wallenberg Foundation (KAW 2017.0100, KAW 2018.0157, KAW 2018.0458, KAW 2019.0447, KAW 2022.0358); Switzerland: Swiss National Science Foundation (SNSF—PCEFP2_194658); United Kingdom: Leverhulme Trust (Leverhulme Trust RPG-2020-004); United States of America: U.S. Department of Energy (ECA DE-AC02-76SF00515), Neubauer Family Foundation.

[1] ATLAS Collaboration, Observation of a new particle in the search for the Standard Model Higgs boson with the ATLAS detector at the LHC, Phys. Lett. B **716**, 1 (2012).
[2] CMS Collaboration, Observation of a new boson at a mass of 125 GeV with the CMS experiment at the LHC, Phys. Lett. B **716**, 30 (2012).
[3] ATLAS Collaboration, The ATLAS experiment at the CERN Large Hadron Collider, J. Instrum. **3**, S08003 (2008).
[4] CMS Collaboration, The CMS experiment at the CERN LHC, J. Instrum. **3**, S08004 (2008).
[5] L. Evans and P. Bryant, LHC Machine, J. Instrum. **3**, S08001 (2008).
[6] ATLAS Collaboration, Study of the spin and parity of the Higgs boson in diboson decays with the ATLAS detector, Eur. Phys. J. C **75**, 476 (2015); Eur. Phys. J. C **76**, 152(E) (2016).
[7] ATLAS Collaboration, *CP* properties of Higgs boson interactions with top quarks in the $t\bar{t}H$ and tH processes using $H \to \gamma\gamma$ with the ATLAS detector, Phys. Rev. Lett. **125**, 061802 (2020).
[8] CMS Collaboration, Constraints on anomalous Higgs boson couplings to vector bosons and fermions in its production and decay using the four-lepton final state, Phys. Rev. D **104**, 052004 (2021).
[9] ATLAS Collaboration, Evidence of off-shell Higgs boson production from ZZ leptonic decay channels and constraints on its total width with the ATLAS detector, Phys. Lett. B **846**, 138223 (2023).
[10] CMS Collaboration, Measurement of the Higgs boson width and evidence of its off-shell contributions to ZZ production, Nat. Phys. **18**, 1329 (2022).
[11] ATLAS Collaboration, A detailed map of Higgs boson interactions by the ATLAS experiment ten years after the discovery, Nature (London) **607**, 52 (2022).
[12] CMS Collaboration, A portrait of the Higgs boson by the CMS experiment ten years after the discovery, Nature (London) **607**, 60 (2022).
[13] F. Englert and R. Brout, Broken symmetry and the mass of gauge vector mesons, Phys. Rev. Lett. **13**, 321 (1964).
[14] P. Higgs, Broken symmetries, massless particles and gauge fields, Phys. Lett. **12**, 132 (1964).
[15] P. W. Higgs, Broken symmetries and the masses of gauge bosons, Phys. Rev. Lett. **13**, 508 (1964).
[16] G. S. Guralnik, C. R. Hagen, and T. W. B. Kibble, Global conservation laws and massless particles, Phys. Rev. Lett. **13**, 585 (1964).
[17] P. W. Higgs, Spontaneous symmetry breakdown without massless bosons, Phys. Rev. **145**, 1156 (1966).
[18] T. W. B. Kibble, Symmetry breaking in non-Abelian gauge theories, Phys. Rev. **155**, 1554 (1967).
[19] ATLAS and CMS Collaborations, Combined measurement of the Higgs boson mass in pp collisions at $\sqrt{s} = 7$ and 8 TeV with the ATLAS and CMS experiments, Phys. Rev. Lett. **114**, 191803 (2015).
[20] ATLAS Collaboration, Combined measurement of the Higgs boson mass from the $H \to \gamma\gamma$ and $H \to ZZ^* \to 4\ell$ decay channels with the ATLAS detector using $\sqrt{s} = 7, 8$, and 13 TeV pp collision data, Phys. Rev. Lett. **131**, 251802 (2023).
[21] P. Agrawal, D. Saha, L.-X. Xu, J.-H. Yu, and C.-P. Yuan, Determining the shape of the Higgs potential at future colliders, Phys. Rev. D **101**, 075023 (2020).
[22] S. Dawson, S. Dittmaier, and M. Spira, Neutral Higgs-boson pair production at hadron colliders: QCD corrections, Phys. Rev. D **58**, 115012 (1998).
[23] S. Borowka *et al.*, Higgs boson pair production in gluon fusion at next-to-leading order with full top-quark mass dependence, Phys. Rev. Lett. **117**, 012001 (2016).
[24] J. Baglio *et al.*, Gluon fusion into Higgs pairs at NLO QCD and the top mass scheme, Eur. Phys. J. C **79**, 459 (2019).
[25] D. de Florian and J. Mazzitelli, Higgs boson pair production at next-to-next-to-leading order in QCD, Phys. Rev. Lett. **111**, 201801 (2013).
[26] D. Y. Shao, C. S. Li, H. T. Li, and J. Wang, Threshold resummation effects in Higgs boson pair production at the LHC, J. High Energy Phys. 07 (2013) 169.
[27] D. de Florian and J. Mazzitelli, Higgs pair production at next-to-next-to-leading logarithmic accuracy at the LHC, J. High Energy Phys. 09 (2015) 053.
[28] M. Grazzini *et al.*, Higgs boson pair production at NNLO with top quark mass effects, J. High Energy Phys. 05 (2018) 059.
[29] J. Baglio *et al.*, $gg \to HH$: Combined uncertainties, Phys. Rev. D **103**, 056002 (2021).
[30] J. Baglio *et al.*, The measurement of the Higgs self-coupling at the LHC: Theoretical status, J. High Energy Phys. 04 (2013) 151.

[31] R. Frederix *et al.*, Higgs pair production at the LHC with NLO and parton-shower effects, Phys. Lett. B **732**, 142 (2014).

[32] L.-S. Ling *et al.*, NNLO QCD corrections to Higgs pair production via vector boson fusion at hadron colliders, Phys. Rev. D **89**, 073001 (2014).

[33] F. A. Dreyer and A. Karlberg, Fully differential vector-boson fusion Higgs pair production at next-to-next-to-leading order, Phys. Rev. D **99**, 074028 (2019).

[34] F. A. Dreyer and A. Karlberg, Vector-boson fusion Higgs pair production at N3LO, Phys. Rev. D **98**, 114016 (2018).

[35] ATLAS Collaboration, Constraints on the Higgs boson self-coupling from single- and double-Higgs production with the ATLAS detector using pp collisions at $\sqrt{s} = 13$ TeV, Phys. Lett. B **843**, 137745 (2023).

[36] ATLAS Collaboration, Search for Higgs boson pair production in the two bottom quarks plus two photons final state in pp collisions at $\sqrt{s} = 13$ TeV with the ATLAS detector, Phys. Rev. D **106**, 052001 (2022).

[37] ATLAS Collaboration, Search for resonant and non-resonant Higgs boson pair production in the $b\bar{b}\tau^+\tau^-$ decay channel using 13 TeV pp collision data from the ATLAS detector, J. High Energy Phys. 07 (2023) 040.

[38] ATLAS Collaboration, Search for nonresonant pair production of Higgs bosons in the $b\bar{b}b\bar{b}$ final state in pp collisions at $\sqrt{s} = 13$ TeV with the ATLAS detector, Phys. Rev. D **108**, 052003 (2023).

[39] CMS Collaboration, Search for nonresonant Higgs boson pair production in final state with two bottom quarks and two tau leptons in proton-proton collisions at $\sqrt{s} = 13$ TeV, Phys. Lett. B **842**, 137531 (2023).

[40] ATLAS Collaboration, The ATLAS Collaboration software and firmware, Report No. ATL-SOFT-PUB-2021-001, 2021, https://cds.cern.ch/record/2767187.

[41] ATLAS Collaboration, ATLAS data quality operations and performance for 2015–2018 data-taking, J. Instrum. **15**, P04003 (2020).

[42] ATLAS Collaboration, Luminosity determination in pp collisions at $\sqrt{s} = 13$ TeV using the ATLAS detector at the LHC, Eur. Phys. J. C **83**, 982 (2023).

[43] G. Avoni *et al.*, The new LUCID-2 detector for luminosity measurement and monitoring in ATLAS, J. Instrum. **13**, P07017 (2018).

[44] ATLAS Collaboration, The ATLAS simulation infrastructure, Eur. Phys. J. C **70**, 823 (2010).

[45] S. Agostinelli *et al.*, Geant4—a simulation toolkit, Nucl. Instrum. Methods Phys. Res., Sect. A **506**, 250 (2003).

[46] S. Alioli, P. Nason, C. Oleari, and E. Re, A general framework for implementing NLO calculations in shower Monte Carlo programs: The POWHEG BOX, J. High Energy Phys. 06 (2010) 043.

[47] R. D. Ball *et al.* (NNPDF Collaboration), Parton distributions for the LHC run II, J. High Energy Phys. 04 (2015) 040.

[48] T. Sjöstrand *et al.*, An introduction to PYTHIA8.2, Comput. Phys. Commun. **191**, 159 (2015).

[49] ATLAS Collaboration, ATLAS PYTHIA8 tunes to 7 TeV data, Report No. ATL-PHYS-PUB-2014-021, 2014, https://cds.cern.ch/record/1966419.

[50] R. D. Ball *et al.* (NNPDF Collaboration), Parton distributions with LHC data, Nucl. Phys. **B867**, 244 (2013).

[51] E. Bothmann *et al.*, Event generation with SHERPA2.2, SciPost Phys. **7**, 034 (2019).

[52] F. Buccioni *et al.*, OpenLoops 2, Eur. Phys. J. C **79**, 866 (2019).

[53] F. Cascioli, P. Maierhöfer, and S. Pozzorini, Scattering amplitudes with open loops, Phys. Rev. Lett. **108**, 111601 (2012).

[54] F. Buccioni, S. Pozzorini, and M. Zoller, On-the-fly reduction of open loops, Eur. Phys. J. C **78**, 70 (2018).

[55] A. Denner, S. Dittmaier, and L. Hofer, Collier: A fortran-based complex one-loop library in extended regularizations, Comput. Phys. Commun. **212**, 220 (2017).

[56] T. Gleisberg and S. Höche, Comix, a new matrix element generator, J. High Energy Phys. 12 (2008) 039.

[57] S. Höche, F. Krauss, M. Schönherr, and F. Siegert, QCD matrix elements + parton showers. The NLO case, J. High Energy Phys. 04 (2013) 027.

[58] J. Butterworth *et al.*, PDF4LHC recommendations for LHC Run II, J. Phys. G **43**, 023001 (2016).

[59] ATLAS Collaboration, Measurement of the Z/γ^* boson transverse momentum distribution in pp collisions at $\sqrt{s} =$ 7 TeV with the ATLAS detector, J. High Energy Phys. 09 (2014) 145.

[60] J. Alwall *et al.*, The automated computation of tree-level and next-to-leading order differential cross sections, and their matching to parton shower simulations, J. High Energy Phys. 07 (2014) 079.

[61] ATLAS Collaboration, Validation of signal Monte Carlo event generation in searches for Higgs boson pairs with the ATLAS detector, Report No. ATL-PHYS-PUB-2019-007, 2019, https://cds.cern.ch/record/2665057.

[62] ATLAS Collaboration, Search for non-resonant Higgs boson pair production in the $2b + 2\ell + E_{\mathrm{T}}^{\mathrm{miss}}$ final state in pp collisions at $\sqrt{s} = 13$ TeV with the ATLAS detector, J. High Energy Phys. 02 (2024) 037.

[63] A. Elagin, P. Murat, A. Pranko, and A. Safonov, A new mass reconstruction technique for resonances decaying to $\tau\tau$, Nucl. Instrum. Methods Phys. Res., Sect. A **654**, 481 (2011).

[64] ATLAS Collaboration, ATLAS flavour-tagging algorithms for the LHC Run 2pp collision dataset, Eur. Phys. J. C **83**, 681 (2023).

[65] A. Hoecker *et al.*, TMVA—Toolkit for multivariate data analysis, arXiv:physics/0703039.

[66] G. Cowan, K. Cranmer, E. Gross, and O. Vitells, Asymptotic formulae for likelihood-based tests of new physics, Eur. Phys. J. C **71**, 1554 (2011); Eur. Phys. J. C **73**, 2501(E) (2013).

[67] C. Bernaciak, M. S. A. Buschmann, A. Butter, and T. Plehn, Fox-Wolfram moments in Higgs physics, Phys. Rev. D **87**, 073014 (2013).

[68] L. A. Spiller, Modification of Fox-Wolfram moments for hadron colliders, J. High Energy Phys. 03 (2016) 027.

[69] C. G. Lester, The stransverse mass, M_{T2}, in special cases, J. High Energy Phys. 05 (2011) 076.

[70] M. L. Graesser and J. Shelton, Hunting mixed top squark decays, Phys. Rev. Lett. **111**, 121802 (2013).

[71] J. H. Kim, K. Kong, K. T. Matchev, and M. Park, Probing the triple higgs self-interaction at the Large Hadron Collider, Phys. Rev. Lett. **122**, 091801 (2019).
[72] R. Barlow and C. Beeston, Fitting using finite Monte Carlo samples, Comput. Phys. Commun. **77**, 219 (1993).
[73] M. Bähr *et al.*, HERWIG++ physics and manual, Eur. Phys. J. C **58**, 639 (2008).
[74] J. Bellm *et al.*, HERWIG7.0/HERWIG++3.0 release note, Eur. Phys. J. C **76**, 196 (2016).
[75] R. Frederix and S. Frixione, Merging meets matching in MC@NLO, J. High Energy Phys. 12 (2012) 061.
[76] S. Frixione, E. Laenen, P. Motylinski, C. White, and B. R. Webber, Single-top hadroproduction in association with a W boson, J. High Energy Phys. 07 (2008) 029.
[77] ATLAS Collaboration, Measurements of inclusive and differential fiducial cross sections of $t\bar{t}$ production with additional heavy-flavour jets in proton-proton collisions at $\sqrt{s} = 13$ TeV with the ATLAS detector, J. High Energy Phys. 04 (2019) 046.
[78] ATLAS Collaboration, Measurement of the cross section for W boson production in association with b-jets in pp collisions at $\sqrt{s} = 7$ TeV with the ATLAS detector, J. High Energy Phys. 06 (2013) 084.
[79] D. de Florian *et al.*, Handbook of LHC Higgs cross sections: 4. Deciphering the nature of the Higgs sector, arXiv:1610.07922.
[80] A. L. Read, Presentation of search results: The CL_S technique, J. Phys. G **28**, 2693 (2002).
[81] G. Heinrich, J. Lang, and L. Scyboz, SMEFT predictions for $gg \to hh$ at full NLO QCD and truncation uncertainties, J. High Energy Phys. 08 (2022) 079; J. High Energy Phys. 10 (2023) 86(E).
[82] E. Bagnaschi, G. Degrassi, and R. Gröber, Higgs boson pair production at NLO in the POWHEG approach and the top quark mass uncertainties, Eur. Phys. J. C **83**, 1054 (2023).
[83] K. G. Hayes, M. L. Perl, and B. Efron, Application of the bootstrap statistical method to the tau-decay-mode problem, Phys. Rev. D **39**, 274 (1989).
[84] ATLAS Collaboration, Studies of new Higgs boson interactions through nonresonant HH production in the $b\bar{b}\gamma\gamma$ final state in pp collisions at $\sqrt{s} = 13$ TeV with the ATLAS detector, J. High Energy Phys. 01 (2024) 066.
[85] B. Grzadkowski, M. Iskrzyński, M. Misiak, and J. Rosiek, Dimension-six terms in the standard model Lagrangian, J. High Energy Phys. 10 (2010) 085.
[86] L. Alasfar *et al.*, Effective field theory descriptions of Higgs boson pair production, Report No. LHCHWG-2022-004, 2023, https://cds.cern.ch/record/2843280.
[87] M. Capozi and G. Heinrich, Exploring anomalous couplings in Higgs boson pair production through shape analysis, J. High Energy Phys. 03 (2020) 091.
[88] ATLAS Collaboration, Interpretations of the ATLAS measurements of Higgs boson production and decay rates and differential cross-sections in pp collisions at $\sqrt{s} = 13$ TeV, arXiv:2402.05742.
[89] ATLAS Collaboration, ATLAS computing acknowledgements, Report No. ATL-SOFT-PUB-2023-001, 2023, https://cds.cern.ch/record/2869272.

G. Aad,[103] E. Aakvaag,[16] B. Abbott,[121] K. Abeling,[55] N. J. Abicht,[49] S. H. Abidi,[29] M. Aboelela,[44] A. Aboulhorma,[35e] H. Abramowicz,[152] H. Abreu,[151] Y. Abulaiti,[118] B. S. Acharya,[69a,69b,b] A. Ackermann,[63a] C. Adam Bourdarios,[4] L. Adamczyk,[86a] S. V. Addepalli,[26] M. J. Addison,[102] J. Adelman,[116] A. Adiguzel,[21c] T. Adye,[135] A. A. Affolder,[137] Y. Afik,[39] M. N. Agaras,[13] J. Agarwala,[73a,73b] A. Aggarwal,[101] C. Agheorghiesei,[27c] A. Ahmad,[36] F. Ahmadov,[38,c] W. S. Ahmed,[105] S. Ahuja,[96] X. Ai,[62e] G. Aielli,[76a,76b] A. Aikot,[164] M. Ait Tamlihat,[35e] B. Aitbenchikh,[35a] I. Aizenberg,[170] M. Akbiyik,[101] T. P. A. Åkesson,[99] A. V. Akimov,[37] D. Akiyama,[169] N. N. Akolkar,[24] S. Aktas,[21a] K. Al Khoury,[41] G. L. Alberghi,[23b] J. Albert,[166] P. Albicocco,[53] G. L. Albouy,[60] S. Alderweireldt,[52] Z. L. Alegria,[122] M. Aleksa,[36] I. N. Aleksandrov,[38] C. Alexa,[27b] T. Alexopoulos,[10] F. Alfonsi,[23b] M. Algren,[56] M. Alhroob,[142] B. Ali,[133] H. M. J. Ali,[92] S. Ali,[149] S. W. Alibocus,[93] M. Aliev,[33c] G. Alimonti,[71a] W. Alkakhi,[55] C. Allaire,[66] B. M. M. Allbrooke,[147] J. F. Allen,[52] C. A. Allendes Flores,[138f] P. P. Allport,[20] A. Aloisio,[72a,72b] F. Alonso,[91] C. Alpigiani,[139] M. Alvarez Estevez,[100] A. Alvarez Fernandez,[101] M. Alves Cardoso,[56] M. G. Alviggi,[72a,72b] M. Aly,[102] Y. Amaral Coutinho,[83b] A. Ambler,[105] C. Amelung,[36] M. Amerl,[102] C. G. Ames,[110] D. Amidei,[107] K. J. Amirie,[156] S. P. Amor Dos Santos,[131a] K. R. Amos,[164] V. Ananiev,[126] C. Anastopoulos,[140] T. Andeen,[11] J. K. Anders,[36] S. Y. Andrean,[47a,47b] A. Andreazza,[71a,71b] S. Angelidakis,[9] A. Angerami,[41,d] A. V. Anisenkov,[37] A. Annovi,[74a] C. Antel,[56] M. T. Anthony,[140] E. Antipov,[146] M. Antonelli,[53] F. Anulli,[75a] M. Aoki,[84] T. Aoki,[154] J. A. Aparisi Pozo,[164] M. A. Aparo,[147] L. Aperio Bella,[48] C. Appelt,[18] A. Apyan,[26] S. J. Arbiol Val,[87] C. Arcangeletti,[53] A. T. H. Arce,[51] E. Arena,[93] J-F. Arguin,[109] S. Argyropoulos,[54] J.-H. Arling,[48] O. Arnaez,[4] H. Arnold,[115] G. Artoni,[75a,75b] H. Asada,[112] K. Asai,[119] S. Asai,[154] N. A. Asbah,[36] K. Assamagan,[29] R. Astalos,[28a] S. Atashi,[160] R. J. Atkin,[33a] M. Atkinson,[163] H. Atmani,[35f] P. A. Atmasiddha,[129] K. Augsten,[133] S. Auricchio,[72a,72b] A. D. Auriol,[20] V. A. Austrup,[102] G. Avolio,[36] K. Axiotis,[56] G. Azuelos,[109,e] D. Babal,[28b]

H. Bachacou,[136] K. Bachas,[153,f] A. Bachiu,[34] F. Backman,[47a,47b] A. Badea,[39] T. M. Baer,[107] P. Bagnaia,[75a,75b] M. Bahmani,[18] D. Bahner,[54] K. Bai,[124] A. J. Bailey,[164] J. T. Baines,[135] L. Baines,[95] O. K. Baker,[173] E. Bakos,[15] D. Bakshi Gupta,[8] V. Balakrishnan,[121] R. Balasubramanian,[115] E. M. Baldin,[37] P. Balek,[86a] E. Ballabene,[23b,23a] F. Balli,[136] L. M. Baltes,[63a] W. K. Balunas,[32] J. Balz,[101] E. Banas,[87] M. Bandieramonte,[130] A. Bandyopadhyay,[24] S. Bansal,[24] L. Barak,[152] M. Barakat,[48] E. L. Barberio,[106] D. Barberis,[57b,57a] M. Barbero,[103] M. Z. Barel,[115] K. N. Barends,[33a] T. Barillari,[111] M-S. Barisits,[36] T. Barklow,[144] P. Baron,[123] D. A. Baron Moreno,[102] A. Baroncelli,[62a] G. Barone,[29] A. J. Barr,[127] J. D. Barr,[97] F. Barreiro,[100] J. Barreiro Guimarães da Costa,[14a] U. Barron,[152] M. G. Barros Teixeira,[131a] S. Barsov,[37] F. Bartels,[63a] R. Bartoldus,[144] A. E. Barton,[92] P. Bartos,[28a] A. Basan,[101] M. Baselga,[49] A. Bassalat,[66,g] M. J. Basso,[157a] R. L. Bates,[59] S. Batlamous,[35e] B. Batool,[142] M. Battaglia,[137] D. Battulga,[18] M. Bauce,[75a,75b] M. Bauer,[36] P. Bauer,[24] L. T. Bazzano Hurrell,[30] J. B. Beacham,[51] T. Beau,[128] J. Y. Beaucamp,[91] P. H. Beauchemin,[159] P. Bechtle,[24] H. P. Beck,[19,h] K. Becker,[168] A. J. Beddall,[82] V. A. Bednyakov,[38] C. P. Bee,[146] L. J. Beemster,[15] T. A. Beermann,[36] M. Begalli,[83d] M. Begel,[29] A. Behera,[146] J. K. Behr,[48] J. F. Beirer,[36] F. Beisiegel,[24] M. Belfkir,[117b] G. Bella,[152] L. Bellagamba,[23b] A. Bellerive,[34] P. Bellos,[20] K. Beloborodov,[37] D. Benchekroun,[35a] F. Bendebba,[35a] Y. Benhammou,[152] K. C. Benkendorfer,[61] L. Beresford,[48] M. Beretta,[53] E. Bergeaas Kuutmann,[162] N. Berger,[4] B. Bergmann,[133] J. Beringer,[17a] G. Bernardi,[5] C. Bernius,[144] F. U. Bernlochner,[24] F. Bernon,[36,103] A. Berrocal Guardia,[13] T. Berry,[96] P. Berta,[134] A. Berthold,[50] S. Bethke,[111] A. Betti,[75a,75b] A. J. Bevan,[95] N. K. Bhalla,[54] M. Bhamjee,[33c] S. Bhatta,[146] D. S. Bhattacharya,[167] P. Bhattarai,[144] K. D. Bhide,[54] V. S. Bhopatkar,[122] R. M. Bianchi,[130] G. Bianco,[23b,23a] O. Biebel,[110] R. Bielski,[124] M. Biglietti,[77a] C. S. Billingsley,[44] M. Bindi,[55] A. Bingul,[21b] C. Bini,[75a,75b] A. Biondini,[93] C. J. Birch-sykes,[102] G. A. Bird,[32] M. Birman,[170] M. Biros,[134] S. Biryukov,[147] T. Bisanz,[49] E. Bisceglie,[43b,43a] J. P. Biswal,[135] D. Biswas,[142] K. Bjørke,[126] I. Bloch,[48] A. Blue,[59] U. Blumenschein,[95] J. Blumenthal,[101] V. S. Bobrovnikov,[37] M. Boehler,[54] B. Boehm,[167] D. Bogavac,[36] A. G. Bogdanchikov,[37] C. Bohm,[47a] V. Boisvert,[96] P. Bokan,[36] T. Bold,[86a] M. Bomben,[5] M. Bona,[95] M. Boonekamp,[136] C. D. Booth,[96] A. G. Borbély,[59] I. S. Bordulev,[37] H. M. Borecka-Bielska,[109] G. Borissov,[92] D. Bortoletto,[127] D. Boscherini,[23b] M. Bosman,[13] J. D. Bossio Sola,[36] K. Bouaouda,[35a] N. Bouchhar,[164] J. Boudreau,[130] E. V. Bouhova-Thacker,[92] D. Boumediene,[40] R. Bouquet,[57b,57a] A. Boveia,[120] J. Boyd,[36] D. Boye,[29] I. R. Boyko,[38] J. Bracinik,[20] N. Brahimi,[4] G. Brandt,[172] O. Brandt,[32] F. Braren,[48] B. Brau,[104] J. E. Brau,[124] R. Brener,[170] L. Brenner,[115] R. Brenner,[162] S. Bressler,[170] D. Britton,[59] D. Britzger,[111] I. Brock,[24] G. Brooijmans,[41] E. Brost,[29] L. M. Brown,[166] L. E. Bruce,[61] T. L. Bruckler,[127] P. A. Bruckman de Renstrom,[87] B. Brüers,[48] A. Bruni,[23b] G. Bruni,[23b] M. Bruschi,[23b] N. Bruscino,[75a,75b] T. Buanes,[16] Q. Buat,[139] D. Buchin,[111] A. G. Buckley,[59] O. Bulekov,[37] B. A. Bullard,[144] S. Burdin,[93] C. D. Burgard,[49] A. M. Burger,[36] B. Burghgrave,[8] O. Burlayenko,[54] J. T. P. Burr,[32] C. D. Burton,[11] J. C. Burzynski,[143] E. L. Busch,[41] V. Büscher,[101] P. J. Bussey,[59] J. M. Butler,[25] C. M. Buttar,[59] J. M. Butterworth,[97] W. Buttinger,[135] C. J. Buxo Vazquez,[108] A. R. Buzykaev,[37] S. Cabrera Urbán,[164] L. Cadamuro,[66] D. Caforio,[58] H. Cai,[130] Y. Cai,[14a,14e] Y. Cai,[14c] V. M. M. Cairo,[36] O. Cakir,[3a] N. Calace,[36] P. Calafiura,[17a] G. Calderini,[128] P. Calfayan,[68] G. Callea,[59] L. P. Caloba,[83b] D. Calvet,[40] S. Calvet,[40] M. Calvetti,[74a,74b] R. Camacho Toro,[128] S. Camarda,[36] D. Camarero Munoz,[26] P. Camarri,[76a,76b] M. T. Camerlingo,[72a,72b] D. Cameron,[36] C. Camincher,[166] M. Campanelli,[97] A. Camplani,[42] V. Canale,[72a,72b] A. C. Canbay,[3a] J. Cantero,[164] Y. Cao,[163] F. Capocasa,[26] M. Capua,[43b,43a] A. Carbone,[71a,71b] R. Cardarelli,[76a] J. C. J. Cardenas,[8] F. Cardillo,[164] G. Carducci,[43b,43a] T. Carli,[36] G. Carlino,[72a] J. I. Carlotto,[13] B. T. Carlson,[130,i] E. M. Carlson,[166,157a] L. Carminati,[71a,71b] A. Carnelli,[136] M. Carnesale,[75a,75b] S. Caron,[114] E. Carquin,[138f] S. Carrá,[71a] G. Carratta,[23b,23a] A. M. Carroll,[124] T. M. Carter,[52] M. P. Casado,[13,j] M. Caspar,[48] F. L. Castillo,[4] L. Castillo Garcia,[13] V. Castillo Gimenez,[164] N. F. Castro,[131a,131e] A. Catinaccio,[36] J. R. Catmore,[126] T. Cavaliere,[4] V. Cavaliere,[29] N. Cavalli,[23b,23a] Y. C. Cekmecelioglu,[48] E. Celebi,[21a] S. Cella,[36] F. Celli,[127] M. S. Centonze,[70a,70b] V. Cepaitis,[56] K. Cerny,[123] A. S. Cerqueira,[83a] A. Cerri,[147] L. Cerrito,[76a,76b] F. Cerutti,[17a] B. Cervato,[142] A. Cervelli,[23b] G. Cesarini,[53] S. A. Cetin,[82] D. Chakraborty,[116] J. Chan,[17a] W. Y. Chan,[154] J. D. Chapman,[32] E. Chapon,[136] B. Chargeishvili,[150b] D. G. Charlton,[20] M. Chatterjee,[19] C. Chauhan,[134] Y. Che,[14c] S. Chekanov,[6] S. V. Chekulaev,[157a] G. A. Chelkov,[38,k] A. Chen,[107] B. Chen,[152] B. Chen,[166] H. Chen,[14c] H. Chen,[29] J. Chen,[62c] J. Chen,[143] M. Chen,[127] S. Chen,[154] S. J. Chen,[14c] X. Chen,[62c,136]

X. Chen,[14b,l] Y. Chen,[62a] C. L. Cheng,[171] H. C. Cheng,[64a] S. Cheong,[144] A. Cheplakov,[38] E. Cheremushkina,[48] E. Cherepanova,[115] R. Cherkaoui El Moursli,[35e] E. Cheu,[7] K. Cheung,[65] L. Chevalier,[136] V. Chiarella,[53] G. Chiarelli,[74a] N. Chiedde,[103] G. Chiodini,[70a] A. S. Chisholm,[20] A. Chitan,[27b] M. Chitishvili,[164] M. V. Chizhov,[38] K. Choi,[11] Y. Chou,[139] E. Y. S. Chow,[114] K. L. Chu,[170] M. C. Chu,[64a] X. Chu,[14a,14e] J. Chudoba,[132] J. J. Chwastowski,[87] D. Cieri,[111] K. M. Ciesla,[86a] V. Cindro,[94] A. Ciocio,[17a] F. Cirotto,[72a,72b] Z. H. Citron,[170] M. Citterio,[71a] D. A. Ciubotaru,[27b] A. Clark,[56] P. J. Clark,[52] C. Clarry,[156] J. M. Clavijo Columbie,[48] S. E. Clawson,[48] C. Clement,[47a,47b] J. Clercx,[48] Y. Coadou,[103] M. Cobal,[69a,69c] A. Coccaro,[57b] R. F. Coelho Barrue,[131a] R. Coelho Lopes De Sa,[104] S. Coelli,[71a] B. Cole,[41] J. Collot,[60] P. Conde Muiño,[131a,131g] M. P. Connell,[33c] S. H. Connell,[33c] E. I. Conroy,[127] F. Conventi,[72a,m] H. G. Cooke,[20] A. M. Cooper-Sarkar,[127] A. Cordeiro Oudot Choi,[128] L. D. Corpe,[40] M. Corradi,[75a,75b] F. Corriveau,[105,n] A. Cortes-Gonzalez,[18] M. J. Costa,[164] F. Costanza,[4] D. Costanzo,[140] B. M. Cote,[120] G. Cowan,[96] K. Cranmer,[171] D. Cremonini,[23b,23a] S. Crépé-Renaudin,[60] F. Crescioli,[128] M. Cristinziani,[142] M. Cristoforetti,[78a,78b] V. Croft,[115] J. E. Crosby,[122] G. Crosetti,[43b,43a] A. Cueto,[100] T. Cuhadar Donszelmann,[160] H. Cui,[14a,14e] Z. Cui,[7] W. R. Cunningham,[59] F. Curcio,[164] J. R. Curran,[52] P. Czodrowski,[36] M. M. Czurylo,[36] M. J. Da Cunha Sargedas De Sousa,[57b,57a] J. V. Da Fonseca Pinto,[83b] C. Da Via,[102] W. Dabrowski,[86a] T. Dado,[49] S. Dahbi,[149] T. Dai,[107] D. Dal Santo,[19] C. Dallapiccola,[104] M. Dam,[42] G. D'amen,[29] V. D'Amico,[110] J. Damp,[101] J. R. Dandoy,[34] M. Danninger,[143] V. Dao,[36] G. Darbo,[57b] S. Darmora,[6] S. J. Das,[29,o] S. D'Auria,[71a,71b] A. D'avanzo,[72a,72b] C. David,[33a] T. Davidek,[134] B. Davis-Purcell,[34] I. Dawson,[95] H. A. Day-hall,[133] K. De,[8] R. De Asmundis,[72a] N. De Biase,[48] S. De Castro,[23b,23a] N. De Groot,[114] P. de Jong,[115] H. De la Torre,[116] A. De Maria,[14c] A. De Salvo,[75a] U. De Sanctis,[76a,76b] F. De Santis,[70a,70b] A. De Santo,[147] J. B. De Vivie De Regie,[60] D. V. Dedovich,[38] J. Degens,[93] A. M. Deiana,[44] F. Del Corso,[23b,23a] J. Del Peso,[100] F. Del Rio,[63a] L. Delagrange,[128] F. Deliot,[136] C. M. Delitzsch,[49] M. Della Pietra,[72a,72b] D. Della Volpe,[56] A. Dell'Acqua,[36] L. Dell'Asta,[71a,71b] M. Delmastro,[4] P. A. Delsart,[60] S. Demers,[173] M. Demichev,[38] S. P. Denisov,[37] L. D'Eramo,[40] D. Derendarz,[87] F. Derue,[128] P. Dervan,[93] K. Desch,[24] C. Deutsch,[24] F. A. Di Bello,[57b,57a] A. Di Ciaccio,[76a,76b] L. Di Ciaccio,[4] A. Di Domenico,[75a,75b] C. Di Donato,[72a,72b] A. Di Girolamo,[36] G. Di Gregorio,[36] A. Di Luca,[78a,78b] B. Di Micco,[77a,77b] R. Di Nardo,[77a,77b] M. Diamantopoulou,[34] F. A. Dias,[115] T. Dias Do Vale,[143] M. A. Diaz,[138a,138b] F. G. Diaz Capriles,[24] M. Didenko,[164] E. B. Diehl,[107] S. Díez Cornell,[48] C. Diez Pardos,[142] C. Dimitriadi,[162,24] A. Dimitrievska,[17a] J. Dingfelder,[24] I-M. Dinu,[27b] S. J. Dittmeier,[63b] F. Dittus,[36] M. Divisek,[134] F. Djama,[103] T. Djobava,[150b] C. Doglioni,[102,99] A. Dohnalova,[28a] J. Dolejsi,[134] Z. Dolezal,[134] K. M. Dona,[39] M. Donadelli,[83c] B. Dong,[108] J. Donini,[40] A. D'Onofrio,[72a,72b] M. D'Onofrio,[93] J. Dopke,[135] A. Doria,[72a] N. Dos Santos Fernandes,[131a] P. Dougan,[102] M. T. Dova,[91] A. T. Doyle,[59] M. A. Draguet,[127] E. Dreyer,[170] I. Drivas-koulouris,[10] M. Drnevich,[118] M. Drozdova,[56] D. Du,[62a] T. A. du Pree,[115] F. Dubinin,[37] M. Dubovsky,[28a] E. Duchovni,[170] G. Duckeck,[110] O. A. Ducu,[27b] D. Duda,[52] A. Dudarev,[36] E. R. Duden,[26] M. D'uffizi,[102] L. Duflot,[66] M. Dührssen,[36] A. E. Dumitriu,[27b] M. Dunford,[63a] S. Dungs,[49] K. Dunne,[47a,47b] A. Duperrin,[103] H. Duran Yildiz,[3a] M. Düren,[58] A. Durglishvili,[150b] B. L. Dwyer,[116] G. I. Dyckes,[17a] M. Dyndal,[86a] B. S. Dziedzic,[87] Z. O. Earnshaw,[147] G. H. Eberwein,[127] B. Eckerova,[28a] S. Eggebrecht,[55] E. Egidio Purcino De Souza,[128] L. F. Ehrke,[56] G. Eigen,[16] K. Einsweiler,[17a] T. Ekelof,[162] P. A. Ekman,[99] S. El Farkh,[35b] Y. El Ghazali,[35b] H. El Jarrari,[36] A. El Moussaouy,[109] V. Ellajosyula,[162] M. Ellert,[162] F. Ellinghaus,[172] N. Ellis,[36] J. Elmsheuser,[29] M. Elsawy,[117a] M. Elsing,[36] D. Emeliyanov,[135] Y. Enari,[154] I. Ene,[17a] S. Epari,[13] P. A. Erland,[87] M. Errenst,[172] M. Escalier,[66] C. Escobar,[164] E. Etzion,[152] G. Evans,[131a] H. Evans,[68] L. S. Evans,[96] A. Ezhilov,[37] S. Ezzarqtouni,[35a] F. Fabbri,[23b,23a] L. Fabbri,[23b,23a] G. Facini,[97] V. Fadeyev,[137] R. M. Fakhrutdinov,[37] D. Fakoudis,[101] S. Falciano,[75a] L. F. Falda Ulhoa Coelho,[36] P. J. Falke,[24] J. Faltova,[134] C. Fan,[163] Y. Fan,[14a] Y. Fang,[14a,14e] M. Fanti,[71a,71b] M. Faraj,[69a,69b] Z. Farazpay,[98] A. Farbin,[8] A. Farilla,[77a] T. Farooque,[108] S. M. Farrington,[52] F. Fassi,[35e] D. Fassouliotis,[9] M. Faucci Giannelli,[76a,76b] W. J. Fawcett,[32] L. Fayard,[66] P. Federic,[134] P. Federicova,[132] O. L. Fedin,[37,k] M. Feickert,[171] L. Feligioni,[103] D. E. Fellers,[124] C. Feng,[62b] M. Feng,[14b] Z. Feng,[115] M. J. Fenton,[160] L. Ferencz,[48] R. A. M. Ferguson,[92] S. I. Fernandez Luengo,[138f] P. Fernandez Martinez,[13] M. J. V. Fernoux,[103] J. Ferrando,[92] A. Ferrari,[162] P. Ferrari,[115,114] R. Ferrari,[73a] D. Ferrere,[56] C. Ferretti,[107] F. Fiedler,[101] P. Fiedler,[133] A. Filipčič,[94]

E. K. Filmer,[1] F. Filthaut,[114] M. C. N. Fiolhais,[131a,131c,p] L. Fiorini,[164] W. C. Fisher,[108] T. Fitschen,[102] P. M. Fitzhugh,[136] I. Fleck,[142] P. Fleischmann,[107] T. Flick,[172] M. Flores,[33d,q] L. R. Flores Castillo,[64a] L. Flores Sanz De Acedo,[36] F. M. Follega,[78a,78b] N. Fomin,[16] J. H. Foo,[156] A. Formica,[136] A. C. Forti,[102] E. Fortin,[36] A. W. Fortman,[17a] M. G. Foti,[17a] L. Fountas,[9,r] D. Fournier,[66] H. Fox,[92] P. Francavilla,[74a,74b] S. Francescato,[61] S. Franchellucci,[56] M. Franchini,[23b,23a] S. Franchino,[63a] D. Francis,[36] L. Franco,[114] V. Franco Lima,[36] L. Franconi,[48] M. Franklin,[61] G. Frattari,[26] W. S. Freund,[83b] Y. Y. Frid,[152] J. Friend,[59] N. Fritzsche,[50] A. Froch,[54] D. Froidevaux,[36] J. A. Frost,[127] Y. Fu,[62a] S. Fuenzalida Garrido,[138f] M. Fujimoto,[103] K. Y. Fung,[64a] E. Furtado De Simas Filho,[83e] M. Furukawa,[154] J. Fuster,[164] A. Gabrielli,[23b,23a] A. Gabrielli,[156] P. Gadow,[36] G. Gagliardi,[57b,57a] L. G. Gagnon,[17a] S. Galantzan,[152] E. J. Gallas,[127] B. J. Gallop,[135] K. K. Gan,[120] S. Ganguly,[154] Y. Gao,[52] F. M. Garay Walls,[138a,138b] B. Garcia,[29] C. García,[164] A. Garcia Alonso,[115] A. G. Garcia Caffaro,[173] J. E. García Navarro,[164] M. Garcia-Sciveres,[17a] G. L. Gardner,[129] R. W. Gardner,[39] N. Garelli,[159] D. Garg,[80] R. B. Garg,[144,s] J. M. Gargan,[52] C. A. Garner,[156] C. M. Garvey,[33a] P. Gaspar,[83b] V. K. Gassmann,[159] G. Gaudio,[73a] V. Gautam,[13] P. Gauzzi,[75a,75b] I. L. Gavrilenko,[37] A. Gavrilyuk,[37] C. Gay,[165] G. Gaycken,[48] E. N. Gazis,[10] A. A. Geanta,[27b] C. M. Gee,[137] A. Gekow,[120] C. Gemme,[57b] M. H. Genest,[60] A. D. Gentry,[113] S. George,[96] W. F. George,[20] T. Geralis,[46] P. Gessinger-Befurt,[36] M. E. Geyik,[172] M. Ghani,[168] M. Ghneimat,[142] K. Ghorbanian,[95] A. Ghosal,[142] A. Ghosh,[160] A. Ghosh,[7] B. Giacobbe,[23b] S. Giagu,[75a,75b] T. Giani,[115] P. Giannetti,[74a] A. Giannini,[62a] S. M. Gibson,[96] M. Gignac,[137] D. T. Gil,[86b] A. K. Gilbert,[86a] B. J. Gilbert,[41] D. Gillberg,[34] G. Gilles,[115] L. Ginabat,[128] D. M. Gingrich,[2,e] M. P. Giordani,[69a,69c] P. F. Giraud,[136] G. Giugliarelli,[69a,69c] D. Giugni,[71a] F. Giuli,[36] I. Gkialas,[9,r] L. K. Gladilin,[37] C. Glasman,[100] G. R. Gledhill,[124] G. Glemža,[48] M. Glisic,[124] I. Gnesi,[43b,t] Y. Go,[29] M. Goblirsch-Kolb,[36] B. Gocke,[49] D. Godin,[109] B. Gokturk,[21a] S. Goldfarb,[106] T. Golling,[56] M. G. D. Gololo,[33g] D. Golubkov,[37] J. P. Gombas,[108] A. Gomes,[131a,131b] G. Gomes Da Silva,[142] A. J. Gomez Delegido,[164] R. Gonçalo,[131a,131c] L. Gonella,[20] A. Gongadze,[150c] F. Gonnella,[20] J. L. Gonski,[144] R. Y. González Andana,[52] S. González de la Hoz,[164] R. Gonzalez Lopez,[93] C. Gonzalez Renteria,[17a] M. V. Gonzalez Rodrigues,[48] R. Gonzalez Suarez,[162] S. Gonzalez-Sevilla,[56] L. Goossens,[36] B. Gorini,[36] E. Gorini,[70a,70b] A. Gorišek,[94] T. C. Gosart,[129] A. T. Goshaw,[51] M. I. Gostkin,[38] S. Goswami,[122] C. A. Gottardo,[36] S. A. Gotz,[110] M. Gouighri,[35b] V. Goumarre,[48] A. G. Goussiou,[139] N. Govender,[33c] I. Grabowska-Bold,[86a] K. Graham,[34] E. Gramstad,[126] S. Grancagnolo,[70a,70b] C. M. Grant,[1,136] P. M. Gravila,[27f] F. G. Gravili,[70a,70b] H. M. Gray,[17a] M. Greco,[70a,70b] C. Grefe,[24] I. M. Gregor,[48] P. Grenier,[144] S. G. Grewe,[111] A. A. Grillo,[137] K. Grimm,[31] S. Grinstein,[13,u] J.-F. Grivaz,[66] E. Gross,[170] J. Grosse-Knetter,[55] J. C. Grundy,[127] L. Guan,[107] C. Gubbels,[165] J. G. R. Guerrero Rojas,[164] G. Guerrieri,[69a,69c] F. Guescini,[111] R. Gugel,[101] J. A. M. Guhit,[107] A. Guida,[18] E. Guilloton,[168] S. Guindon,[36] F. Guo,[14a,14e] J. Guo,[62c] L. Guo,[48] Y. Guo,[107] R. Gupta,[48] R. Gupta,[130] S. Gurbuz,[24] S. S. Gurdasani,[54] G. Gustavino,[36] M. Guth,[56] P. Gutierrez,[121] L. F. Gutierrez Zagazeta,[129] M. Gutsche,[50] C. Gutschow,[97] C. Gwenlan,[127] C. B. Gwilliam,[93] E. S. Haaland,[126] A. Haas,[118] M. Habedank,[48] C. Haber,[17a] H. K. Hadavand,[8] A. Hadef,[50] S. Hadzic,[111] A. I. Hagan,[92] J. J. Hahn,[142] E. H. Haines,[97] M. Haleem,[167] J. Haley,[122] J. J. Hall,[140] G. D. Hallewell,[103] L. Halser,[19] K. Hamano,[166] M. Hamer,[24] G. N. Hamity,[52] E. J. Hampshire,[96] J. Han,[62b] K. Han,[62a] L. Han,[14c] L. Han,[62a] S. Han,[17a] Y. F. Han,[156] K. Hanagaki,[84] M. Hance,[137] D. A. Hangal,[41] H. Hanif,[143] M. D. Hank,[129] J. B. Hansen,[42] P. H. Hansen,[42] K. Hara,[158] D. Harada,[56] T. Harenberg,[172] S. Harkusha,[37] M. L. Harris,[104] Y. T. Harris,[127] J. Harrison,[13] N. M. Harrison,[120] P. F. Harrison,[168] N. M. Hartman,[111] N. M. Hartmann,[110] Y. Hasegawa,[141] F. Haslbeck,[127] R. Hauser,[108] C. M. Hawkes,[20] R. J. Hawkings,[36] Y. Hayashi,[154] S. Hayashida,[112] D. Hayden,[108] C. Hayes,[107] R. L. Hayes,[115] C. P. Hays,[127] J. M. Hays,[95] H. S. Hayward,[93] F. He,[62a] M. He,[14a,14e] Y. He,[155] Y. He,[48] Y. He,[97] N. B. Heatley,[95] V. Hedberg,[99] A. L. Heggelund,[126] N. D. Hehir,[95,a] C. Heidegger,[54] K. K. Heidegger,[54] W. D. Heidorn,[81] J. Heilman,[34] S. Heim,[48] T. Heim,[17a] J. G. Heinlein,[129] J. J. Heinrich,[124] L. Heinrich,[111,v] J. Hejbal,[132] A. Held,[171] S. Hellesund,[16] C. M. Helling,[165] S. Hellman,[47a,47b] R. C. W. Henderson,[92] L. Henkelmann,[32] A. M. Henriques Correia,[36] H. Herde,[99] Y. Hernández Jiménez,[146] L. M. Herrmann,[24] T. Herrmann,[50] G. Herten,[54] R. Hertenberger,[110] L. Hervas,[36] M. E. Hesping,[101] N. P. Hessey,[157a] E. Hill,[156] S. J. Hillier,[20] J. R. Hinds,[108] F. Hinterkeuser,[24] M. Hirose,[125] S. Hirose,[158] D. Hirschbuehl,[172] T. G. Hitchings,[102] B. Hiti,[94] J. Hobbs,[146] R. Hobincu,[27e] N. Hod,[170] M. C. Hodgkinson,[140] B. H. Hodkinson,[127]

A. Hoecker,[36] D. D. Hofer,[107] J. Hofer,[48] T. Holm,[24] M. Holzbock,[111] L. B. A. H. Hommels,[32] B. P. Honan,[102] J. Hong,[62c] T. M. Hong,[130] B. H. Hooberman,[163] W. H. Hopkins,[6] Y. Horii,[112] S. Hou,[149] A. S. Howard,[94] J. Howarth,[59] J. Hoya,[6] M. Hrabovsky,[123] A. Hrynevich,[48] T. Hryn'ova,[4] P. J. Hsu,[65] S.-C. Hsu,[139] Q. Hu,[62a] S. Huang,[64b] X. Huang,[14a,14e] Y. Huang,[140] Y. Huang,[14a] Z. Huang,[102] Z. Hubacek,[133] M. Huebner,[24] F. Huegging,[24] T. B. Huffman,[127] C. A. Hugli,[48] M. Huhtinen,[36] S. K. Huiberts,[16] R. Hulsken,[105] N. Huseynov,[12] J. Huston,[108] J. Huth,[61] R. Hyneman,[144] G. Iacobucci,[56] G. Iakovidis,[29] I. Ibragimov,[142] L. Iconomidou-Fayard,[66] J. P. Iddon,[36] P. Iengo,[72a,72b] R. Iguchi,[154] T. Iizawa,[127] Y. Ikegami,[84] N. Ilic,[156] H. Imam,[35a] M. Ince Lezki,[56] T. Ingebretsen Carlson,[47a,47b] G. Introzzi,[73a,73b] M. Iodice,[77a] V. Ippolito,[75a,75b] R. K. Irwin,[93] M. Ishino,[154] W. Islam,[171] C. Issever,[18,48] S. Istin,[21a,w] H. Ito,[169] R. Iuppa,[78a,78b] A. Ivina,[170] J. M. Izen,[45] V. Izzo,[72a] P. Jacka,[132,133] P. Jackson,[1] B. P. Jaeger,[143] C. S. Jagfeld,[110] G. Jain,[157a] P. Jain,[54] K. Jakobs,[54] T. Jakoubek,[170] J. Jamieson,[59] K. W. Janas,[86a] M. Javurkova,[104] L. Jeanty,[124] J. Jejelava,[150a,x] P. Jenni,[54,y] C. E. Jessiman,[34] C. Jia,[62b] J. Jia,[146] X. Jia,[61] X. Jia,[14a,14e] Z. Jia,[14c] S. Jiggins,[48] J. Jimenez Pena,[13] S. Jin,[14c] A. Jinaru,[27b] O. Jinnouchi,[155] P. Johansson,[140] K. A. Johns,[7] J. W. Johnson,[137] D. M. Jones,[32] E. Jones,[48] P. Jones,[32] R. W. L. Jones,[92] T. J. Jones,[93] H. L. Joos,[55,36] R. Joshi,[120] J. Jovicevic,[15] X. Ju,[17a] J. J. Junggeburth,[104] T. Junkermann,[63a] A. Juste Rozas,[13,u] M. K. Juzek,[87] S. Kabana,[138e] A. Kaczmarska,[87] M. Kado,[111] H. Kagan,[120] M. Kagan,[144] A. Kahn,[41] A. Kahn,[129] C. Kahra,[101] T. Kaji,[154] E. Kajomovitz,[151] N. Kakati,[170] I. Kalaitzidou,[54] C. W. Kalderon,[29] N. J. Kang,[137] D. Kar,[33g] K. Karava,[127] M. J. Kareem,[157b] E. Karentzos,[54] I. Karkanias,[153] O. Karkout,[115] S. N. Karpov,[38] Z. M. Karpova,[38] V. Kartvelishvili,[92] A. N. Karyukhin,[37] E. Kasimi,[153] J. Katzy,[48] S. Kaur,[34] K. Kawade,[141] M. P. Kawale,[121] C. Kawamoto,[88] T. Kawamoto,[62a] E. F. Kay,[36] F. I. Kaya,[159] S. Kazakos,[108] V. F. Kazanin,[37] Y. Ke,[146] J. M. Keaveney,[33a] R. Keeler,[166] G. V. Kehris,[61] J. S. Keller,[34] A. S. Kelly,[97] J. J. Kempster,[147] P. D. Kennedy,[101] O. Kepka,[132] B. P. Kerridge,[135] S. Kersten,[172] B. P. Kerševan,[94] L. Keszeghova,[28a] S. Ketabchi Haghighat,[156] R. A. Khan,[130] A. Khanov,[122] A. G. Kharlamov,[37] T. Kharlamova,[37] E. E. Khoda,[139] M. Kholodenko,[37] T. J. Khoo,[18] G. Khoriauli,[167] J. Khubua,[150b] Y. A. R. Khwaira,[66] B. Kibirige,[33g] A. Kilgallon,[124] D. W. Kim,[47a,47b] Y. K. Kim,[39] N. Kimura,[97] M. K. Kingston,[55] A. Kirchhoff,[55] C. Kirfel,[24] F. Kirfel,[24] J. Kirk,[135] A. E. Kiryunin,[111] C. Kitsaki,[10] O. Kivernyk,[24] M. Klassen,[63a] C. Klein,[34] L. Klein,[167] M. H. Klein,[44] S. B. Klein,[56] U. Klein,[93] P. Klimek,[36] A. Klimentov,[29] T. Klioutchnikova,[36] P. Kluit,[115] S. Kluth,[111] E. Kneringer,[79] T. M. Knight,[156] A. Knue,[49] R. Kobayashi,[88] D. Kobylianskii,[170] S. F. Koch,[127] M. Kocian,[144] P. Kodyš,[134] D. M. Koeck,[124] P. T. Koenig,[24] T. Koffas,[34] O. Kolay,[50] I. Koletsou,[4] T. Komarek,[123] K. Köneke,[54] A. X. Y. Kong,[1] T. Kono,[119] N. Konstantinidis,[97] P. Kontaxakis,[56] B. Konya,[99] R. Kopeliansky,[41] S. Koperny,[86a] K. Korcyl,[87] K. Kordas,[153,z] A. Korn,[97] S. Korn,[55] I. Korolkov,[13] N. Korotkova,[37] B. Kortman,[115] O. Kortner,[111] S. Kortner,[111] W. H. Kostecka,[116] V. V. Kostyukhin,[142] A. Kotsokechagia,[136] A. Kotwal,[51] A. Koulouris,[36] A. Kourkoumeli-Charalampidi,[73a,73b] C. Kourkoumelis,[9] E. Kourlitis,[111,v] O. Kovanda,[124] R. Kowalewski,[166] W. Kozanecki,[136] A. S. Kozhin,[37] V. A. Kramarenko,[37] G. Kramberger,[94] P. Kramer,[101] M. W. Krasny,[128] A. Krasznahorkay,[36] J. W. Kraus,[172] J. A. Kremer,[48] T. Kresse,[50] J. Kretzschmar,[93] K. Kreul,[18] P. Krieger,[156] S. Krishnamurthy,[104] M. Krivos,[134] K. Krizka,[20] K. Kroeninger,[49] H. Kroha,[111] J. Kroll,[132] J. Kroll,[129] K. S. Krowpman,[108] U. Kruchonak,[38] H. Krüger,[24] N. Krumnack,[81] M. C. Kruse,[51] O. Kuchinskaia,[37] S. Kuday,[3a] S. Kuehn,[36] R. Kuesters,[54] T. Kuhl,[48] V. Kukhtin,[38] Y. Kulchitsky,[37,k] S. Kuleshov,[138d,138b] M. Kumar,[33g] N. Kumari,[48] P. Kumari,[157b] A. Kupco,[132] T. Kupfer,[49] A. Kupich,[37] O. Kuprash,[54] H. Kurashige,[85] L. L. Kurchaninov,[157a] O. Kurdysh,[66] Y. A. Kurochkin,[37] A. Kurova,[37] M. Kuze,[155] A. K. Kvam,[104] J. Kvita,[123] T. Kwan,[105] N. G. Kyriacou,[107] L. A. O. Laatu,[103] C. Lacasta,[164] F. Lacava,[75a,75b] H. Lacker,[18] D. Lacour,[128] N. N. Lad,[97] E. Ladygin,[38] A. Lafarge,[40] B. Laforge,[128] T. Lagouri,[173] F. Z. Lahbabi,[35a] S. Lai,[55] I. K. Lakomiec,[86a] N. Lalloue,[60] J. E. Lambert,[166] S. Lammers,[68] W. Lampl,[7] C. Lampoudis,[153,z] G. Lamprinoudis,[101] A. N. Lancaster,[116] E. Lançon,[29] U. Landgraf,[54] M. P. J. Landon,[95] V. S. Lang,[54] O. K. B. Langrekken,[126] A. J. Lankford,[160] F. Lanni,[36] K. Lantzsch,[24] A. Lanza,[73a] A. Lapertosa,[57b,57a] J. F. Laporte,[136] T. Lari,[71a] F. Lasagni Manghi,[23b] M. Lassnig,[36] V. Latonova,[132] A. Laudrain,[101] A. Laurier,[151] S. D. Lawlor,[140] Z. Lawrence,[102] R. Lazaridou,[168] M. Lazzaroni,[71a,71b] B. Le,[102] E. M. Le Boulicaut,[51] B. Leban,[23b,23a] A. Lebedev,[81] M. LeBlanc,[102] F. Ledroit-Guillon,[60] A. C. A. Lee,[97] S. C. Lee,[149] S. Lee,[47a,47b] T. F. Lee,[93] L. L. Leeuw,[33c] H. P. Lefebvre,[96] M. Lefebvre,[166] C. Leggett,[17a] G. Lehmann Miotto,[36] M. Leigh,[56]

W. A. Leight,[104] W. Leinonen,[114] A. Leisos,[153,aa] M. A. L. Leite,[83c] C. E. Leitgeb,[18] R. Leitner,[134] K. J. C. Leney,[44] T. Lenz,[24] S. Leone,[74a] C. Leonidopoulos,[52] A. Leopold,[145] C. Leroy,[109] R. Les,[108] C. G. Lester,[32] M. Levchenko,[37] J. Levêque,[4] L. J. Levinson,[170] G. Levrini,[23b,23a] M. P. Lewicki,[87] D. J. Lewis,[4] A. Li,[5] B. Li,[62b] C. Li,[62a] C-Q. Li,[111] H. Li,[62a] H. Li,[62b] H. Li,[14c] H. Li,[14b] H. Li,[62b] J. Li,[62c] K. Li,[139] L. Li,[62c] M. Li,[14a,14e] Q. Y. Li,[62a] S. Li,[14a,14e] S. Li,[62d,62c,bb] T. Li,[5] X. Li,[105] Z. Li,[127] Z. Li,[154] Z. Li,[14a,14e] S. Liang,[14a,14e] Z. Liang,[14a] M. Liberatore,[136] B. Liberti,[76a] K. Lie,[64c] J. Lieber Marin,[83b] H. Lien,[68] K. Lin,[108] R. E. Lindley,[7] J. H. Lindon,[2] E. Lipeles,[129] A. Lipniacka,[16] A. Lister,[165] J. D. Little,[4] B. Liu,[14a] B. X. Liu,[143] D. Liu,[62d,62c] E. H. L. Liu,[20] J. B. Liu,[62a] J. K. K. Liu,[32] K. Liu,[62d] K. Liu,[62d,62c] M. Liu,[62a] M. Y. Liu,[62a] P. Liu,[14a] Q. Liu,[62d,139,62c] X. Liu,[62a] X. Liu,[62b] Y. Liu,[14d,14e] Y. L. Liu,[62b] Y. W. Liu,[62a] J. Llorente Merino,[143] S. L. Lloyd,[95] E. M. Lobodzinska,[48] P. Loch,[7] T. Lohse,[18] K. Lohwasser,[140] E. Loiacono,[48] M. Lokajicek,[132,a] J. D. Lomas,[20] J. D. Long,[163] I. Longarini,[160] L. Longo,[70a,70b] R. Longo,[163] I. Lopez Paz,[67] A. Lopez Solis,[48] N. Lorenzo Martinez,[4] A. M. Lory,[110] G. Löschcke Centeno,[147] O. Loseva,[37] X. Lou,[47a,47b] X. Lou,[14a,14e] A. Lounis,[66] P. A. Love,[92] G. Lu,[14a,14e] M. Lu,[80] S. Lu,[129] Y. J. Lu,[65] H. J. Lubatti,[139] C. Luci,[75a,75b] F. L. Lucio Alves,[14c] F. Luehring,[68] I. Luise,[146] O. Lukianchuk,[66] O. Lundberg,[145] B. Lund-Jensen,[145,a] N. A. Luongo,[6] M. S. Lutz,[36] A. B. Lux,[25] D. Lynn,[29] R. Lysak,[132] E. Lytken,[99] V. Lyubushkin,[38] T. Lyubushkina,[38] M. M. Lyukova,[146] H. Ma,[29] K. Ma,[62a] L. L. Ma,[62b] W. Ma,[62a] Y. Ma,[122] D. M. Mac Donell,[166] G. Maccarrone,[53] J. C. MacDonald,[101] P. C. Machado De Abreu Farias,[83b] R. Madar,[40] T. Madula,[97] J. Maeda,[85] T. Maeno,[29] H. Maguire,[140] V. Maiboroda,[136] A. Maio,[131a,131b,131d] K. Maj,[86a] O. Majersky,[48] S. Majewski,[124] N. Makovec,[66] V. Maksimovic,[15] B. Malaescu,[128] Pa. Malecki,[87] V. P. Maleev,[37] F. Malek,[60,cc] M. Mali,[94] D. Malito,[96] U. Mallik,[80] S. Maltezos,[10] S. Malyukov,[38] J. Mamuzic,[13] G. Mancini,[53] M. N. Mancini,[26] G. Manco,[73a,73b] J. P. Mandalia,[95] I. Mandić,[94] L. Manhaes de Andrade Filho,[83a] I. M. Maniatis,[170] J. Manjarres Ramos,[90] D. C. Mankad,[170] A. Mann,[110] S. Manzoni,[36] L. Mao,[62c] X. Mapekula,[33c] A. Marantis,[153,aa] G. Marchiori,[5] M. Marcisovsky,[132] C. Marcon,[71a] M. Marinescu,[20] S. Marium,[48] M. Marjanovic,[121] M. Markovitch,[66] E. J. Marshall,[92] Z. Marshall,[17a] S. Marti-Garcia,[164] T. A. Martin,[168] V. J. Martin,[52] B. Martin dit Latour,[16] L. Martinelli,[75a,75b] M. Martinez,[13,u] P. Martinez Agullo,[164] V. I. Martinez Outschoorn,[104] P. Martinez Suarez,[13] S. Martin-Haugh,[135] G. Martinovicova,[134] V. S. Martoiu,[27b] A. C. Martyniuk,[97] A. Marzin,[36] D. Mascione,[78a,78b] L. Masetti,[101] T. Mashimo,[154] J. Masik,[102] A. L. Maslennikov,[37] P. Massarotti,[72a,72b] P. Mastrandrea,[74a,74b] A. Mastroberardino,[43b,43a] T. Masubuchi,[154] T. Mathisen,[162] J. Matousek,[134] N. Matsuzawa,[154] J. Maurer,[27b] A. J. Maury,[66] B. Maček,[94] D. A. Maximov,[37] R. Mazini,[149] I. Maznas,[116] M. Mazza,[108] S. M. Mazza,[137] E. Mazzeo,[71a,71b] C. Mc Ginn,[29] J. P. Mc Gowan,[166] S. P. Mc Kee,[107] C. C. McCracken,[165] E. F. McDonald,[106] A. E. McDougall,[115] J. A. Mcfayden,[147] R. P. McGovern,[129] G. Mchedlidze,[150b] R. P. Mckenzie,[33g] T. C. Mclachlan,[48] D. J. Mclaughlin,[97] S. J. McMahon,[135] C. M. Mcpartland,[93] R. A. McPherson,[166,n] S. Mehlhase,[110] A. Mehta,[93] D. Melini,[164] B. R. Mellado Garcia,[33g] A. H. Melo,[55] F. Meloni,[48] A. M. Mendes Jacques Da Costa,[102] H. Y. Meng,[156] L. Meng,[92] S. Menke,[111] M. Mentink,[36] E. Meoni,[43b,43a] G. Mercado,[116] C. Merlassino,[69a,69c] L. Merola,[72a,72b] C. Meroni,[71a,71b] J. Metcalfe,[6] A. S. Mete,[6] C. Meyer,[68] J-P. Meyer,[136] R. P. Middleton,[135] L. Mijović,[52] G. Mikenberg,[170] M. Mikestikova,[132] M. Mikuž,[94] H. Mildner,[101] A. Milic,[36] D. W. Miller,[39] E. H. Miller,[144] L. S. Miller,[34] A. Milov,[170] D. A. Milstead,[47a,47b] T. Min,[14c] A. A. Minaenko,[37] I. A. Minashvili,[150b] L. Mince,[59] A. I. Mincer,[118] B. Mindur,[86a] M. Mineev,[38] Y. Mino,[88] L. M. Mir,[13] M. Miralles Lopez,[59] M. Mironova,[17a] A. Mishima,[154] M. C. Missio,[114] A. Mitra,[168] V. A. Mitsou,[164] Y. Mitsumori,[112] O. Miu,[156] P. S. Miyagawa,[95] T. Mkrtchyan,[63a] M. Mlinarevic,[97] T. Mlinarevic,[97] M. Mlynarikova,[36] S. Mobius,[19] P. Mogg,[110] M. H. Mohamed Farook,[113] A. F. Mohammed,[14a,14e] S. Mohapatra,[41] G. Mokgatitswane,[33g] L. Moleri,[170] B. Mondal,[142] S. Mondal,[133] K. Mönig,[48] E. Monnier,[103] L. Monsonis Romero,[164] J. Montejo Berlingen,[13] M. Montella,[120] F. Montereali,[77a,77b] F. Monticelli,[91] S. Monzani,[69a,69c] N. Morange,[66] A. L. Moreira De Carvalho,[131a] M. Moreno Llácer,[164] C. Moreno Martinez,[56] P. Morettini,[57b] S. Morgenstern,[36] M. Morii,[61] M. Morinaga,[154] F. Morodei,[75a,75b] L. Morvaj,[36] P. Moschovakos,[36] B. Moser,[36] M. Mosidze,[150b] T. Moskalets,[54] P. Moskvitina,[114] J. Moss,[31,dd] A. Moussa,[35d] E. J. W. Moyse,[104] O. Mtintsilana,[33g] S. Muanza,[103] J. Mueller,[130] D. Muenstermann,[92] R. Müller,[19] G. A. Mullier,[162] A. J. Mullin,[32] J. J. Mullin,[129] D. P. Mungo,[156] D. Munoz Perez,[164] F. J. Munoz Sanchez,[102] M. Murin,[102] W. J. Murray,[168,135] M. Muškinja,[94]

C. Mwewa,[29] A. G. Myagkov,[37,k] A. J. Myers,[8] G. Myers,[107] M. Myska,[133] B. P. Nachman,[17a] O. Nackenhorst,[49] K. Nagai,[127] K. Nagano,[84] J. L. Nagle,[29,o] E. Nagy,[103] A. M. Nairz,[36] Y. Nakahama,[84] K. Nakamura,[84] K. Nakkalil,[5] H. Nanjo,[125] R. Narayan,[44] E. A. Narayanan,[113] I. Naryshkin,[37] M. Naseri,[34] S. Nasri,[117b] C. Nass,[24] G. Navarro,[22a] J. Navarro-Gonzalez,[164] R. Nayak,[152] A. Nayaz,[18] P. Y. Nechaeva,[37] F. Nechansky,[48] L. Nedic,[127] T. J. Neep,[20] A. Negri,[73a,73b] M. Negrini,[23b] C. Nellist,[115] C. Nelson,[105] K. Nelson,[107] S. Nemecek,[132] M. Nessi,[36,ee] M. S. Neubauer,[163] F. Neuhaus,[101] J. Neundorf,[48] R. Newhouse,[165] P. R. Newman,[20] C. W. Ng,[130] Y. W. Y. Ng,[48] B. Ngair,[117a] H. D. N. Nguyen,[109] R. B. Nickerson,[127] R. Nicolaidou,[136] J. Nielsen,[137] M. Niemeyer,[55] J. Niermann,[55] N. Nikiforou,[36] V. Nikolaenko,[37,k] I. Nikolic-Audit,[128] K. Nikolopoulos,[20] P. Nilsson,[29] I. Ninca,[48] H. R. Nindhito,[56] G. Ninio,[152] A. Nisati,[75a] N. Nishu,[2] R. Nisius,[111] J-E. Nitschke,[50] E. K. Nkadimeng,[33g] T. Nobe,[154] D. L. Noel,[32] T. Nommensen,[148] M. B. Norfolk,[140] R. R. B. Norisam,[97] B. J. Norman,[34] M. Noury,[35a] J. Novak,[94] T. Novak,[48] L. Novotny,[133] R. Novotny,[113] L. Nozka,[123] K. Ntekas,[160] N. M. J. Nunes De Moura Junior,[83b] J. Ocariz,[128] A. Ochi,[85] I. Ochoa,[131a] S. Oerdek,[48,ff] J. T. Offermann,[39] A. Ogrodnik,[134] A. Oh,[102] C. C. Ohm,[145] H. Oide,[84] R. Oishi,[154] M. L. Ojeda,[48] Y. Okumura,[154] L. F. Oleiro Seabra,[131a] S. A. Olivares Pino,[138d] D. Oliveira Damazio,[29] D. Oliveira Goncalves,[83a] J. L. Oliver,[160] Ö. O. Öncel,[54] A. P. O'Neill,[19] A. Onofre,[131a,131e] P. U. E. Onyisi,[11] M. J. Oreglia,[39] G. E. Orellana,[91] D. Orestano,[77a,77b] N. Orlando,[13] R. S. Orr,[156] V. O'Shea,[59] L. M. Osojnak,[129] R. Ospanov,[62a] G. Otero y Garzon,[30] H. Otono,[89] P. S. Ott,[63a] G. J. Ottino,[17a] M. Ouchrif,[35d] F. Ould-Saada,[126] T. Ovsiannikova,[139] M. Owen,[59] R. E. Owen,[135] K. Y. Oyulmaz,[21a] V. E. Ozcan,[21a] F. Ozturk,[87] N. Ozturk,[8] S. Ozturk,[82] H. A. Pacey,[127] A. Pacheco Pages,[13] C. Padilla Aranda,[13] G. Padovano,[75a,75b] S. Pagan Griso,[17a] G. Palacino,[68] A. Palazzo,[70a,70b] J. Pampel,[24] J. Pan,[173] T. Pan,[64a] D. K. Panchal,[11] C. E. Pandini,[115] J. G. Panduro Vazquez,[96] H. D. Pandya,[1] H. Pang,[14b] P. Pani,[48] G. Panizzo,[69a,69c] L. Panwar,[128] L. Paolozzi,[56] S. Parajuli,[163] A. Paramonov,[6] C. Paraskevopoulos,[53] D. Paredes Hernandez,[64b] A. Pareti,[73a,73b] K. R. Park,[41] T. H. Park,[156] M. A. Parker,[32] F. Parodi,[57b,57a] E. W. Parrish,[116] V. A. Parrish,[52] J. A. Parsons,[41] U. Parzefall,[54] B. Pascual Dias,[109] L. Pascual Dominguez,[152] E. Pasqualucci,[75a] S. Passaggio,[57b] F. Pastore,[96] P. Patel,[87] U. M. Patel,[51] J. R. Pater,[102] T. Pauly,[36] C. I. Pazos,[159] J. Pearkes,[144] M. Pedersen,[126] R. Pedro,[131a] S. V. Peleganchuk,[37] O. Penc,[36] E. A. Pender,[52] G. D. Penn,[173] K. E. Penski,[110] M. Penzin,[37] B. S. Peralva,[83d] A. P. Pereira Peixoto,[139] L. Pereira Sanchez,[144] D. V. Perepelitsa,[29,o] E. Perez Codina,[157a] M. Perganti,[10] H. Pernegger,[36] O. Perrin,[40] K. Peters,[48] R. F. Y. Peters,[102] B. A. Petersen,[36] T. C. Petersen,[42] E. Petit,[103] V. Petousis,[133] C. Petridou,[153,z] T. Petru,[134] A. Petrukhin,[142] M. Pettee,[17a] N. E. Pettersson,[36] A. Petukhov,[37] K. Petukhova,[134] R. Pezoa,[138f] L. Pezzotti,[36] G. Pezzullo,[173] T. M. Pham,[171] T. Pham,[106] P. W. Phillips,[135] G. Piacquadio,[146] E. Pianori,[17a] F. Piazza,[124] R. Piegaia,[30] D. Pietreanu,[27b] A. D. Pilkington,[102] M. Pinamonti,[69a,69c] J. L. Pinfold,[2] B. C. Pinheiro Pereira,[131a] A. E. Pinto Pinoargote,[101,136] L. Pintucci,[69a,69c] K. M. Piper,[147] A. Pirttikoski,[56] D. A. Pizzi,[34] L. Pizzimento,[64b] A. Pizzini,[115] M.-A. Pleier,[29] V. Plesanovs,[54] V. Pleskot,[134] E. Plotnikova,[38] G. Poddar,[95] R. Poettgen,[99] L. Poggioli,[128] I. Pokharel,[55] S. Polacek,[134] G. Polesello,[73a] A. Poley,[143,157a] A. Polini,[23b] C. S. Pollard,[168] Z. B. Pollock,[120] E. Pompa Pacchi,[75a,75b] D. Ponomarenko,[114] L. Pontecorvo,[36] S. Popa,[27a] G. A. Popeneciu,[27d] A. Poreba,[36] D. M. Portillo Quintero,[157a] S. Pospisil,[133] M. A. Postill,[140] P. Postolache,[27c] K. Potamianos,[168] P. A. Potepa,[86a] I. N. Potrap,[38] C. J. Potter,[32] H. Potti,[1] J. Poveda,[164] M. E. Pozo Astigarraga,[36] A. Prades Ibanez,[164] J. Pretel,[54] D. Price,[102] M. Primavera,[70a] M. A. Principe Martin,[100] R. Privara,[123] T. Procter,[59] M. L. Proffitt,[139] N. Proklova,[129] K. Prokofiev,[64c] G. Proto,[111] J. Proudfoot,[6] M. Przybycien,[86a] W. W. Przygoda,[86b] A. Psallidas,[46] J. E. Puddefoot,[140] D. Pudzha,[37] D. Pyatiizbyantseva,[37] J. Qian,[107] D. Qichen,[102] Y. Qin,[13] T. Qiu,[52] A. Quadt,[55] M. Queitsch-Maitland,[102] G. Quetant,[56] R. P. Quinn,[165] G. Rabanal Bolanos,[61] D. Rafanoharana,[54] F. Ragusa,[71a,71b] J. L. Rainbolt,[39] J. A. Raine,[56] S. Rajagopalan,[29] E. Ramakoti,[37] I. A. Ramirez-Berend,[34] K. Ran,[48,14e] N. P. Rapheeha,[33g] H. Rasheed,[27b] V. Raskina,[128] D. F. Rassloff,[63a] A. Rastogi,[17a] S. Rave,[101] B. Ravina,[55] I. Ravinovich,[170] M. Raymond,[36] A. L. Read,[126] N. P. Readioff,[140] D. M. Rebuzzi,[73a,73b] G. Redlinger,[29] A. S. Reed,[111] K. Reeves,[26] J. A. Reidelsturz,[172] D. Reikher,[152] A. Rej,[49] C. Rembser,[36] M. Renda,[27b] M. B. Rendel,[111] F. Renner,[48] A. G. Rennie,[160] A. L. Rescia,[48] S. Resconi,[71a] M. Ressegotti,[57b,57a] S. Rettie,[36] J. G. Reyes Rivera,[108] E. Reynolds,[17a] O. L. Rezanova,[37] P. Reznicek,[134] H. Riani,[35d] N. Ribaric,[92] E. Ricci,[78a,78b] R. Richter,[111] S. Richter,[47a,47b]

E. Richter-Was,[86b] M. Ridel,[128] S. Ridouani,[35d] P. Rieck,[118] P. Riedler,[36] E. M. Riefel,[47a,47b] J. O. Rieger,[115] M. Rijssenbeek,[146] M. Rimoldi,[36] L. Rinaldi,[23b,23a] T. T. Rinn,[29] M. P. Rinnagel,[110] G. Ripellino,[162] I. Riu,[13] J. C. Rivera Vergara,[166] F. Rizatdinova,[122] E. Rizvi,[95] B. R. Roberts,[17a] S. H. Robertson,[105,n] D. Robinson,[32] C. M. Robles Gajardo,[138f] M. Robles Manzano,[101] A. Robson,[59] A. Rocchi,[76a,76b] C. Roda,[74a,74b] S. Rodriguez Bosca,[36] Y. Rodriguez Garcia,[22a] A. Rodriguez Rodriguez,[54] A. M. Rodríguez Vera,[116] S. Roe,[36] J. T. Roemer,[160] A. R. Roepe-Gier,[137] J. Roggel,[172] O. Røhne,[126] R. A. Rojas,[104] C. P. A. Roland,[128] J. Roloff,[29] A. Romaniouk,[37] E. Romano,[73a,73b] M. Romano,[23b] A. C. Romero Hernandez,[163] N. Rompotis,[93] L. Roos,[128] S. Rosati,[75a] B. J. Rosser,[39] E. Rossi,[127] E. Rossi,[72a,72b] L. P. Rossi,[61] L. Rossini,[54] R. Rosten,[120] M. Rotaru,[27b] B. Rottler,[54] C. Rougier,[90] D. Rousseau,[66] D. Rousso,[32] A. Roy,[163] S. Roy-Garand,[156] A. Rozanov,[103] Z. M. A. Rozario,[59] Y. Rozen,[151] A. Rubio Jimenez,[164] A. J. Ruby,[93] V. H. Ruelas Rivera,[18] T. A. Ruggeri,[1] A. Ruggiero,[127] A. Ruiz-Martinez,[164] A. Rummler,[36] Z. Rurikova,[54] N. A. Rusakovich,[38] H. L. Russell,[166] G. Russo,[75a,75b] J. P. Rutherfoord,[7] S. Rutherford Colmenares,[32] K. Rybacki,[92] M. Rybar,[134] E. B. Rye,[126] A. Ryzhov,[44] J. A. Sabater Iglesias,[56] P. Sabatini,[164] H. F-W. Sadrozinski,[137] F. Safai Tehrani,[75a] B. Safarzadeh Samani,[135] M. Safdari,[144] S. Saha,[1] M. Sahinsoy,[111] A. Saibel,[164] M. Saimpert,[136] M. Saito,[154] T. Saito,[154] D. Salamani,[36] A. Salnikov,[144] J. Salt,[164] A. Salvador Salas,[152] D. Salvatore,[43b,43a] F. Salvatore,[147] A. Salzburger,[36] D. Sammel,[54] E. Sampson,[92] D. Sampsonidis,[153,z] D. Sampsonidou,[124] J. Sánchez,[164] V. Sanchez Sebastian,[164] H. Sandaker,[126] C. O. Sander,[48] J. A. Sandesara,[104] M. Sandhoff,[172] C. Sandoval,[22b] D. P. C. Sankey,[135] T. Sano,[88] A. Sansoni,[53] L. Santi,[75a,75b] C. Santoni,[40] H. Santos,[131a,131b] A. Santra,[170] K. A. Saoucha,[161] J. G. Saraiva,[131a,131d] J. Sardain,[7] O. Sasaki,[84] K. Sato,[158] C. Sauer,[63b] F. Sauerburger,[54] E. Sauvan,[4] P. Savard,[156,e] R. Sawada,[154] C. Sawyer,[135] L. Sawyer,[98] I. Sayago Galvan,[164] C. Sbarra,[23b] A. Sbrizzi,[23b,23a] T. Scanlon,[97] J. Schaarschmidt,[139] U. Schäfer,[101] A. C. Schaffer,[66,44] D. Schaile,[110] R. D. Schamberger,[146] C. Scharf,[18] M. M. Schefer,[19] V. A. Schegelsky,[37] D. Scheirich,[134] F. Schenck,[18] M. Schernau,[160] C. Scheulen,[55] C. Schiavi,[57b,57a] M. Schioppa,[43b,43a] B. Schlag,[144,s] K. E. Schleicher,[54] S. Schlenker,[36] J. Schmeing,[172] M. A. Schmidt,[172] K. Schmieden,[101] C. Schmitt,[101] N. Schmitt,[101] S. Schmitt,[48] L. Schoeffel,[136] A. Schoening,[63b] P. G. Scholer,[34] E. Schopf,[127] M. Schott,[101] J. Schovancova,[36] S. Schramm,[56] T. Schroer,[56] H-C. Schultz-Coulon,[63a] M. Schumacher,[54] B. A. Schumm,[137] Ph. Schune,[136] A. J. Schuy,[139] H. R. Schwartz,[137] A. Schwartzman,[144] T. A. Schwarz,[107] Ph. Schwemling,[136] R. Schwienhorst,[108] A. Sciandra,[137] G. Sciolla,[26] F. Scuri,[74a] C. D. Sebastiani,[93] K. Sedlaczek,[116] P. Seema,[18] S. C. Seidel,[113] A. Seiden,[137] B. D. Seidlitz,[41] C. Seitz,[48] J. M. Seixas,[83b] G. Sekhniaidze,[72a] L. Selem,[60] N. Semprini-Cesari,[23b,23a] D. Sengupta,[56] V. Senthilkumar,[164] L. Serin,[66] L. Serkin,[69a,69b] M. Sessa,[76a,76b] H. Severini,[121] F. Sforza,[57b,57a] A. Sfyrla,[56] Q. Sha,[14a] E. Shabalina,[55] R. Shaheen,[145] J. D. Shahinian,[129] D. Shaked Renous,[170] L. Y. Shan,[14a] M. Shapiro,[17a] A. Sharma,[36] A. S. Sharma,[165] P. Sharma,[80] P. B. Shatalov,[37] K. Shaw,[147] S. M. Shaw,[102] A. Shcherbakova,[37] Q. Shen,[62c,5] D. J. Sheppard,[143] P. Sherwood,[97] L. Shi,[97] X. Shi,[14a] C. O. Shimmin,[173] J. D. Shinner,[96] I. P. J. Shipsey,[127] S. Shirabe,[89] M. Shiyakova,[38,gg] J. Shlomi,[170] M. J. Shochet,[39] J. Shojaii,[106] D. R. Shope,[126] B. Shrestha,[121] S. Shrestha,[120,hh] E. M. Shrif,[33g] M. J. Shroff,[166] P. Sicho,[132] A. M. Sickles,[163] E. Sideras Haddad,[33g] A. Sidoti,[23b] F. Siegert,[50] Dj. Sijacki,[15] F. Sili,[91] J. M. Silva,[52] M. V. Silva Oliveira,[29] S. B. Silverstein,[47a] S. Simion,[66] R. Simoniello,[36] E. L. Simpson,[59] H. Simpson,[147] L. R. Simpson,[107] N. D. Simpson,[99] S. Simsek,[82] S. Sindhu,[55] P. Sinervo,[156] S. Singh,[156] S. Sinha,[48] S. Sinha,[102] M. Sioli,[23b,23a] I. Siral,[36] E. Sitnikova,[48] J. Sjölin,[47a,47b] A. Skaf,[55] E. Skorda,[20] P. Skubic,[121] M. Slawinska,[87] V. Smakhtin,[170] B. H. Smart,[135] S. Yu. Smirnov,[37] Y. Smirnov,[37] L. N. Smirnova,[37,k] O. Smirnova,[99] A. C. Smith,[41] E. A. Smith,[39] H. A. Smith,[127] J. L. Smith,[102] R. Smith,[144] M. Smizanska,[92] K. Smolek,[133] A. A. Snesarev,[37] S. R. Snider,[156] H. L. Snoek,[115] S. Snyder,[29] R. Sobie,[166,n] A. Soffer,[152] C. A. Solans Sanchez,[36] E. Yu. Soldatov,[37] U. Soldevila,[164] A. A. Solodkov,[37] S. Solomon,[26] A. Soloshenko,[38] K. Solovieva,[54] O. V. Solovyanov,[40] V. Solovyev,[37] P. Sommer,[36] A. Sonay,[13] W. Y. Song,[157b] A. Sopczak,[133] A. L. Sopio,[97] F. Sopkova,[28b] J. D. Sorenson,[113] I. R. Sotarriva Alvarez,[155] V. Sothilingam,[63a] O. J. Soto Sandoval,[138c,138b] S. Sottocornola,[68] R. Soualah,[161] Z. Soumaimi,[35e] D. South,[48] N. Soybelman,[170] S. Spagnolo,[70a,70b] M. Spalla,[111] D. Sperlich,[54] G. Spigo,[36] S. Spinali,[92] D. P. Spiteri,[59] M. Spousta,[134] E. J. Staats,[34] R. Stamen,[63a] A. Stampekis,[20] M. Standke,[24] E. Stanecka,[87] M. V. Stange,[50] B. Stanislaus,[17a] M. M. Stanitzki,[48] B. Stapf,[48] E. A. Starchenko,[37] G. H. Stark,[137] J. Stark,[90] P. Staroba,[132] P. Starovoitov,[63a]

S. Stärz,[105] R. Staszewski,[87] G. Stavropoulos,[46] J. Steentoft,[162] P. Steinberg,[29] B. Stelzer,[143,157a] H. J. Stelzer,[130] O. Stelzer-Chilton,[157a] H. Stenzel,[58] T. J. Stevenson,[147] G. A. Stewart,[36] J. R. Stewart,[122] M. C. Stockton,[36] G. Stoicea,[27b] M. Stolarski,[131a] S. Stonjek,[111] A. Straessner,[50] J. Strandberg,[145] S. Strandberg,[47a,47b] M. Stratmann,[172] M. Strauss,[121] T. Strebler,[103] P. Strizenec,[28b] R. Ströhmer,[167] D. M. Strom,[124] R. Stroynowski,[44] A. Strubig,[47a,47b] S. A. Stucci,[29] B. Stugu,[16] J. Stupak,[121] N. A. Styles,[48] D. Su,[144] S. Su,[62a] W. Su,[62d] X. Su,[62a] D. Suchy,[28a] K. Sugizaki,[154] V. V. Sulin,[37] M. J. Sullivan,[93] D. M. S. Sultan,[127] L. Sultanaliyeva,[37] S. Sultansoy,[3b] T. Sumida,[88] S. Sun,[107] S. Sun,[171] O. Sunneborn Gudnadottir,[162] N. Sur,[103] M. R. Sutton,[147] H. Suzuki,[158] M. Svatos,[132] M. Swiatlowski,[157a] T. Swirski,[167] I. Sykora,[28a] M. Sykora,[134] T. Sykora,[134] D. Ta,[101] K. Tackmann,[48,ff] A. Taffard,[160] R. Tafirout,[157a] J. S. Tafoya Vargas,[66] Y. Takubo,[84] M. Talby,[103] A. A. Talyshev,[37] K. C. Tam,[64b] N. M. Tamir,[152] A. Tanaka,[154] J. Tanaka,[154] R. Tanaka,[66] M. Tanasini,[57b,57a] Z. Tao,[165] S. Tapia Araya,[138f] S. Tapprogge,[101] A. Tarek Abouelfadl Mohamed,[108] S. Tarem,[151] K. Tariq,[14a] G. Tarna,[103,27b] G. F. Tartarelli,[71a] P. Tas,[134] M. Tasevsky,[132] E. Tassi,[43b,43a] A. C. Tate,[163] G. Tateno,[154] Y. Tayalati,[35e,ii] G. N. Taylor,[106] W. Taylor,[157b] A. S. Tee,[171] R. Teixeira De Lima,[144] P. Teixeira-Dias,[96] J. J. Teoh,[156] K. Terashi,[154] J. Terron,[100] S. Terzo,[13] M. Testa,[53] R. J. Teuscher,[156,n] A. Thaler,[79] O. Theiner,[56] N. Themistokleous,[52] T. Theveneaux-Pelzer,[103] O. Thielmann,[172] D. W. Thomas,[96] J. P. Thomas,[20] E. A. Thompson,[17a] P. D. Thompson,[20] E. Thomson,[129] R. E. Thornberry,[44] Y. Tian,[55] V. Tikhomirov,[37,k] Yu. A. Tikhonov,[37] S. Timoshenko,[37] D. Timoshyn,[134] E. X. L. Ting,[1] P. Tipton,[173] S. H. Tlou,[33g] K. Todome,[155] S. Todorova-Nova,[134] S. Todt,[50] M. Togawa,[84] J. Tojo,[89] S. Tokár,[28a] K. Tokushuku,[84] O. Toldaiev,[68] R. Tombs,[32] M. Tomoto,[84,112] L. Tompkins,[144,s] K. W. Topolnicki,[86b] E. Torrence,[124] H. Torres,[90] E. Torró Pastor,[164] M. Toscani,[30] C. Tosciri,[39] M. Tost,[11] D. R. Tovey,[140] A. Traeet,[16] I. S. Trandafir,[27b] T. Trefzger,[167] A. Tricoli,[29] I. M. Trigger,[157a] S. Trincaz-Duvoid,[128] D. A. Trischuk,[26] B. Trocmé,[60] L. Truong,[33c] M. Trzebinski,[87] A. Trzupek,[87] F. Tsai,[146] M. Tsai,[107] A. Tsiamis,[153,z] P. V. Tsiareshka,[37] S. Tsigaridas,[157a] A. Tsirigotis,[153,aa] V. Tsiskaridze,[156] E. G. Tskhadadze,[150a] M. Tsopoulou,[153] Y. Tsujikawa,[88] I. I. Tsukerman,[37] V. Tsulaia,[17a] S. Tsuno,[84] K. Tsuri,[119] D. Tsybychev,[146] Y. Tu,[64b] A. Tudorache,[27b] V. Tudorache,[27b] A. N. Tuna,[61] S. Turchikhin,[57b,57a] I. Turk Cakir,[3a] R. Turra,[71a] T. Turtuvshin,[38,jj] P. M. Tuts,[41] S. Tzamarias,[153,z] E. Tzovara,[101] F. Ukegawa,[158] P. A. Ulloa Poblete,[138c,138b] E. N. Umaka,[29] G. Unal,[36] A. Undrus,[29] G. Unel,[160] J. Urban,[28b] P. Urquijo,[106] P. Urrejola,[138a] G. Usai,[8] R. Ushioda,[155] M. Usman,[109] Z. Uysal,[82] V. Vacek,[133] B. Vachon,[105] K. O. H. Vadla,[126] T. Vafeiadis,[36] A. Vaitkus,[97] C. Valderanis,[110] E. Valdes Santurio,[47a,47b] M. Valente,[157a] S. Valentinetti,[23b,23a] A. Valero,[164] E. Valiente Moreno,[164] A. Vallier,[90] J. A. Valls Ferrer,[164] D. R. Van Arneman,[115] T. R. Van Daalen,[139] A. Van Der Graaf,[49] P. Van Gemmeren,[6] M. Van Rijnbach,[126] S. Van Stroud,[97] I. Van Vulpen,[115] P. Vana,[134] M. Vanadia,[76a,76b] W. Vandelli,[36] E. R. Vandewall,[122] D. Vannicola,[152] L. Vannoli,[53] R. Vari,[75a] E. W. Varnes,[7] C. Varni,[17b] T. Varol,[149] D. Varouchas,[66] L. Varriale,[164] K. E. Varvell,[148] M. E. Vasile,[27b] L. Vaslin,[84] G. A. Vasquez,[166] A. Vasyukov,[38] R. Vavricka,[101] F. Vazeille,[40] T. Vazquez Schroeder,[36] J. Veatch,[31] V. Vecchio,[102] M. J. Veen,[104] I. Veliscek,[29] L. M. Veloce,[156] F. Veloso,[131a,131c] S. Veneziano,[75a] A. Ventura,[70a,70b] S. Ventura Gonzalez,[136] A. Verbytskyi,[111] M. Verducci,[74a,74b] C. Vergis,[24] M. Verissimo De Araujo,[83b] W. Verkerke,[115] J. C. Vermeulen,[115] C. Vernieri,[144] M. Vessella,[104] M. C. Vetterli,[143,e] A. Vgenopoulos,[153,z] N. Viaux Maira,[138f] T. Vickey,[140] O. E. Vickey Boeriu,[140] G. H. A. Viehhauser,[127] L. Vigani,[63b] M. Villa,[23b,23a] M. Villaplana Perez,[164] E. M. Villhauer,[52] E. Vilucchi,[53] M. G. Vincter,[34] G. S. Virdee,[20] A. Vishwakarma,[52] A. Visibile,[115] C. Vittori,[36] I. Vivarelli,[23b,23a] E. Voevodina,[111] F. Vogel,[110] J. C. Voigt,[50] P. Vokac,[133] Yu. Volkotrub,[86b] J. Von Ahnen,[48] E. Von Toerne,[24] B. Vormwald,[36] V. Vorobel,[134] K. Vorobev,[37] M. Vos,[164] K. Voss,[142] M. Vozak,[115] L. Vozdecky,[121] N. Vranjes,[15] M. Vranjes Milosavljevic,[15] M. Vreeswijk,[115] N. K. Vu,[62d,62c] R. Vuillermet,[36] O. Vujinovic,[101] I. Vukotic,[39] S. Wada,[158] C. Wagner,[104] J. M. Wagner,[17a] W. Wagner,[172] S. Wahdan,[172] H. Wahlberg,[91] M. Wakida,[112] J. Walder,[135] R. Walker,[110] W. Walkowiak,[142] A. Wall,[129] E. J. Wallin,[99] T. Wamorkar,[6] A. Z. Wang,[137] C. Wang,[101] C. Wang,[11] H. Wang,[17a] J. Wang,[64c] R.-J. Wang,[101] R. Wang,[61] R. Wang,[6] S. M. Wang,[149] S. Wang,[62b] T. Wang,[62a] W. T. Wang,[80] W. Wang,[14a] X. Wang,[14c] X. Wang,[163] X. Wang,[62c] Y. Wang,[62d] Y. Wang,[14c] Z. Wang,[107] Z. Wang,[62d,51,62c] Z. Wang,[107] A. Warburton,[105] R. J. Ward,[20] N. Warrack,[59] S. Waterhouse,[96] A. T. Watson,[20] H. Watson,[59] M. F. Watson,[20] E. Watton,[59,135] G. Watts,[139] B. M. Waugh,[97] C. Weber,[29] H. A. Weber,[18] M. S. Weber,[19] S. M. Weber,[63a]

C. Wei,[62a] Y. Wei,[127] A. R. Weidberg,[127] E. J. Weik,[118] J. Weingarten,[49] M. Weirich,[101] C. Weiser,[54] C. J. Wells,[48] T. Wenaus,[29] B. Wendland,[49] T. Wengler,[36] N. S. Wenke,[111] N. Wermes,[24] M. Wessels,[63a] A. M. Wharton,[92] A. S. White,[61] A. White,[8] M. J. White,[1] D. Whiteson,[160] L. Wickremasinghe,[125] W. Wiedenmann,[171] M. Wielers,[135] C. Wiglesworth,[42] D. J. Wilbern,[121] H. G. Wilkens,[36] D. M. Williams,[41] H. H. Williams,[129] S. Williams,[32] S. Willocq,[104] B. J. Wilson,[102] P. J. Windischhofer,[39] F. I. Winkel,[30] F. Winklmeier,[124] B. T. Winter,[54] J. K. Winter,[102] M. Wittgen,[144] M. Wobisch,[98] Z. Wolffs,[115] J. Wollrath,[160] M. W. Wolter,[87] H. Wolters,[131a,131c] M. C. Wong,[137] E. L. Woodward,[41] S. D. Worm,[48] B. K. Wosiek,[87] K. W. Woźniak,[87] S. Wozniewski,[55] K. Wraight,[59] C. Wu,[20] M. Wu,[14d] M. Wu,[114] S. L. Wu,[171] X. Wu,[56] Y. Wu,[62a] Z. Wu,[4] J. Wuerzinger,[111,v] T. R. Wyatt,[102] B. M. Wynne,[52] S. Xella,[42] L. Xia,[14c] M. Xia,[14b] J. Xiang,[64c] M. Xie,[62a] X. Xie,[62a] S. Xin,[14a,14e] A. Xiong,[124] J. Xiong,[17a] D. Xu,[14a] H. Xu,[62a] L. Xu,[62a] R. Xu,[129] T. Xu,[107] Y. Xu,[14b] Z. Xu,[52] Z. Xu,[14c] B. Yabsley,[148] S. Yacoob,[33a] Y. Yamaguchi,[155] E. Yamashita,[154] H. Yamauchi,[158] T. Yamazaki,[17a] Y. Yamazaki,[85] J. Yan,[62c] S. Yan,[59] Z. Yan,[104] H. J. Yang,[62c,62d] H. T. Yang,[62a] S. Yang,[62a] T. Yang,[64c] X. Yang,[36] X. Yang,[14a] Y. Yang,[44] Y. Yang,[62a] Z. Yang,[62a] W-M. Yao,[17a] H. Ye,[14c] H. Ye,[55] J. Ye,[14a] S. Ye,[29] X. Ye,[62a] Y. Yeh,[97] I. Yeletskikh,[38] B. K. Yeo,[17b] M. R. Yexley,[97] P. Yin,[41] K. Yorita,[169] S. Younas,[27b] C. J. S. Young,[36] C. Young,[144] C. Yu,[14a,14e] Y. Yu,[62a] M. Yuan,[107] R. Yuan,[62b] L. Yue,[97] M. Zaazoua,[62a] B. Zabinski,[87] E. Zaid,[52] Z. K. Zak,[87] T. Zakareishvili,[164] N. Zakharchuk,[34] S. Zambito,[56] J. A. Zamora Saa,[138d,138b] J. Zang,[154] D. Zanzi,[54] O. Zaplatilek,[133] C. Zeitnitz,[172] H. Zeng,[14a] J. C. Zeng,[163] D. T. Zenger Jr.,[26] O. Zenin,[37] T. Ženiš,[28a] S. Zenz,[95] S. Zerradi,[35a] D. Zerwas,[66] M. Zhai,[14a,14e] D. F. Zhang,[140] J. Zhang,[62b] J. Zhang,[6] K. Zhang,[14a,14e] L. Zhang,[14c] P. Zhang,[14a,14e] R. Zhang,[171] S. Zhang,[107] S. Zhang,[44] T. Zhang,[154] X. Zhang,[62c] X. Zhang,[62b] Y. Zhang,[62c,5] Y. Zhang,[97] Y. Zhang,[14c] Z. Zhang,[17a] Z. Zhang,[66] H. Zhao,[139] T. Zhao,[62b] Y. Zhao,[137] Z. Zhao,[62a] A. Zhemchugov,[38] J. Zheng,[14c] K. Zheng,[163] X. Zheng,[62a] Z. Zheng,[144] D. Zhong,[163] B. Zhou,[107] H. Zhou,[7] N. Zhou,[62c] Y. Zhou,[14c] Y. Zhou,[7] C. G. Zhu,[62b] J. Zhu,[107] Y. Zhu,[62c] Y. Zhu,[62a] X. Zhuang,[14a] K. Zhukov,[37] N. I. Zimine,[38] J. Zinsser,[63b] M. Ziolkowski,[142] L. Živković,[15] A. Zoccoli,[23b,23a] K. Zoch,[61] T. G. Zorbas,[140] O. Zormpa,[46] W. Zou,[41] and L. Zwalinski[36]

(ATLAS Collaboration)

[1]*Department of Physics, University of Adelaide, Adelaide, Australia*
[2]*Department of Physics, University of Alberta, Edmonton, Alberta, Canada*
[3a]*Department of Physics, Ankara University, Ankara, Türkiye*
[3b]*Division of Physics, TOBB University of Economics and Technology, Ankara, Türkiye*
[4]*LAPP, Université Savoie Mont Blanc, CNRS/IN2P3, Annecy, France*
[5]*APC, Université Paris Cité, CNRS/IN2P3, Paris, France*
[6]*High Energy Physics Division, Argonne National Laboratory, Argonne, Illinois, USA*
[7]*Department of Physics, University of Arizona, Tucson, Arizona, USA*
[8]*Department of Physics, University of Texas at Arlington, Arlington, Texas, USA*
[9]*Physics Department, National and Kapodistrian University of Athens, Athens, Greece*
[10]*Physics Department, National Technical University of Athens, Zografou, Greece*
[11]*Department of Physics, University of Texas at Austin, Austin, Texas, USA*
[12]*Institute of Physics, Azerbaijan Academy of Sciences, Baku, Azerbaijan*
[13]*Institut de Física d'Altes Energies (IFAE), Barcelona Institute of Science and Technology, Barcelona, Spain*
[14a]*Institute of High Energy Physics, Chinese Academy of Sciences, Beijing, China*
[14b]*Physics Department, Tsinghua University, Beijing, China*
[14c]*Department of Physics, Nanjing University, Nanjing, China*
[14d]*School of Science, Shenzhen Campus of Sun Yat-sen University, China*
[14e]*University of Chinese Academy of Science (UCAS), Beijing, China*
[15]*Institute of Physics, University of Belgrade, Belgrade, Serbia*
[16]*Department for Physics and Technology, University of Bergen, Bergen, Norway*
[17a]*Physics Division, Lawrence Berkeley National Laboratory, Berkeley, California, USA*
[17b]*University of California, Berkeley, California, USA*
[18]*Institut für Physik, Humboldt Universität zu Berlin, Berlin, Germany*

[19]Albert Einstein Center for Fundamental Physics and Laboratory for High Energy Physics, University of Bern, Bern, Switzerland
[20]School of Physics and Astronomy, University of Birmingham, Birmingham, United Kingdom
[21a]Department of Physics, Bogazici University, Istanbul, Türkiye
[21b]Department of Physics Engineering, Gaziantep University, Gaziantep, Türkiye
[21c]Department of Physics, Istanbul University, Istanbul, Türkiye
[22a]Facultad de Ciencias y Centro de Investigaciónes, Universidad Antonio Nariño, Bogotá, Colombia
[22b]Departamento de Física, Universidad Nacional de Colombia, Bogotá, Colombia
[23a]Dipartimento di Fisica e Astronomia A. Righi, Università di Bologna, Bologna, Italy
[23b]INFN Sezione di Bologna, Italy
[24]Physikalisches Institut, Universität Bonn, Bonn, Germany
[25]Department of Physics, Boston University, Boston, Massachusetts, USA
[26]Department of Physics, Brandeis University, Waltham, Massachusetts, USA
[27a]Transilvania University of Brasov, Brasov, Romania
[27b]Horia Hulubei National Institute of Physics and Nuclear Engineering, Bucharest, Romania
[27c]Department of Physics, Alexandru Ioan Cuza University of Iasi, Iasi, Romania
[27d]National Institute for Research and Development of Isotopic and Molecular Technologies, Physics Department, Cluj-Napoca, Romania
[27e]National University of Science and Technology Politechnica, Bucharest, Romania
[27f]West University in Timisoara, Timisoara, Romania
[27g]Faculty of Physics, University of Bucharest, Bucharest, Romania
[28a]Faculty of Mathematics, Physics and Informatics, Comenius University, Bratislava, Slovak Republic
[28b]Department of Subnuclear Physics, Institute of Experimental Physics of the Slovak Academy of Sciences, Kosice, Slovak Republic
[29]Physics Department, Brookhaven National Laboratory, Upton, New York, USA
[30]Universidad de Buenos Aires, Facultad de Ciencias Exactas y Naturales, Departamento de Física, y CONICET, Instituto de Física de Buenos Aires (IFIBA), Buenos Aires, Argentina
[31]California State University, California, USA
[32]Cavendish Laboratory, University of Cambridge, Cambridge, United Kingdom
[33a]Department of Physics, University of Cape Town, Cape Town, South Africa
[33b]iThemba Labs, Western Cape, South Africa
[33c]Department of Mechanical Engineering Science, University of Johannesburg, Johannesburg, South Africa
[33d]National Institute of Physics, University of the Philippines Diliman (Philippines), Philippines
[33e]University of South Africa, Department of Physics, Pretoria, South Africa
[33f]University of Zululand, KwaDlangezwa, South Africa
[33g]School of Physics, University of the Witwatersrand, Johannesburg, South Africa
[34]Department of Physics, Carleton University, Ottawa, Ontario, Canada
[35a]Faculté des Sciences Ain Chock, Université Hassan II de Casablanca, Morocco
[35b]Faculté des Sciences, Université Ibn-Tofail, Kénitra, Morocco
[35c]Faculté des Sciences Semlalia, Université Cadi Ayyad, LPHEA-Marrakech, Morocco
[35d]LPMR, Faculté des Sciences, Université Mohamed Premier, Oujda, Morocco
[35e]Faculté des sciences, Université Mohammed V, Rabat, Morocco
[35f]Institute of Applied Physics, Mohammed VI Polytechnic University, Ben Guerir, Morocco
[36]CERN, Geneva, Switzerland
[37]Affiliated with an institute covered by a cooperation agreement with CERN
[38]Affiliated with an international laboratory covered by a cooperation agreement with CERN
[39]Enrico Fermi Institute, University of Chicago, Chicago, Illinois, USA
[40]LPC, Université Clermont Auvergne, CNRS/IN2P3, Clermont-Ferrand, France
[41]Nevis Laboratory, Columbia University, Irvington, New York, USA
[42]Niels Bohr Institute, University of Copenhagen, Copenhagen, Denmark
[43a]Dipartimento di Fisica, Università della Calabria, Rende, Italy
[43b]INFN Gruppo Collegato di Cosenza, Laboratori Nazionali di Frascati, Italy
[44]Physics Department, Southern Methodist University, Dallas, Texas, USA
[45]Physics Department, University of Texas at Dallas, Richardson, Texas, USA
[46]National Centre for Scientific Research "Demokritos", Agia Paraskevi, Greece
[47a]Department of Physics, Stockholm University, Sweden
[47b]Oskar Klein Centre, Stockholm, Sweden
[48]Deutsches Elektronen-Synchrotron DESY, Hamburg and Zeuthen, Germany
[49]Fakultät Physik, Technische Universität Dortmund, Dortmund, Germany

[50]*Institut für Kern- und Teilchenphysik, Technische Universität Dresden, Dresden, Germany*
[51]*Department of Physics, Duke University, Durham, North Carolina, USA*
[52]*SUPA—School of Physics and Astronomy, University of Edinburgh, Edinburgh, United Kingdom*
[53]*INFN e Laboratori Nazionali di Frascati, Frascati, Italy*
[54]*Physikalisches Institut, Albert-Ludwigs-Universität Freiburg, Freiburg, Germany*
[55]*II. Physikalisches Institut, Georg-August-Universität Göttingen, Göttingen, Germany*
[56]*Département de Physique Nucléaire et Corpusculaire, Université de Genève, Genève, Switzerland*
[57a]*Dipartimento di Fisica, Università di Genova, Genova, Italy*
[57b]*INFN Sezione di Genova, Italy*
[58]*II. Physikalisches Institut, Justus-Liebig-Universität Giessen, Giessen, Germany*
[59]*SUPA—School of Physics and Astronomy, University of Glasgow, Glasgow, United Kingdom*
[60]*LPSC, Université Grenoble Alpes, CNRS/IN2P3, Grenoble INP, Grenoble, France*
[61]*Laboratory for Particle Physics and Cosmology, Harvard University, Cambridge, Massachusetts, USA*
[62a]*Department of Modern Physics and State Key Laboratory of Particle Detection and Electronics, University of Science and Technology of China, Hefei, China*
[62b]*Institute of Frontier and Interdisciplinary Science and Key Laboratory of Particle Physics and Particle Irradiation (MOE), Shandong University, Qingdao, China*
[62c]*School of Physics and Astronomy, Shanghai Jiao Tong University, Key Laboratory for Particle Astrophysics and Cosmology (MOE), SKLPPC, Shanghai, China*
[62d]*Tsung-Dao Lee Institute, Shanghai, China*
[62e]*School of Physics and Microelectronics, Zhengzhou University, China*
[63a]*Kirchhoff-Institut für Physik, Ruprecht-Karls-Universität Heidelberg, Heidelberg, Germany*
[63b]*Physikalisches Institut, Ruprecht-Karls-Universität Heidelberg, Heidelberg, Germany*
[64a]*Department of Physics, Chinese University of Hong Kong, Shatin, N.T., Hong Kong, China*
[64b]*Department of Physics, University of Hong Kong, Hong Kong, China*
[64c]*Department of Physics and Institute for Advanced Study, Hong Kong University of Science and Technology, Clear Water Bay, Kowloon, Hong Kong, China*
[65]*Department of Physics, National Tsing Hua University, Hsinchu, Taiwan*
[66]*IJCLab, Université Paris-Saclay, CNRS/IN2P3, 91405, Orsay, France*
[67]*Centro Nacional de Microelectrónica (IMB-CNM-CSIC), Barcelona, Spain*
[68]*Department of Physics, Indiana University, Bloomington, Indiana, USA*
[69a]*INFN Gruppo Collegato di Udine, Sezione di Trieste, Udine, Italy*
[69b]*ICTP, Trieste, Italy*
[69c]*Dipartimento Politecnico di Ingegneria e Architettura, Università di Udine, Udine, Italy*
[70a]*INFN Sezione di Lecce, Italy*
[70b]*Dipartimento di Matematica e Fisica, Università del Salento, Lecce, Italy*
[71a]*INFN Sezione di Milano, Italy*
[71b]*Dipartimento di Fisica, Università di Milano, Milano, Italy*
[72a]*INFN Sezione di Napoli, Italy*
[72b]*Dipartimento di Fisica, Università di Napoli, Napoli, Italy*
[73a]*INFN Sezione di Pavia, Italy*
[73b]*Dipartimento di Fisica, Università di Pavia, Pavia, Italy*
[74a]*INFN Sezione di Pisa, Italy*
[74b]*Dipartimento di Fisica E. Fermi, Università di Pisa, Pisa, Italy*
[75a]*INFN Sezione di Roma, Italy*
[75b]*Dipartimento di Fisica, Sapienza Università di Roma, Roma, Italy*
[76a]*INFN Sezione di Roma Tor Vergata, Italy*
[76b]*Dipartimento di Fisica, Università di Roma Tor Vergata, Roma, Italy*
[77a]*INFN Sezione di Roma Tre, Italy*
[77b]*Dipartimento di Matematica e Fisica, Università Roma Tre, Roma, Italy*
[78a]*INFN-TIFPA, Italy*
[78b]*Università degli Studi di Trento, Trento, Italy*
[79]*Universität Innsbruck, Department of Astro and Particle Physics, Innsbruck, Austria*
[80]*University of Iowa, Iowa City, Iowa, USA*
[81]*Department of Physics and Astronomy, Iowa State University, Ames, Iowa, USA*
[82]*Istinye University, Sariyer, Istanbul, Türkiye*
[83a]*Departamento de Engenharia Elétrica, Universidade Federal de Juiz de Fora (UFJF), Juiz de Fora, Brazil*
[83b]*Universidade Federal do Rio De Janeiro COPPE/EE/IF, Rio de Janeiro, Brazil*
[83c]*Instituto de Física, Universidade de São Paulo, São Paulo, Brazil*

[83d]Rio de Janeiro State University, Rio de Janeiro, Brazil
[83e]Federal University of Bahia, Bahia, Brazil
[84]KEK, High Energy Accelerator Research Organization, Tsukuba, Japan
[85]Graduate School of Science, Kobe University, Kobe, Japan
[86a]AGH University of Krakow, Faculty of Physics and Applied Computer Science, Krakow, Poland
[86b]Marian Smoluchowski Institute of Physics, Jagiellonian University, Krakow, Poland
[87]Institute of Nuclear Physics Polish Academy of Sciences, Krakow, Poland
[88]Faculty of Science, Kyoto University, Kyoto, Japan
[89]Research Center for Advanced Particle Physics and Department of Physics, Kyushu University, Fukuoka, Japan
[90]L2IT, Université de Toulouse, CNRS/IN2P3, UPS, Toulouse, France
[91]Instituto de Física La Plata, Universidad Nacional de La Plata and CONICET, La Plata, Argentina
[92]Physics Department, Lancaster University, Lancaster, United Kingdom
[93]Oliver Lodge Laboratory, University of Liverpool, Liverpool, United Kingdom
[94]Department of Experimental Particle Physics, Jožef Stefan Institute and Department of Physics, University of Ljubljana, Ljubljana, Slovenia
[95]School of Physics and Astronomy, Queen Mary University of London, London, United Kingdom
[96]Department of Physics, Royal Holloway University of London, Egham, United Kingdom
[97]Department of Physics and Astronomy, University College London, London, United Kingdom
[98]Louisiana Tech University, Ruston, Louisiana, USA
[99]Fysiska institutionen, Lunds universitet, Lund, Sweden
[100]Departamento de Física Teorica C-15 and CIAFF, Universidad Autónoma de Madrid, Madrid, Spain
[101]Institut für Physik, Universität Mainz, Mainz, Germany
[102]School of Physics and Astronomy, University of Manchester, Manchester, United Kingdom
[103]CPPM, Aix-Marseille Université, CNRS/IN2P3, Marseille, France
[104]Department of Physics, University of Massachusetts, Amherst, Massachusetts, USA
[105]Department of Physics, McGill University, Montreal, Quebec, Canada
[106]School of Physics, University of Melbourne, Victoria, Australia
[107]Department of Physics, University of Michigan, Ann Arbor, Michigan, USA
[108]Department of Physics and Astronomy, Michigan State University, East Lansing, Michigan, USA
[109]Group of Particle Physics, University of Montreal, Montreal, Quebec, Canada
[110]Fakultät für Physik, Ludwig-Maximilians-Universität München, München, Germany
[111]Max-Planck-Institut für Physik (Werner-Heisenberg-Institut), München, Germany
[112]Graduate School of Science and Kobayashi-Maskawa Institute, Nagoya University, Nagoya, Japan
[113]Department of Physics and Astronomy, University of New Mexico, Albuquerque, New Mexico, USA
[114]Institute for Mathematics, Astrophysics and Particle Physics, Radboud University/Nikhef, Nijmegen, Netherlands
[115]Nikhef National Institute for Subatomic Physics and University of Amsterdam, Amsterdam, Netherlands
[116]Department of Physics, Northern Illinois University, DeKalb, Illinois, USA
[117a]New York University Abu Dhabi, Abu Dhabi, United Arab Emirates
[117b]United Arab Emirates University, Al Ain, United Arab Emirates
[118]Department of Physics, New York University, New York, New York, USA
[119]Ochanomizu University, Otsuka, Bunkyo-ku, Tokyo, Japan
[120]Ohio State University, Columbus, Ohio, USA
[121]Homer L. Dodge Department of Physics and Astronomy, University of Oklahoma, Norman, Oklahoma, USA
[122]Department of Physics, Oklahoma State University, Stillwater, Oklahoma, USA
[123]Palacký University, Joint Laboratory of Optics, Olomouc, Czech Republic
[124]Institute for Fundamental Science, University of Oregon, Eugene, Oregon, USA
[125]Graduate School of Science, Osaka University, Osaka, Japan
[126]Department of Physics, University of Oslo, Oslo, Norway
[127]Department of Physics, Oxford University, Oxford, United Kingdom
[128]LPNHE, Sorbonne Université, Université Paris Cité, CNRS/IN2P3, Paris, France
[129]Department of Physics, University of Pennsylvania, Philadelphia, Pennsylvania, USA
[130]Department of Physics and Astronomy, University of Pittsburgh, Pittsburgh, Pennsylvania, USA
[131a]Laboratório de Instrumentação e Física Experimental de Partículas—LIP, Lisboa, Portugal
[131b]Departamento de Física, Faculdade de Ciências, Universidade de Lisboa, Lisboa, Portugal
[131c]Departamento de Física, Universidade de Coimbra, Coimbra, Portugal
[131d]Centro de Física Nuclear da Universidade de Lisboa, Lisboa, Portugal
[131e]Departamento de Física, Universidade do Minho, Braga, Portugal

[131f]*Departamento de Física Teórica y del Cosmos, Universidad de Granada, Granada (Spain), Spain*
[131g]*Departamento de Física, Instituto Superior Técnico, Universidade de Lisboa, Lisboa, Portugal*
[132]*Institute of Physics of the Czech Academy of Sciences, Prague, Czech Republic*
[133]*Czech Technical University in Prague, Prague, Czech Republic*
[134]*Charles University, Faculty of Mathematics and Physics, Prague, Czech Republic*
[135]*Particle Physics Department, Rutherford Appleton Laboratory, Didcot, United Kingdom*
[136]*IRFU, CEA, Université Paris-Saclay, Gif-sur-Yvette, France*
[137]*Santa Cruz Institute for Particle Physics, University of California Santa Cruz, Santa Cruz, California, USA*
[138a]*Departamento de Física, Pontificia Universidad Católica de Chile, Santiago, Chile*
[138b]*Millennium Institute for Subatomic physics at high energy frontier (SAPHIR), Santiago, Chile*
[138c]*Instituto de Investigación Multidisciplinario en Ciencia y Tecnología, y Departamento de Física, Universidad de La Serena, Chile*
[138d]*Universidad Andres Bello, Department of Physics, Santiago, Chile*
[138e]*Instituto de Alta Investigación, Universidad de Tarapacá, Arica, Chile*
[138f]*Departamento de Física, Universidad Técnica Federico Santa María, Valparaíso, Chile*
[139]*Department of Physics, University of Washington, Seattle, Washington, USA*
[140]*Department of Physics and Astronomy, University of Sheffield, Sheffield, United Kingdom*
[141]*Department of Physics, Shinshu University, Nagano, Japan*
[142]*Department Physik, Universität Siegen, Siegen, Germany*
[143]*Department of Physics, Simon Fraser University, Burnaby, British Columbia, Canada*
[144]*SLAC National Accelerator Laboratory, Stanford, California, USA*
[145]*Department of Physics, Royal Institute of Technology, Stockholm, Sweden*
[146]*Departments of Physics and Astronomy, Stony Brook University, Stony Brook, New York, USA*
[147]*Department of Physics and Astronomy, University of Sussex, Brighton, United Kingdom*
[148]*School of Physics, University of Sydney, Sydney, Australia*
[149]*Institute of Physics, Academia Sinica, Taipei, Taiwan*
[150a]*E. Andronikashvili Institute of Physics, Iv. Javakhishvili Tbilisi State University, Tbilisi, Georgia*
[150b]*High Energy Physics Institute, Tbilisi State University, Tbilisi, Georgia*
[150c]*University of Georgia, Tbilisi, Georgia*
[151]*Department of Physics, Technion, Israel Institute of Technology, Haifa, Israel*
[152]*Raymond and Beverly Sackler School of Physics and Astronomy, Tel Aviv University, Tel Aviv, Israel*
[153]*Department of Physics, Aristotle University of Thessaloniki, Thessaloniki, Greece*
[154]*International Center for Elementary Particle Physics and Department of Physics, University of Tokyo, Tokyo, Japan*
[155]*Department of Physics, Tokyo Institute of Technology, Tokyo, Japan*
[156]*Department of Physics, University of Toronto, Toronto, Ontario, Canada*
[157a]*TRIUMF, Vancouver, British Columbia, Canada*
[157b]*Department of Physics and Astronomy, York University, Toronto, Ontario, Canada*
[158]*Division of Physics and Tomonaga Center for the History of the Universe, Faculty of Pure and Applied Sciences, University of Tsukuba, Tsukuba, Japan*
[159]*Department of Physics and Astronomy, Tufts University, Medford, Massachusetts, USA*
[160]*Department of Physics and Astronomy, University of California Irvine, Irvine, California, USA*
[161]*University of Sharjah, Sharjah, United Arab Emirates*
[162]*Department of Physics and Astronomy, University of Uppsala, Uppsala, Sweden*
[163]*Department of Physics, University of Illinois, Urbana, Illinois, USA*
[164]*Instituto de Física Corpuscular (IFIC), Centro Mixto Universidad de Valencia—CSIC, Valencia, Spain*
[165]*Department of Physics, University of British Columbia, Vancouver, British Columbia, Canada*
[166]*Department of Physics and Astronomy, University of Victoria, Victoria, British Columbia, Canada*
[167]*Fakultät für Physik und Astronomie, Julius-Maximilians-Universität Würzburg, Würzburg, Germany*
[168]*Department of Physics, University of Warwick, Coventry, United Kingdom*
[169]*Waseda University, Tokyo, Japan*
[170]*Department of Particle Physics and Astrophysics, Weizmann Institute of Science, Rehovot, Israel*
[171]*Department of Physics, University of Wisconsin, Madison, Wisconsin, USA*
[172]*Fakultät für Mathematik und Naturwissenschaften, Fachgruppe Physik, Bergische Universität Wuppertal, Wuppertal, Germany*
[173]*Department of Physics, Yale University, New Haven, Connecticut, USA*

[a]Deceased.
[b]Also at Department of Physics, King's College London, London, United Kingdom.

[c]Also at Institute of Physics, Azerbaijan Academy of Sciences, Baku, Azerbaijan.
[d]Also at Lawrence Livermore National Laboratory, Livermore, USA.
[e]Also at TRIUMF, Vancouver, British Columbia, Canada.
[f]Also at Department of Physics, University of Thessaly, Greece.
[g]Also at An-Najah National University, Nablus, Palestine.
[h]Also at Department of Physics, University of Fribourg, Fribourg, Switzerland.
[i]Also at Department of Physics, Westmont College, Santa Barbara, USA.
[j]Also at Departament de Fisica de la Universitat Autonoma de Barcelona, Barcelona, Spain.
[k]Also at Affiliated with an institute covered by a cooperation agreement with CERN.
[l]Also at The Collaborative Innovation Center of Quantum Matter (CICQM), Beijing, China.
[m]Also at Università di Napoli Parthenope, Napoli, Italy.
[n]Also at Institute of Particle Physics (IPP), Canada.
[o]Also at University of Colorado Boulder, Department of Physics, Colorado, USA.
[p]Also at Borough of Manhattan Community College, City University of New York, New York, New York, USA.
[q]Also at National Institute of Physics, University of the Philippines Diliman (Philippines), Philippines.
[r]Also at Department of Financial and Management Engineering, University of the Aegean, Chios, Greece.
[s]Also at Department of Physics, Stanford University, Stanford, California, USA.
[t]Also at Centro Studi e Ricerche Enrico Fermi, Italy.
[u]Also at Institucio Catalana de Recerca i Estudis Avancats, ICREA, Barcelona, Spain.
[v]Also at Technical University of Munich, Munich, Germany.
[w]Also at Yeditepe University, Physics Department, Istanbul, Türkiye.
[x]Also at Institute of Theoretical Physics, Ilia State University, Tbilisi, Georgia.
[y]Also at CERN, Geneva, Switzerland.
[z]Also at Center for Interdisciplinary Research and Innovation (CIRI-AUTH), Thessaloniki, Greece.
[aa]Also at Hellenic Open University, Patras, Greece.
[bb]Also at Center for High Energy Physics, Peking University, China.
[cc]Also at Department of Physics, Stellenbosch University, South Africa.
[dd]Also at Department of Physics, California State University, Sacramento, USA.
[ee]Also at Département de Physique Nucléaire et Corpusculaire, Université de Genève, Genève, Switzerland.
[ff]Also at Institut für Experimentalphysik, Universität Hamburg, Hamburg, Germany.
[gg]Also at Institute for Nuclear Research and Nuclear Energy (INRNE) of the Bulgarian Academy of Sciences, Sofia, Bulgaria.
[hh]Also at Washington College, Chestertown, Maryland, USA.
[ii]Also at Institute of Applied Physics, Mohammed VI Polytechnic University, Ben Guerir, Morocco.
[jj]Also at Institute of Physics and Technology, Mongolian Academy of Sciences, Ulaanbaatar, Mongolia.